1976

Electrical Properties Of Ammonium-perchlorate

Ah Mee Hor

ELECTRICAL PROPERTIES OF AMMONIUM PERCHLORATE

by

Ah Mee Hor

Department of Chemistry

Submitted in partial fulfillment
of the requirements for the degree of
Doctor of Philosophy

Faculty of Graduate Studies
The University of Western Ontario
London, Ontario
June, 1976

ABSTRACT

Electrical measurements are some of the most important techniques for studying defects in ionic crystals. A literature survey of previous work done on ammonium perchlorate (AP) indicates that only its conductivity has been studied and that serious discrepancies exist between the results of various authors. In this project, the electrical properties of pure AP, in nitrogen, ammonia and water vapor, and of doped AP have been investigated by studying d.c. conductivity, thermal depolarization and d.c. polarization currents.

The conductivity of pure AP in nitrogen consists of low temperature and high temperature regions with activation energies for conduction of 0.56 and 0.87 eV respectively. Ammonia and water vapor at low coverages enhance the conductivity but do not alter the activation energies. AP doped with SO_4^{2-} and CrO_4^{2-} have a larger conductivity than pure AP; the conductivity of the doped crystals has a single activation energy, 0.66 eV for SO_4^{2-} and 0.72 eV for CrO_4^{2-}. Doping AP crystals with Pb^{2+} causes a decrease in the conductivity but there are two activation energies as for pure AP. The conductivity is 5 or 6 times higher when the electric field is applied perpendicularly to (210) faces than when the field is normal to (001) faces. A conduction mechanism involving proton jumps in the ClO_4^- sublattice is proposed.

Ammonia-treated AP, and AP doped with SO_4^{2-} and CrO_4^{2-} display two peaks in their thermal depolarization currents.

The high temperature peak with an activation energy 0.50 eV appears at 287 K. It is common to all three samples and is ascribed to the relaxation of $HClO_4$. For AP doped with SO_4^{2-} and CrO_4^{2-} the low temperature peak at 236 K has an activation energy of 0.25 eV, which is ascribed to the relaxation of ammonia-anion vacancy complexes. The low temperature peak of ammonia-treated AP has a higher activation energy of 0.35 eV and occurs at 252 K, due to the different environment for the relaxation of ammonia.

D.c. polarization currents are complicated by the distribution of traps at large defects such as dislocations and further work will be needed for a better understanding of this phenomenon.

ACKNOWLEDGMENT

I would like to express my gratitude to my supervisor, Professor P.W.M. Jacobs for suggesting this research topic and for his constant guidance and encouragement throughout this work.

I would also like to thank Professor S. Radhakrishna for his useful suggestions on growing doped AP crystals and Professor J.H. Crawford, Jr. for his advice on the thermal depolarization apparatus. I am also indebted to the graduate students, postdoctoral fellows, faculty members and staff who have contributed to my education at Western.

Finally, I would like to give special thanks to my wife for her understanding, faith and help.

TABLE OF CONTENTS

LIST OF TABLES

LIST OF FIGURES

CHAPTER 1

INTRODUCTION

1-1 Review of Previous Work

Ammonium perchlorate NH_4ClO_4 (hereinafter abbreviated to AP) has been extensively studied, and especially for its thermal decomposition (1,2) because of its widespread use in solid propellants and explosives. As charge migration is suspected to be closely related to its thermal decomposition electrical conduction in AP has been the subject of several investigations. The identification of the conducting species would not only explain the conductivity of AP but also give us some insight into the mechanism of its thermal decomposition.

The first conductivity measurements were carried out by Zirkind and Freeman (3) on the pellet samples in three kinds of environments namely, vacuum, oxygen and argon atmospheres. Electronic and ionic conduction mechanisms were suggested. Wise (4) compared the conductivity of AP pellets in N_2 and NH_3 above 450 K and found that NH_3 increased the conductivity but lowered the activation energy for conduction from 1.4 to 0.9 eV. He interpreted this data in terms of a proton transfer mechanism. Maycock et al. (5,6) using d.c. measurements on single crystals observed several linear regions in

the conductivity plot. They noticed polarization effects between 298 and 398 K but did not indicate whether their quoted values of conductivity referred to zero time, infinite time or some intermediate time. The assignment of conduction mechanisms like surface conduction, interstitial NH_4^+ conduction, etc. to various temperature regions seems rather arbitrary. Jacobs, Lovatt and Ng (7,8) studied the a.c. conductivity of pure and doped AP at 1591 Hz. The effect of thermal cycling, water vapor, NH_3, and dopants Ba^{2+} and SO_4^{2-} were studied. They suggested a mechanism of formation of proton holes (NH_3 molecules at cation lattice sites) followed by migration of these defects in the bulk crystal by the transfer of protons from adjacent ammonium ions. The activation energy for the proton migration was estimated to be very small. Owen, Thomas & Williams (9,10) measured the d.c. conductivity of pure and doped AP and pure rubidium perchlorate (RP). RP has practically the same unit cell dimension and ion sizes as AP. The similarity in both the activation energy of 1.1 to 1.2 eV and the magnitude of the conductivity which was observed for the two compounds in the temperature region 390 to 410 K led these authors to reject a proton transfer mechanism. Instead the migration of cations, NH_4^+ in AP and Rb^+ in RP, was said to be responsible for the conduction. Their findings that the conductivity of AP was increased by SO_4^{2-} but not affected by Ba^{2+} lead them to propose interstitial NH_4^+ ions as the major charge carriers. From the dielectric loss and d.c.

conductivity of AP doped with HSO_4^-, Khairetdinov and Boldyrev (11) obtained an activation energy of 0.76 - 0.81 eV for the migration of charge carriers and proposed a proton conduction mechanism involving the reorientation of $HClO_4$ formed. Recently Keenan and Ohanian (12) reported the d.c. conductivity of pure AP from room temperature to 450 K. Two linear regions were observed and the activation energies in the low and high temperature regions were 0.12 and 1.04 eV respectively. Their conductivity reading referred to those obtained at 1 minute after the application of electric field. To explain the extremely low activation energy of 0.12 eV, they worked out a proton conduction mechanism in which interstitial water molecules act as both proton donor and acceptor sites. At the high temperature, the migration of NH_4^+ via cation vacancies was thought to prevail over the proton conduction mechanism.

A theoretical analysis of electrical conductivity in AP has been published by Goldstein and Keenan (13). The model used was that of polarizable point ions and a computer simulation technique was employed. The ions considered were NH_4^+ and ClO_4^-, and a Schottky defect pair was found to have the smallest formation energy, 1.66 eV compared with 4.05 eV for a Frenkel defect pair. Accordingly conduction by interstitial NH_4^+ was concluded to be negligible. A turnstile mechanism involving slow synchronous rotations of two adjacent perchlorate ions to allow the passage of NH_4^+ into

a cation vacancy was proposed for the conduction in the temperature region 520 to 550°K. The energy of migration of a cation vacancy was found to be 4.53 eV. Unfortunately, their model did not take into consideration the existence of NH_3 and $HClO_4$ species.

1-2 Defects in Ionic Solids

The concept of defects in crystals, originally introduced by Frenkel, Schottky and Wagner, has been widely used in explaining the observed electrical, mechanical and chemical properties of ionic crystals. Comprehensive discussions of the subject can be found in several reviews (14,15,16,17).

The simplest possible types of defects, generally known as point defects, are vacancies, interstitial ions and impurity ions. Large defects are also known such as dislocations (linear defects) and grain boundaries and surface (planar defects). For the sake of simplicity, a two-dimensional lattice of a monovalent ionic crystal M^+X^-, schematically depicted in Fig. 1 is used for a general discussion. The charge of defects is usually described in terms of effective charge, i.e. the difference between the local charge states after and before the formation or incorporation of the defect. For example, the effective charge of a cation vacancy in a uni-univalent crystal is -1 and of an impurity divalent cation at the normal cation site is +1. Electric neutrality requires the incorporation of at least two kinds of defects with opposite charge.

The absence of both a cation and an anion from their respective lattice sites forms a Schottky defect pair, Fig. 1(b). A Frenkel defect pair is formed when a normal lattice ion migrates to an interstitial position thus leaving behind a vacancy on its own sublattice, Fig. 1(c). Both cation and anion Frenkel defects may occur. The thermally generated Schottky and Frenkel defects are intrinsic defects to be distinguished from defects created by other means. The introduction of impurity ions (doping) may create point defects in the lattice, e.g. for charge compensation, the presence of a divalent impurity ion Mi^{2+} at the cation site would introduce either a vacancy at another cation site or an extra anion X^- at an interstitial site, Fig. 1(d). Similar arguments can be used for other kinds of doping.

An electric dipole is formed when two defects of opposite charge are situated close to each other. In Fig. 1(e) impurity Mi^{2+} ions form two types of dipoles with cation vacancies depending on their relative positions, and in Fig. 1(f) a pair of cation and anion vacancies also constitutes a dipole. Larger aggregates of dipoles such as dimers, trimers etc. form when the dipole are located in close proximity.

Large defects including dislocations and grain boundaries are known to affect the physical and chemical properties of solids (18). Dislocations can function as traps as well as providing effective migration paths for point defects.

The migration of defects under the action of forces

gives rise to the transport of matter and electric charge which can be studied by a variety of experimental techniques. Migration of charged defects in an applied electric field results in ionic conduction and polarization. Chemical forces due to the presence of concentration gradients could effect the diffusion of defects. Thermal gradients may generate a thermoelectric power and mechanical stress produce deformation and diffusional creep due to the migration of dislocations and point defects. As this project mainly deals with the electrical properties of defects in AP, only the related theoretical background will be discussed briefly.

1-3 Ionic Conductivity

The migration of defects under the action of an applied field violates the conditions of thermodynamic equilibrium. An exact treatment of this subject should use non-equilibrium thermodynamics, as has been done by Howard and Lidiard (19). However the commonly used simple model of thermally activated jumps can also account for the essential phenomenological features of atomic migration processes. According to this model, a defect must surmount a potential barrier when it jumps from one site to the other. In the absence of applied field, the jump is random and characterized by a frequency.

$$w = \nu \exp(-\Delta g/kT) \qquad (1.1)$$

$$= \nu \exp(\Delta s/k) \exp(-\Delta h/kT) \qquad (1.2)$$

where Δg = Gibbs free energy of activation

Δs = entropy of activation

Δh = enthalpy of activation

ν = lattice vibrational frequency

k = Boltzmann's constant

and T = absolute temperature

An applied electric field lowers the height of energy barrier Δg for the defect jump in the direction of field by an amount $\frac{1}{2} \varepsilon aq$, where ε is the magnitude of the field, a the component of the jump distance along the direction of the field and q is the effective charge of the defect. The energy barrier is raised by same amount for the jump opposite to the field. The excess number of jumps in the direction of the field results in a net current flow. The conductivity σ due to the migration of charged defects is

$$\sigma = n\mu q \qquad (1.3)$$

where n = concentration of defects

μ = mobility of defects

q = effective charge of defect

or, on substituting for μ,

$$\sigma = \frac{nq^2a^2}{kT} \nu \exp\left(\frac{\Delta s}{k}\right) \exp\left(\frac{-\Delta h}{kT}\right) \qquad (1.4)$$

The low-temperature conductivity of an ionic solid is referred to as extrinsic conductivity since the defects responsible for conduction are generally introduced by the aliovalent impurity ions. When the temperature is increased the formation of intfinsic defects become energetically

feasible. Therefore an increase in both the conductivity and its activation energy are observed and the expression for the conductivity will have to take the formation energy into account,

$$\sigma = \frac{Nq^2a^2\nu}{kT}\exp\left(\frac{\Delta s + \frac{1}{2}s}{k}\right)\exp\left[\frac{-(\Delta h + \frac{1}{2}h)}{kT}\right] \qquad (1.5)$$

where N = no. of lattice sites

s = entropy associated with defect formation

h = enthalpy associated with defect formation

For compounds such as alkali halides, silver halides and alkaline earth Halides, the conductivity is measured over a large temperature range and hence the values of Δh, h, Δs and s can be calculated by means of computer fitting. When the number of data points is few and the measurements are restricted to a short temperature range, a simplified form of analysis must be adopted. The conductivity equation is re-written as

$$\sigma T = A \exp(-E/kT) \qquad (1.6)$$

where A = pre-exponential factor term

E = activation energy which in fact means an enthalpy of activation

The conductivity results are plotted graphically as log σ T vs. T^{-1} and the slopes of the various linear regions give the values of E.

1-4 D.C. Polarization Current

An electric dipole in a solid reorients with a characteristic relaxation time constant

$$\tau = \tau_o \exp(E_r/kT) \qquad (1.7)$$

where E_r = activation energy of reorientation

τ_o = pre-exponential factor

For instance, each of the impurity Mi^{2+} - cation vacancy dipoles in Fig. 1(e) can change its direction through the jump of the vacancy into a number of crystallographically equivalent positions around Mi^{2+}. τ_o depends on jump frequency w, and a geometrical factor decided by the no. of equivalent positions. The application of a static field would bring the dipoles into their preferred orientations in the direction of the field and this produces a polarization current which decreases with time due to a readjustment of the dipole distribution to an equilibrium value. The polarization current I_p at time t is calculated from

$$I_p(t) = I(t) - I_\infty \qquad (1.8)$$

where I(t) = current at time t after application of field

I_∞ = final steady-state current

The polarization current can usually be analysed into one or more exponential terms (20,21,22) as

$$I_p(t) = \sum_i Ai \exp(-t/\tau_i) \qquad (1.9)$$

where τ_i is a characteristic relaxation time for the process involved and A_i is a constant which depends on the material and may vary from specimen to specimen of the same material. By measuring the polarization current at several temperatures, a set of values is obtained for each τ_i and these may be used in plots of log τ^{-1} vs. T^{-1} to determine E_r in eq. (1.7).

1-5 Thermal Depolarization Current (TDC)

The thermal depolarization technique for studying the electric dipoles in ionic crystals was first introduced by Bucci and co-workers (23) who introduced the name of ionic thermocurrent (ITC). Later this method was used to investigate electronic defects in solids, and dielectric relaxation of polymers and liquids which may not involve any ionic conduction. Thus thermal depolarization current (TDC) is a more general and more descriptive term than ITC.

The procedure of a typical TDC experiment is schematically represented in Fig. 2 and described as follows: (i) In the absence of an electric field the dipoles are randomly oriented. (ii) The dipoles are oriented into some preferential directions by an electric field ε applied at a temperature T_p for a time t_p. If $t_p >> \tau(T_p)$, essentially all the dipole will become oriented so that the polarization approaches the saturation value. A d.c. polarization current will be observed in the meantime. (iii) With the field still applied the sample is cooled to a temperature T_o at which $\tau(T_o)$ is several hours or longer, so that the dipoles remain frozen in

the same configuration as that adopted in step (ii). (iv) The field ε is then removed and the sample is warmed at a constant rate $b = dT/dt$. The relaxation time of dipoles (eq. (1.7)) gets shorter and shorter as temperature T rises and a depolarization current J will be detected as the dipoles lose their preferred orientation.

The depolarization current is given by (23)

$$J(T) = \frac{P_o}{\tau_o} \exp\left(\frac{-E_r}{kT}\right) \exp\left[-(b\tau_o)^{-1} \int_{T_o}^{T} \exp\left(\frac{-E_r}{kT'}\right) dT' \right] \quad (1.10)$$

where P_o is the total released charge (= total polarization x area, S).

The curve traced by J as a function of T is an asymmetric curve with a maximum at a temperature

$$T_m = [\, bE_r \tau(T_m)/k]^{-1} \quad (1.11)$$

$$= [\, bE_r \tau_o \exp(E_r/kT_m)/k]^{-1} \quad (1.12)$$

which is independent of ε and T_p. The initial current rise at low temperature is approximated by

$$J(T) \doteq \frac{P_o}{\tau_o} \exp(-E_r/kT) \quad (1.13)$$

when the existing polarization is still not very different from (P_o/S). The area under the TDC curve gives the total polarization,

$$P_o = \int_o^\infty J(t)dt \quad (1.14)$$

$$= \frac{n\alpha d^2 \varepsilon S}{kT_p} \quad (1.15)$$

which is related to the n no. of dipoles of moment d, and α, a geometrical factor accounting for crystallographically equivalent orientations of dipoles.

If there is more than one type of dipole, multiple peaks will be found and the eq. (1.10) can be replaced by a summation. Although these may be separated by selective polarization and peak cleaning technique, data analysis is best done by computer fitting techniques (24,25).

1-6 Properties of Ammonium Perchlorate

AP is a white crystalline solid. At low temperature its orthorhombic structure has unit cell dimensions a_o = 9.202 Å, b_o = 5.816 Å and C_o = 7.449 Å. Each unit cell contains four formula units. At 513 K it transforms into a cubic structure. While the ammonium ion undergoes free or almost free rotation with a low energy barrier of about 0.1 eV, the free rotation of perchlorate ions does not occur until the transition temperature of 513 K is reached.

AP is stable at room temperature but decomposes at measurable rates at temperatures greater than 420 K. The following two equations seem to best represent the overall product distribution for the thermal decomposition of AP:

$$\text{At } T < 573 \text{ K}, \quad 4NH_4ClO_4 = 2Cl_2 + 2N_2O + 3O_2 + 8H_2O \qquad (1.16)$$

$$\text{At } T > 573 \text{ K}, \quad 2NH_4ClO_4 = Cl_2 + 2NO + O_2 + 4H_2O \qquad (1.17)$$

The cleavage planes for the orthorhombic AP are (210) and (001), and hence a cleaved crystal has two rhombic (001) faces

and four rectangular (210) faces. The solubility of AP at 303 K is 26.0 g per 100 ml of H_2O.

1-7 Objectives of this research

The inconsistencies between the conductivity results published by different authors are indeed very serious, amounting for instance, to a factor of 100 in the conductivity of pure AP. While the earlier experiments were usually performed on the pellet samples for which an irreproducible conductivity is understandable, the situation does not seem to be improved much when single crystals were used in more recent work. Poor reproducibility of conductivity apparently arises from the following factors:

(i) Crystals used are not of good quality, generally due to an improper method of preparation.

(ii) Thermal instability of AP is not taken into consideration though the products of decomposition are known to affect the conductivity.

(iii) Polarization effects in d.c. measurements have not been carefully studied.

(iv) Improper annealing treatment of samples.

The common mistake committed in all previously published work is that the authors always proposed some conduction mechanisms without paying proper attention to the crystal structure of AP. They seemed to assume isotropic conductivity for orthorhombic AP. One reason may be that their irreproducible results masked the anisotropic property. Except in one

investigation in which the dielectric loss was measured, all the studies involved only the measurements of a.c. and d.c. conductivity.

In view of the incomplete nature of and the large discrepancies in previous investigations, this research project had the following objectives: (i) The growth of large single crystals of good quality, of both pure and doped AP. (ii) The investigation of the d.c. conductivity in different crystal orientations. (iii) The use of additional techniques, thermal depolarization and d.c. polarization, to study the defects in AP. It was hoped that results obtained from such a careful investigation would clarify the present incomplete understanding of electrical conduction in AP.

CHAPTER 2

EXPERIMENTAL

2-1. Sample Preparation

AP powder was purchased from the Fisher Scientific Company. It was 99.99% pure and contained traces of chlorate, sulfate, chloride and metallic impurities. The powder was ground further in an agate mortar and then compressed into pellets of diameter 12.96 mm and height about 2 mm by means of a hydraulic press operated at a pressure of 14,000 psi. These pellets were mechanically rigid and had a density equal to 98.6% of the density of a single crystal.

Large single crystals of pure and doped AP were grown from saturated aqueous solution of AP. They were cleaved along two planes (210) and (001) into prisms of desired sizes. Other planes were obtainable by polishing the crystal with fine emery paper. The dopants used were respectively, $Pb(ClO_4)_2 \cdot 3H_2O$ and $Ba(ClO_4)_2 \cdot 3H_2O$ from Alfa Products, $(NH_4)_2CrO_4$ from Allied Chemicals, and $(NH_4)_2SO_4$ from British Drug Houses. Doped crystals grown were 1% AP:Ba^{2+}, 5% AP:Pb^{2+}, 0.1% AP:SO_4^{2-}, 0.1% and 1% AP:CrO_4^{2-}. The stated figures refer to the mole percentages of impurities added to the AP solution used for growing the crystals and not to the amount of the impurities incorporated into the crystals, which is unknown. More details on the crystal growing

technique used will be presented in the next section.

Early measurements indicated that the d.c. conductivity of AP crystals, when measured with Pt foil electrodes under a mild pressure, could vary from one sample to another by a factor of as much as five, mainly due to the irreproducible electrical contact between the sample surfaces and the electrodes. This problem was solved by coating the surface of crystal with either a thin conducting film of silver paint or vacuum deposited palladium. Both kinds of coating yielded the same results in the conductivity measurements and in thermal depolarization studies.

2-2 Crystal Growth

AP is thermally unstable and therefore cannot be grown from melt or vapor. The large single crystals used in this work were grown from the saturated aqueous solutions of AP. The crystal growth apparatus consisted of a growth tank, a rotating unit and a temperature control unit.

The growth tank (Fig.3) was constructed from a two-liter beaker fitted with a plexiglass lid. It is imperative that dust be prevented from entering into the growth tank. The glass "tree" which was mounted on the shaft H of the rotating unit had three sets of four branches each. The upper set Q formed a propeller whose main function was to stir the top part of the solution in order to prevent any crystallization on the solution surface. The remaining two sets of branches were arranged in a staggered configuration such that the

maximum room was available for the crystals to grow. Thin glass plates V, hung from those branches by means of Pt wires, stirred the solution when the tree was rotated. At the end of each branch a small vertical tube acted as a holder for a tiny glass rod carrying a seed cemented onto its tip with epoxy resin. A thermometer T and the probe P of the temperature controller were inserted into the solution through small holes into the lid.

The rotating unit (Fig. 4) consisted of a 25 r.p.m. Bodine electric motor which was coupled to the shaft H via a rack and pinion. By this device the glass tree was rotated continuously in alternate directions, three and a half revolutions each, so as to ensure equal growth on opposite faces of the crystals. The rack R was moved to and fro by an arm E attached eccentrically to the motor shaft, and by means of the pinion G produced the desired rotation of shaft H. The speed of rotation varies sinusoidally, a gradual deceleration and acceleration occurring before and after each reversal of the direction of rotation. The agitation of the solution over the faces of the growing crystals was thereby minimized.

The growth tank was insulated thermally from its surroundings by placing it in a larger beaker with an inch of air gap between the two beakers. The temperature of the solution was generally kept at about 10° K above the room temperature by two infrared lamps sited on opposite sides of the growth tank and slightly above it so that the radiation was directed at an angle of about 45° to the solution level. The lamps

were regulated by a Fisher proportional temperature control, and the solution temperature could be kept constant to within 0.01 K of the set temperature.

The seeds were prepared by slowly evaporating a saturated solution of AP in a small beaker. Only seeds of good quality were selected for the crystal growth. Alternatively, seeds of size 2×2×1 mm were cut from the large crystals harvested from the growth tank. The seeds were glued with epoxy resin to the tips of tiny glass rods. The resin would harden after 24 hours of setting at room temperature.

The growth tank was filled with 1.6 liters of saturated AP solution which was prepared by dissolving an appropriate amount of AP powder in doubly distilled water from a Corning distillation apparatus. The temperature of the solution was raised to 0.5 K above its saturation point and the seeds were then installed on the branches of the glass tree. The surface of the seeds was allowed to dissolve to remove surface irregularities and the solution was then brought back to its original saturation temperature. Crystal growth was effected by lowering the solution temperature by about 0.1 K per day. Too fast a cooling rate would produce crystals of poor quality which contained large visible imperfections. The seeds grew slowly into crystals of size 15×15×5 mm in one month. These crystals were removed from the solutions and kept in a desiccator until needed.

2.3 Conductivity Cell

The conductivity cell used in this work is shown in Fig.5. The cell body was made of a quartz tube, 7 cm in O.D. and 35 cm in length, sealed to a Quickfit joint. Inside the cell, a sample holder was suspended from the top of the cell by two tungsten wires W. The sample holder (Fig. 6) had two quartz plates P to keep the sample X and insulating alumina discs A in a fixed position when the screw B was tightened to exert a mild pressure through springs S and quartz sleeves T onto the quartz plates. The sample was sandwiched between two Pt electrodes which were insulated from the quartz plates by alumina discs. Thin Pt wires were spot-welded to the electrodes. A Pt vs. Pt + 13% Rh thermocouple was placed close (~2 mm) to the sample. The electrode and thermocouple leads were each insulated by quartz tubing and exited from four narrow sleeves L at the top of the cell. The tips of the sleeves were sealed with epoxy resin. After leaving the cell, the electrode leads were soldered to coaxially shielded wires terminating in BNC connectors.

The conductivity cell was heated by a nichrome-wire wound furnace. A nickel sheet N was placed in between the furnace and the cell, and the remaining exposed parts of the cell was covered with aluminum foil. The nickel sheet and aluminum foil were both appropriately grounded. As a result, the conductivity cell was well shielded from the stray external electric fields of its surroundings as well as from the effects of the furnace windings, which were non-inductively

wound as an added precaution. Proper shielding is absolutely essential when the current to be measured lies in the range of 10^{-12} to 10^{-14} A.

The conductivity cell C was connected to a vacuum line, as shown in Fig. 7. The cell could be evacuated to a vacuum of 10^{-6} torr with a mercury diffusion pump backed up by a rotary pump. The sample was usually annealed at about 380 K in vacuum for 16 hours or more to get rid of any adsorbed moisture or gases. Without this annealing treatment the conductivity results tended to be less reproducible.

Nitrogen or ammonia gas from cylinders was passed through a P_2O_5 drying column D before it entered the conductivity cell. The nitrogen gas served as an inert atmosphere which suppressed the sublimation of AP and also acted as a heat-transfer medium as well. Water vapor was introduced into the cell by evaporating some water, previously frozen by liquid N_2, from a small tube attached to the bottom of the cell.

To determine the d.c. conductivity of a sample, a d.c. voltage (40 V/mm) from a Hewlett Packard power supply was applied across the sample and the resulting current was measured by a Cary 401 vibrating-reed electrometer and simultaneously displayed on a strip chart recorder. The applied voltage was chosen to lie within the ohmic region of the current vs. voltage plot. Guarded and unguarded samples gave identical results. At the end of each measurement, the sample was shorted to discharge any accumulated charge completely.

2-4 Thermal Depolarization Apparatus

The apparatus used for studying TDC in AP is shown in Fig. 8. It consisted of two chambers both made from stainless steel. An Inconel-shielded, MgO - insulated Thermocoax wire W was wound around the outside wall of the inner chamber to provide internal heating without introducing undesirable electrical interference. The sample S sat on a Pt electrode B which was insulated from the steel platform P by a high-quality sapphire insulator (I). The measuring junction of an chromel-alumel thermocouple and the sensor of a temperature controller probe (both not shown in diagram) were positioned in the close vicinity of the sample. The upper electrode, which was surrounded by a steel shield A, was a rigid steel tubing with a spring-loaded tip T in touch with the sample.

Figure 9 reveals the arrangement of leads and connectors on the top of the apparatus. Through a Veeco valve V the apparatus could be evacuated and dry helium introduced to act as an exchange gas in heating the sample. The chromel-alumel thermocouple and temperature controller probe were inserted through CAJON ultra-torr adapters C and P respectively. The terminals H and H' of the Thermocoax wire were mounted from inside the apparatus with flanges such that the wire could be removed, along with the inner chamber to allow the installation of a sample. Of two BNC teflon connectors, E was linked to the upper electrode and D to the bottom electrode by Pt wires.

During the polarization of a sample, the bottom electrode was connected to the high voltage end of a d.c. power supply

and the top electrode to the input terminal of a Cary 401 electrometer. To measure the TDC, the bottom electrode was grounded and the top electrode remained connected to the electrometer. In this depolarization circuit, the sapphire insulator was grounded on both sides so that any depolarization from the sapphire would not be detected by electrometer. Furthermore, the insulation of the upper electrode was always at room temperature and could not therefore give rise to any thermal depolarization signal. This arrangement of the necessary insulations was considered desirable if spurious depolarization currents were to be excluded from the measuring circuit. The noise level of the present apparatus was usually found to be about 5×10^{-15} A.

In a typical TDC experiment, the apparatus was evacuated and then filled with 500 torr of dry He. The sample was polarized by an electric field of strength 2000 V/cm, at the chosen temperature T_p for a certain time. The apparatus was then cooled by immersing it in a liquid nitrogen bath. When the sample had been cooled to the required temperature, the electric field was removed and the sample was warmed at a constant rate of 4 K per minute. The constant heating rate was controlled by a Stanton Redcroft Model 681 linear temperature programmer. The TDC and thermocouple reading were simultaneously displayed on a 2-pen Hewlett Packard chart recorder. A higher heating rate generally produces a sharper peak in TDC but also a greater temperature gradient across the sample. Many investigators seemed to have ignored the latter

effect on their measurements.

2-5 Data Analysis

(i) Conductivity

The results of conductivity measurements were plotted as log σT vs. T^{-1} and each linear section was fitted by the method of least squares. The slope of each straight line gives the value of E in eq. (1.6), and the quoted error is the standard deviation in E.

(ii) D.C. Polarization Current

The analysis of d.c. polarization currents was partly done by a graphical method. The polarization current I_p was plotted logarithmically against time and, according to eq. (1.9), the curve obtained was further resolved into one or more components, each of which is a straight line whose slope equals τ_i^{-1}. The activation energies were then obtained from the slope of plots of log τ_i^{-1} vs. T^{-1} using a set of τ_i at several temperatures obtained as described above.

(iii) Thermal Depolarization Current

The computer fitting routine used for analysing the TDC is known as NLIN 2 program (26) which is based on a general model of the form

$$\hat{J}_i = f(X_{i1}, X_{i2} \ldots X_{im}; b_1, b_2 \ldots b_k) \qquad (2.1)$$

which contains m (max. no. = 10) independent variables X and k (max. no. = 50) parameters b. The program provides the predicted values $\hat{J}_i$ for each observation i, by adjusting each

of the parameters b such that

$$\underline{\phi} = \sum_{i=1}^{n} (J_i - \hat{J}_i)^2 \qquad (2.2)$$

is a minimum. For TDC, the only independent variable is temperature, J_i is the observed current and $\hat{J}_i$ the predicted one at i^{th} point. Each TDC peak is characterized by three parameters P_o, τ_o and E_r in eq. (1.10) and their initial guessed values are supplied in addition to the current, temperature and heating rate, as input data to the NLIN 2 program. The plot of log (initial current rise) against T^{-1} provides an estimate of E_r in eV [eq.(1.13)], area of the TDC peak gives the value of P_o in coulombs and finally τ_o is determined when T_m, E_r and b are given [eq.(1.12)]. The standard deviation in E_r for each TDC peak is about 0.03 eV.

CHAPTER 3

RESULTS ON CONDUCTIVITY

When a d.c. electric field was applied across an AP crystal, the current was found to decay gradually with increasing time to a constant value. The conductivity determined from this final constant current is generally known as the steady-state conductivity and will be denoted by σ_∞ in the text to follow. The time taken for the current to reach its steady-state value depended on the temperature, the nautre of incorporated impurities, annealing treatment etc. The measuring equipment, which consisted of an electrometer coupled to a strip-chart recorder, was found to have a total response time of about 3 seconds. Hence the initial conductivity σ_o quoted here in fact referred to the highest point of the recorded current in each measurement. Extrapolation of current vs. time curves to obtain the zero-time conductivity was not attempted for the obvious reason that the very fast decay which occurred in the first few seconds would not permit an accurate determination of the zero-time current. Most of the measurements were performed by applying an electric field perpendicular to either (001) or (210) cleaved faces of crystals. Handy notations like $\sigma_o(210)$, $\sigma_\infty(001)$ etc. will be used to represent the kinds of conductivity measured,

eg. $\sigma_o^{\perp}(210)$ means the initial conductivity obtained when $\varepsilon \perp (210)$.

3-1 AP Pellets

After the AP pellet had been thoroughly annealed at 383 K in a vacuum of 10^{-5} torr for about two days, reproducible conductivity results were obtained in several repeated runs provided the pellet was not heated to well above 498 K. The conductivity plot (Fig. 10) yields an activation energy of 1.08 eV between 391 and 423 K. Below 391 K the activation energy was roughly estimated to be 0.90 eV because of insufficient points in the lower temperature region. When the pellet was first heated to about 453 K the conductivity plot extended linearly with a constant activation energy of 1.08 eV. Subsequent repeated measurements after this run would generally result in a higher conductivity and a greater scatter of the data, as indicated by the crosses in Fig. 10.

3-2 AP Pellets in Ammonia

The effect of dry ammonia gas on the conductivity of an AP pellet is shown in Fig. 11. The conductivity increased with the pressure of ammonia as observed from the measurements made at four different pressures namely, 50, 100, 200 and 300 torr. The conductivity plots are a set of curves which show varying but increasing activation energies with temperature. The enhancement of conductivity by dry NH_3 was most pronounced in the low temperature region. In Table 1, the normalized conductivities of an AP pellet in NH_3 are compared with

those in N_2 at two chosen temperatures 370 and 410 K. Although the nonlinearity of these conductivity plots prevents one from calculating the exact values of activation energies one can certainly say the ammonia gas has significantly lowered the activation energies for conduction processes in AP. Rough values of the activation energy as low as 0.45 and 0.70 eV were observed, respectively, for low and high temperature measurements on AP in NH_3 .

The NH_3 was also found to adsorb physically onto the AP because the conductivity returned to its original value in N_2 after the system was evacuated for 24 hours. Points A and B were obtained on removal of NH_3 at the completion of the third and fifth runs.

3-3 Pure AP Single Crystals

The conductivity of AP single crystals was measured from room temperature to 423 K after they had been annealed at 378 K in vacuum for 16 hours. The annealing time required for obtaining a reproducible conductivity was shorter than for pellets. This is mainly due to the fact that more moisture and adsorbed gaseous impurities are present in the AP powder from which the pellets were made. The results of conductivity σ (001) measurements on an AP single crystal are shown in Fig.12. The conductivity σ_∞ plot consists of two linear regions from which the values of the activation energy were determined to be 0.87 ± 0.05 eV (from 393 to 423 K) and 0.56 ± 0.05 eV (below 393 K) respectively. After several runs, the low

temperature conductivity tended to increase slowly to produce an extra linear region of ~0.44 eV in activation energy.

In constrast with the steady-state conductivity, the initial conductivity σ_o varied little over most of the temperature range studied, the activation energy being only 0.06 eV. Above 400 K the initial conductivity increased more quickly but the short curve available in the high temperature region precluded the accurate determination of activation energy.

σ_∞ (210) obtained from another piece of pure AP was about 30% larger than the σ_∞ (001) just described but only a qualitative comparison can be made here because different crystals were employed.

3-4 Pure AP Single Crystal in Water Vapor

After the conductivity of an AP crystal had been measured, 19 torr of water vapor was evaporated into the conductivity cell. The crystal was allowed to equilibrate with the water vapor at 397 K overnight, and its conductivity was then found to have decreased by as much as 40 percent. Conductivity measurements were carried out at first with decreasing temperature and then with increasing temperature. During the cooling run the sample was kept at the two temperatures 363 and 330 K each for 12 hours. The conductivities were reproduced with 3 percent of their original values at each of these temperatures, indicating that equilibrium between AP and water vapor was always maintained. At the end of cooling run, the sample was left at 310 K and its conductivity was noticed to

increase gradually by 15% in 12 hours. This seemed due to the adsorption of water on AP. The heating run showed considerable hysteresis at the low temperature and in general the conductivity was higher than that measured during the cooling run. However the conductivity returned to the value measured in the cooling run when the sample was held at 340 K for about 17 hours. Above 360 K, the measured conductivities from the heating and cooling runs were nearly identical without showing any hysteresis. At the end of the heating run the conductivity cell was evacuated and the crystal was then annealed at 380 K for 40 hours. Conductivity measurements were then repeated in a nitrogen atmosphere.

Figure 13 shows the results of four runs carried out in investigating the effects of water vapor on the conductivity of an AP crystal. Runs 1 and 4 represent the results obtained before and after the water vapor experiment while runs 2 and 3 are the cooling and heating runs in water vapor. The drop in conductivity 16 hours after the admission of water vapor was likely caused by the dissolution of the crystal surface resulting in a smaller contact area between the crystal and electrodes. Therefore the effect of water vapor should be deduced from comparing the results observed in water vapor with that after its removal (run 4). Water vapor had a profound effect only on the low temperature conductivity. Below 340 K the conductivity was greatly enhanced and the activation energy reduced to almost zero. When the temperature was brought above 360 K, the conductivity though slightly higher in magnitude,

was essentially similar to that in nitrogen.

A water vapor experiment at higher pressures appeared very attractive if a more complete study was to be carried out. Unfortunately, the condensation of water on the sleeves of the conductivity cell, causing large electrical leakages, made the conductivity results unreliable. Attempts to measure the conductivity of AP at higher pressure of water were therefore abandoned.

3-5 Pure AP Single Crystals in Ammonia

The effect of ammonia on the conductivity of an AP crystal was studied at 3 different pressures and the results are represented in Fig. 14. The data from run 1 show results obtained for an AP crystal in nitrogen after it had received the usual annealing treatment. This run acts as a reference to which the later observation in ammonia may be compared. The ammonia experiment was begun with the lowest pressure used by admitting 65 torr of dry ammonia gas into the conductivity cell at about 353 K. The AP was allowed to equilibrate with ammonia for 24 hours and then the conductivity was measured with increasing temperature. After completing the run in about 10 hours, the conductivity cell was evacuated and the sample was annealed at 390 K followed by checking the conductivity at a few temperatures. Runs 3 and 4 were performed, respectively at 120 and 210 torr of ammonia in the same fashion as run 2. Although the conductivity of AP was evidently increased by the presence of ammonia, the activation energies

for conduction processes remained unchanged. The greater the pressure of ammonia the more the whole conductivity plot was shifted towards higher values of conductivity.

The removal of ammonia accompanied by prolonged annealing after each run never returned the conductivity of AP to its original value before the ammonia experiment. The dots in Fig. 14 represent the results obtained after run 2. The crosses are for those after run 4; one and six days of annealing yielded essentially identical results. This observation was very much different from that made using an AP pellet, in which desorption of ammonia was generally complete and original conductivities were regained in a period of 12 hours. The adsorption of ammonia on an AP crystal was apparently not a simple physical process and some ammonia tended to be permanently associated with the crystal.

The observation that the activation energy for conduction was unaffected by ammonia should not be taken too literally because the situation is complicated by the slow approach to equilibrium between the AP and ammonia, as revealed by some adsorption and desorption experiments. If similar ammonia experiments were to be carried out over longer periods of time, it is to be expected that a system closer to equilibrium would be achieved. Figure 15 shows that in run 2 the conductivity results obtained over a 12 hour interval and a temperature range of 30 K. The activation energy is 0.34 eV. Run 3 was performed over a period of 48 hours and this produced a still lower activation energy of 0.25 eV. Both these

values are much smaller than the ones obtained in measurements carried out over a shorter period of time.

3-6 Barium and Lead-doped AP Crystals

Generally speaking the conductivity σ_∞ plots of AP crystals doped with divalent cation impurities resembled that of a pure crystal, i.e. they consisted of two linear sections within the temperature range studied. However, the kink in the conductivity plot corresponding to a change in activation energy was shifted to a lower temperature.

The 1% AP:Ba^{2+} crystal showed an almost identical conductivity to that of a pure crystal except for a slightly higher conductivity in the high temperature region (Fig. 16). The values of the activation energy calculated from this curve were 0.80 ± 0.03 and 0.56 ± 0.02 eV for high and low temperature regions, respectively. No further work was done on 1% AP:Ba^{2+} because it seemed that Ba^{2+} was not incorporated into the AP lattice.

In contrast, the 5% AP:Pb^{2+} crystal showed a substantial decrease in conductivity compared to that of a pure crystal. Figure 17 shows the results of two runs made by applying the electric field perpendicularly to the (001) and (210) cleavage faces respectively of the same piece of crystal. σ_∞(210) is about 5 times larger than σ_∞(001) and contains an extra feature in the low temperature region where a fairly flat conductivity curve was observed with a low activation energy of 0.20 eV. At higher temperatures the value of the activation

energy were 0.88 ± 0.03 and 0.56 ± 0.05 eV for both cases. The extremely small conductivity in the [001] direction of Pb^{2+}-doped AP did not permit any reliable measurement below 373 K, resulting in rather short line for $\sigma_\infty(001)$. The initial conductivity σ_0 of Pb^{2+}-doped AP did not show any temperature dependence.

3-7 Sulfate-doped AP Crystals

The conductivity of 0.1% AP:SO_4^{2-} is shown in Fig. 18. On first heating the crystal, the $\sigma_\infty(001)$ plot gave an activation energy of about 0.74 eV. After 16 hours of annealing at 378 K, the conductivity was found to be very reproducible over several runs involving thermal cycling between room temperature and 410 K, and an activation energy of 0.66 ± 0.02 eV was obtained.

The conductivity obtained by applying the electric field perpendicularly to the (210) faces was found to be 7 times that of $\sigma_\infty(001)$; the activation energy was found to be 0.70 ± 0.02 eV. The temperature dependence of $\sigma_0(210)$ was more significant than that of both pure AP and AP:Pb^{2+}. Not shown in the figure is the $\sigma_\infty(010)$ which was only 15% higher than $\sigma_\infty(210)$.

3-8 Chromate-doped AP Crystals

The chromate ions were found to incorporate very well into the AP lattice. Both 0.1% and 1% chromate-doped AP were lightly tinted with a yellow coloration. The conductivity

of 0.1% AP:CrO_4^{2-} was about five times that of 0.1% AP:SO_4^{2-}.

The results of conductivity measurements on 0.1% AP:CrO_4^{2-} are shown in Fig. 19. In the first heating run for the sample with an electric field normal to (001) faces, the conductivity plot initially remained linear up to 345 K, then it increased rather rapidly up to 357 K and finally transformed into another straight line parallel to the low temperature one. The crystal was annealed at 380 K for 16 hours and its conductivity fell slightly (~10%). The conductivity of the annealed crystal was measured from 392 K to room temperature and a straight line with a slope of 0.72 ± 0.02 eV was obtained in the conductivity plot.

$\sigma_\infty(210)$ and $\sigma_\infty(100)$ were respectively found to be 10 and 7 times $\sigma_\infty(001)$ but only a qualitative comparison can be made here because different crystals were employed. The $\sigma_0(001)$ and $\sigma_0(210)$ displayed the simialr feature as observed for the AP:SO_4^{2-} crystals.

At room temperature the conductivity of 1% AP:CrO_4^{2-} was almost identical to that of 0.1% AP:CrO_4^{2-}. Figure 20 shows the results of conductivity measurement of 1% AP:CrO_4^{2-} when $\varepsilon \perp (001)$. On first heating the crystal, there was an abrupt increase in its conductivity at 320 K. The conductivity plot then increased linearly with an activation energy of 0.85 eV. The sample was annealed at 380 K and its conductivity reduced by 30%. The annealed crystal produced two linear regions in the conductivity plot: the high temperature region (393 to 338 K) has an activation energy of 0.85 ± 0.05 eV

and the low temperature region (338 to 300 K) being 0.74 ± 0.05 eV.

The conductivities of the same piece of 1% AP:CrO_4^{2-} are shown in Fig. 21. Again $\sigma_\infty(210)$ was found to be about 6 times $\sigma_\infty(001)$ but with the same activation energies of 0.85 & 0.74 eV.

The increase in the initial conductivity σ_0 occurred at a much lower temperature as compared with that of pure AP.

CHAPTER 4

RESULTS ON THERMAL DEPOLARIZATION CURRENT (TDC)

There have been no previous investigations of the thermal depolarization of AP and consequently a considerable amount of time and effort was devoted to studying this phenomenon as completely as possible. The thermal depolarization apparatus was tested with a crystal of Sr^{2+}-doped KCl for which a single TDC peak at 223 K was found in good agreement with other observers(23).

For pure AP the TDC obtained was very small ($\sim 2\times10^{-14}$A) and therefore barely visible on the recorder chart. Two peaks appeared at about 240 and 290 K. Although the high temperature peak was somewhat larger than the low temperature peak, for both peaks, the signal-to-noise ratio was too small to permit any accurate analysis. However, divalent anion doped crystals gave strong TDC, just as these same crystals displayed a larger d.c. conductivity than pure AP. Also it was found that the observations of TDC were most successful for crystals which had been previously polarized by an electric field perpendicular to their (210) faces.

4-1 Sulfate-doped AP crystals

Figure 22 shows the results of three TDC experiments

performed on a 0.1% AP:SO_4^{2-} crystal by applying an electric field perpendicularly to its (210) faces. A fairly constant current of about 0.18×10^{-13} A, not shown in this figure, was detected even when no polarization field was applied to the sample, indicating that some spontaneous polarization processes analogous to ferroelectric or pyroelectric effects were triggered during the heating cycle. Further investigation revealed that a current of the same magnitude flowed in the opposite direction during the cooling cycle. Also the direction of this constant background current was reversed if the crystal was inverted. Spectrum 1 was obtained after the sample had been polarized at 300 K. The high temperature peak (283 K) was almost twice as high as the low temperature peak (241 K). By lowering the polarization temperature to 240 K, spectrum 2 was obtained. It consisted of two peaks of equal heights occurring at the same temperatures as the peaks in spectrum 1. The high temperature peak was about one third of its previous size whereas the low temperature peak still retained about 60% of its original size. Spectrum 3 was produced after applying the peak cleaning technique to remove the low temperature peak. The sample was originally polarized at 240 K and then allowed to depolarize up to 260 K from which temperature it was re-cooled without further application of the polarizing field. Only a single TDC peak appeared at 285 K.

For all three spectra, especially the first one, the high temperature tail did not return to zero as quickly as

a dipolar TDC should. The lowering of the polarization temperature to 240 K has significantly reduced it. The reason for this broad TDC peak extending above 300 K was not clear; its presence was unfortunate because it would complicate the analysis of TDC spectra. Similar observations have been made in several investigations of other ionic crystals and these have been attributed to the presence of microprecipitates (27), the formation of space charge (28), the dissociation of complexes (29), etc. Without further investigation it can only be surmised that one or more of these effects were operating in the 0.1% AP:SO_4^{2-} crystals.

Table 2 lists the results of analysis of TDC by computer fitting. The high temperature peak occurred at ~284 K with E_r = 0.54 - 0.65 eV and the low temperature peak at 241 K with E_r = 0.26 - 0.29 eV. Both peaks were found to have unusually large τ_0 values.

A typical plot of log J vs. T^{-1}, where J is the observed thermal depolarization current is shown in Fig. 23. The solid curve represents the experimental observations and the circles are the fitted points. The high temperature ends could not be fitted accurately for the reasons mentioned previously.

Additional experiments were performed by applying an electric field normal to (001) and (010) faces. The former gave only weak peaks but the latter showed TDC peaks similar to those obtained when the field was normal to (210) faces. However, the spontaneous background current was absent in both cases if no electric field was applied.

4-2 Chromate-doped AP Crystal

The 0.1% AP:CrO_4^{2-} behaved similarly to 0.1% AP:SO_4^{2-} in that it produced a substantial spontaneous current of about 0.15×10^{-13} A normal to the (210) faces while being warmed up from low temperatures. The TDC of a 0.1% AP:CrO_4^{2-} are shown in Fig. 24 and 25. The polarizing field was applied perpendicularly to (210) faces successively at three temperatures 200, 220 and 300 K. The resulting TDC spectra displayed two peaks at about 236 and 292 K. The intensity of TDC peaks increased with increasing polarization temperature, the high temperature peak being found to increase at a much faster rate than the low temperature one. Only at the lowest polarization temperature did the TDC decay quickly to zero like that for a normal dipole relaxation.

The results of computer fitting of the TDC spectra are shown in Table 3. The values of the parameters E_r and τ_o obtained from the spectra for crystals polarized at low temperatures were fairly consistent but polarization at high temperatures led to a higher E_r and a shorter τ_o. The fitting of spectrum 3 was considered very good (standard deviation in current fitted = 0.6×10^{-14} A) but for spectra 1 and 2 the finite currents at high temperatures rendered a good fit to the data impossible.

For 1% AP:CrO_4^{2-} the TDC was found to be rather complicated. In a series of measurements the conditions of polarization were set at 215 K and $\varepsilon \perp (210)$. A spontaneous background current of 0.15×10^{-13} A was detected for the

unpolarized sample. The sample gave weak TDC peaks before any annealing treatment. In Fig. 26, the spectrum 1 was obtained after 12 hours annealing at 346 K. An additional five hours annealing at 373 K resulted in spectrum 2 with more intense peaks at 232 and 292 K. Further annealing at 373 K for an extra 16 hours yielded spectrum 3 in which the peaks were shifted towards higher temperatures, appearing at 252 and 300 K. A very intense but inverted TDC peak, not shown in the diagram, occurred above 340 K in spectrum 1 and was also obtained with the unannealed sample. This peak seems to be related to the dissolution of precipitates which was also observed during the conductivity measurements. An interesting observation noted was that the spontaneous background current decreased after each successive annealing, diminishing from its original value of 0.15×10^{-13} A to almost zero in the final run.

Table 4 lists the results of analysis of the three spectra. The high temperature peak of spectrum 1 showed a rather small E_r, apparently due to some cancellation of TDC signal by the large and overlapping negative peak occurring above 340 K. The E_r value of the low temperature peak was not affected by this phenomenon. The results of spectrum 1 were obtained by the graphical method and are listed merely for comparison purposes. Figures 27 and 28 give the computer fit to the spectra 2 and 3 and show that a good fit to the experimental observations was achieved in both cases. For spectrum 2, the values of τ_o, E_r and T_m were comparable to those obtained for

0.1% AP:CrO_4^{2-} whereas spectrum 3 gave a higher peak temperature and a larger E_r for the low temperature peak.

4-3 Lead-doped AP Crystals

When an unpolarized AP:Pb^{2+} crystal was warmed up gradually from 120 K, a constant current of about 0.15×10^{-13} A was detected flowing perpendicularly to both the (001) and (210) faces. Figure 29 shows the TDC for an AP:Pb^{2+} obtained after polarization with the field normal to the (210) faces. It consists of a normal low temperature peak and an unusually broad high temperature peak. Increasing the polarization temperature enhanced the high temperature peak as well as shifting it to higher temperatures. However, the position of the low temperature peak was independent of polarization temperature. No computer fitting was attempted because of the uncertain characteristics of high temperature peak. The activation energy for the low temperature peak was determined graphically to be 0.20 eV and τ_o was estimated to be 0.80×10^{-2} seconds.

4-4 Ammonia-treated AP Crystals

As ammonia had already been found to enhance the conductivity of an AP crystal, it seemed worthwhile to investigate its possible effect on the TDC. As ammonia is known to condense below 195 K, it seemed inappropriate to attempt to measure the TDC of AP in an ammonia atmosphere. To get around this difficulty a modified approach was adopted in which the

sample was first exposed to 760 torr of ammonia in a closed vessel for 12 hours and then transferred to the TDC cell. The TDC spectra of an ammonia-treated AP crystal are shown in Fig. 30. Polarizations ($\varepsilon \perp (\bar{2}10)$) at two different temperatures 260 and 300 K produced similar TDC spectra whose peaks emerged at 253 and 285 K. The results of the double peak fit to the experimental spectra are listed in Table 5. The low temperature peak is characterized by $E_{r_2} = 0.36$ eV and $\tau_{o2} = 0.18 \times 10^{-4}$ s whereas the high temperature peak has $E_{r_1} = 0.50$ eV and $\tau_{o1} = 0.30 \times 10^{-6}$ s. Again the fit was found to be better for the lower polarization temperature.

CHAPTER 5

RESULTS ON D.C. POLARIZATION CURRENT

It has already been mentioned that the current flowing through an AP crystal under a constant applied d.c. voltage decreases with increasing time. For a particular sample under investigation, the time required for the current to decay from its initial value to a final steady value depended strongly on the temperature. The time could vary from a few seconds at high temperatures to several hours at low temperatures. In this work only the polarization currents recorded within the temperature range between 300 and 360 K were analysed. This was mainly due to: (i) the measuring equipment used was not suitable for following very fast polarizations with time constants of less than few seconds, and (ii) it seemed unpractical to study the very slow current decays taking of the order of several hours.

As the polarization currents were being recorded during the conductivity measurements, which were usually preceded by annealing treatment, the results obtained thus refer to annealed samples. The annealing treatment was found to enhance the polarization current.

The polarization currents in pure and doped AP were studied with the electric field ε perpendicular to either (001)

or (210) faces. Larger polarization currents were found for the latter orientation. The results will be described in two separate sections on the basis of the direction of the applied field. For clarity, not all of the polarization currents will be shown in the current vs. time plots.

5-1 Polarization Currents When $\perp$ (001)

The polarization currents in a pure AP crystal from 304 to 340 K were found to be almost superimposible on one another, as shown in Fig. 31. This implied that the temperature dependence of the polarization current was very small. The polarization currents were readily analysed as the sum of two exponential terms, each characterized by a separate time constant. Although the fast polarization process was about 10 times quicker than the slow one, neither showed a significant temperature dependence. Plots of log τ^{-1} vs. T^{-1} are shown in Fig. 32, from which the activation energies for both processes were estimated to be less than 0.1 eV.

Figures 33 and 34 indicate that the presence of SO_4^{2-} or CrO_4^{2-} in AP increased the polarization currents. Also the fast component of the polarization current became relatively less important than the slow one. Consequently, only the analysis of the slow process was feasible. The final results are displayed in the form of plots of log τ^{-1} vs. T^{-1}, shown in Fig. 35. 0.1% AP:SO_4^{2-} is characterized by E_r = 0.56 eV whereas for 0.1% AP:CrO_4^{2-} E_r = 0.66 eV. The time constants at corresponding temperatures are shorter for the latter crystals.

5-2 Polarization Currents when $E \perp (210)$

When the electric field was applied perpendicularly to (210) faces of pure and doped AP crystals, the polarization currents were found to be distinctly different from the previous case studied, both with respect to their magnitudes and their rate of decay. Larger currents and faster decays were generally observed.

The polarization currents in pure AP crystals were found to obey a single exponential decay (Fig. 36) and the activation energy associated with this polarization process was determined to be 0.45 eV from the $\log \tau^{-1}$ vs. T^{-1} plot in Fig. 39.

0.1% AP:CrO_4^{2-} showed a very fast current decay (Fig. 37) during polarization with a time constant about 2 orders of magnitude smaller than that for pure AP at the same temperature. The polarization currents were dominated by a single exponential decay whose activation energy was found to be 0.40 eV (Fig. 39).

Polarization currents in 0.1% AP:SO_4^{2-} show an extra slow process (Fig. 38). After decomposing each polarization currents into its two components, the fast polarization process was found to be characterized by E_τ = 0.36 eV and the $\log \tau^{-1}$ vs. T^{-1} plot was noticed to run closely parallel to that for 0.1% AP:CrO_4^{2-} (Fig. 39). The slow process was found to correspond an activation energy of 0.50 eV with its time constant about one tenth of the fast one.

CHAPTER 6

DISCUSSION

6-1 General

At first sight the prospect of devising a consistent explanation for the results obtained from the 3 principal investigations made on pure and doped AP appears to be so formidable that a straightforward explanation seems quite improbable. This position is strengthened by a closer look into the structure, properties and sample preparation of AP, all of which differ greatly from those of the alkali and alkaline earth halides upon which the modern theory of defects in ionic crystals has been established.

Instead of simple ions occupying each lattice site AP consists of tetrahedral polyatomic groups at both cation and anion sites. The translational motions of large polyatomic groups are sterically unfavorable as compared to the simple atomic jumps of almost spherical ions in an alkali or alkaline earth halides. Nevertheless the vibrations and rotations of these polyatomic ions can be very important in facilitating the transfer of charge carriers, as already suggested for the conduction processes in ice (30), KH_2PO_4 (31,32), alcohols (33), and imidazole (34).

The alkali and alkaline earth halides are cubic and isotropic but the orthorhombic crystal structure of AP may lead to some anistropy in its physical properties.

Conductivity measurements on AP were made at temperatures above the highest temperature reached during crystal growth. This should lead to the dissolution of impurities, and the elimination of occluded water and adsorbed gases but in addition other effects might result from such thermal treatment of an unstable compound like AP, e.g. the introduction of additional structural disorder. The partial decomposition of AP produces water among other products and also the multiplication of dislocations. In contrast, in alkali and alkaline earth halides preliminary annealing and conductivity measurements are performed in the temperature range below temperatures at which the crystals were grown. Annealing may remove dislocations and point defects and hence reduce structural disorder. With these points borne in mind it is necessary to proceed cautiously in adopting the well-established theory for ionic crystals to the present systems.

The electrical conductivity of an ionic solid is determined by the concentration of free charge carriers and their mobilities, while transient phenomena like polarization and depolarization are related to the bound carriers in complexes, or to carriers trapped at special sites such as the crystal-electrode interface, grain boundaries, dislocations, etc. The concentration and effectiveness of the traps would affect

the magnitude of such transients. Sutter and Nowick (35) reported that the steady-state conductivity of NaCl varied independently of the transients after mechanical, thermal and irradiation treatments. This is a good indication that different causes exist for the two kinds of observations.

6-2 Conductivity of AP

The results of the conductivity measurements on pure and doped AP revealed some important findings which will be presented, along with references to others' work, in the following summary:

1. The study on AP pellets showed that the decomposition of AP in the temperature range between 430 and 450 K was already significant enough to affect the conductivity. Pellets showed a higher conductivity and activation energy than AP single crystals, primarily due to differences in surface effects. Since pellets were made by compressing powder, they are expected to possess a large internal surface and more imperfections. Surface effects causing higher conductivity and a higher activation energy also occur for ice (36).

2. Pure and Ba^{2+}-doped AP showed the same σ_∞ and the same activation energies. AP:Pb^{2+} exhibited a lower conductivity though the type of conductivity plot was retained. The activation energies for pure and divalent cation doped AP were determined to be 0.87 and 0.56 eV respectively for the high and low temperature regions. Crystals of AP doped with

divalent anions were characterized by only one activation energy ranging from 0.66 to 0.72 eV over the entire temperature range studied. The heavily doped 1% AP:$CrO_4^=$ was an exception, showing an extra activation energy of 0.85 eV in the high temperature region.

3. NH_3 increased the conductivity of the pellets but lowered the activation energy for the conduction processes. Pellets have a large internal surface which adsorbs NH_3 and the effects of NH_3 seem to stem mainly from its modification of the surface properties of pellets.

4. The effect of NH_3 on the conductivity of crystals was complicated by the slow attainment of equilibrium between the sample and NH_3. Although the conductivity was always increased by NH_3, the activation energy became dependent on the length of time over which a complete run of measurement was carred out. The activation energies of 0.87 and 0.56 eV in the high and low temperature regions were maintained if the run was completed within 12 hours. Prolonging the measurement time tended to reduce the activation energy. The desorption of NH_3 from the crystals was never complete indicating that NH_3 might become part of the crystal, hence changing its bulk properties. A more disturbing fact is that a complex $NH_4ClO_4:2NH_3$ might have been formed. This complex shows an activation energy for a.c. conductivity of 0.25 eV (97).

5. Above 350 K, water increased the conductivity of AP slightly and did not affect the activation energies. Below that it increased the conductivity tremendously and reduced the activation energy to almost zero. For pure AP studied in a N_2 atmosphere, the small increase in the low temperature conductivity could be due to the water produced from the decomposition of AP.

6. For all the crystals studied the smallest σ_∞ was obtained when the electric field ε was perpendicular to the (001) faces. The conductivities measured where the electrodes were placed on (210), (100) and (010) faces were about of the same magnitude, and all about 5 to 7 times higher than the results with $\varepsilon \perp (001)$. This anisotropy in conductivity has not been observed previously by any other investigators; possibly it was concealed by the poor reproducibility in their measurements (9). The arbitrary and as we have seen unjustified assumption of isotropic conductivity has also been made (12).

7. The crystals displayed distinctively different plots of log σT vs T^{-1} for σ_o and σ_∞. The σ_o plots were fairly flat at low temperature and showed the first sign of large increase with temperature at a much lower temperature for the highly conducting samples such as AP:CrO_4^{2-} and AP:SO_4^{2-} than for pure and AP:Pb^{2+}. The initial charge transport process appeared to be related to σ_∞ in some way. The σ_o curves were very similar to the a.c. conductivity obtained by Ng et al.

(8,38) in the appearance of a flat region at low temperature.

The time required for conductivity to diminish from σ_0 to σ_∞ increased when the temperature was lowered. Measurements with incomplete polarizations would therefore lead to arbitrary values lying between σ_0 and σ_∞. The results obtained by Keenan and Ohanian (12) using one minute as their polarization times would therefore have yielded higher values of conductivity than σ_∞ and consequently lower value of activation energy at the low temperature, because of increasing errors in their values of σ_∞ with decreasing temperature. Differences in the activation energies obtained by different authors are probably due to their ignoring polarization effects.

The σ_0 curves have a very low activation energy of about 0.1 eV. Only the transfer of protons can account for such a low value. The similarity of σ_0 for pure and doped crystals suggests that the proton jump initiates the conduction processes.

6-3 Proposed Conduction Mechanism

The presence of defects is essential for the migration of ions in crystals, well-known examples being cation and anion vacancies in alkali halides, interstitial Ag^+ and cation vacancies in silver halides, and interstitial F^- and anion vacancies in alkaline earth fluorides. Over the past two decades evidence has accumulated that proton conduction is operating in a large number of solids, inorganic, organic,

polymeric and biomolecular. Two recent reviews (39,40) have discussed the subject in rather great detail. Proton conductors can be divided roughly into two main classes: (i) those in which no chain of hydrogen exists and in which proton conduction must therefore be by interstitial motion; and (ii) chain hydrogen-bonded substances, in which cooperative proton transfer processes may occur. An illustration shown in the following equation would serve to clarify this cooperative process:

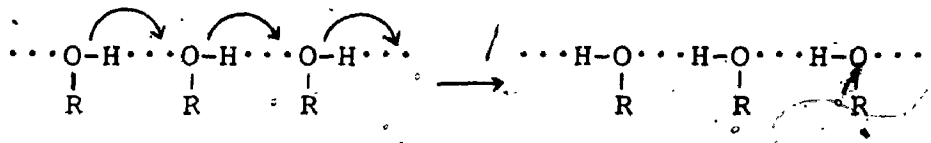

where ROH = ice, alcohols etc.

Along the hydrogen-bonded chain, a cooperative proton transfer occurs as indicated by the arrows and the net effect of this process is to transfer a H atom from one end of the chain to the other. The new hydrogen-bonded chain created is in a reverse orientation from that in which it originally was, and is unable to permit any further proton transfer. A cooperative reorientation process is needed to bring the new chain into its original configuration,

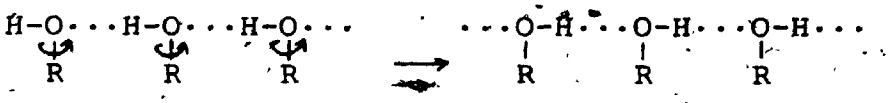

In alcohols the rotation of C-O bonds is sufficient to achieve this while the main hydrocarbon chains remains fixed.

However, there are systems in which the hydrogen bonds are

broken by intramolecular links, eg. in KH_2PO_4.

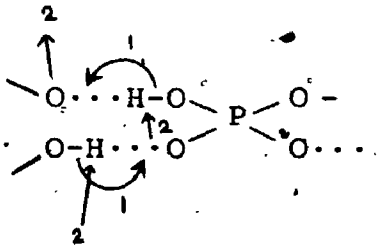

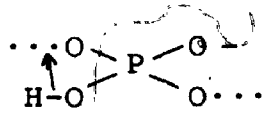

direct transfer process

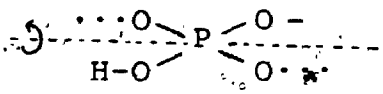

rotation of phosphate

The initial proton transfer (process 1) may be followed by an intramolecular transfer (process 2) of the proton. Process 2 can be accomplished either by a direct transfer of the proton or by a rotation of the intervening phosphate group. The original orientation of the chain is then restored and a repetition of the two processes together would result in proton conduction.

The resemblance of AP to some well-known proton conductors NH_4Cl, $(NH_4)_2SO_4$ and $NH_4H_2PO_4$ in several aspects prompts one to consider that a similar type of proton conduction might occur in AP. Electrolysis of AP (41) between 293-373 K has been shown to yield only hydrogen at the cathode, the amount produced obeying Faraday's law. Time-of-flight measurements (42,43) have demonstrated that AP vaporizes as NH_3 and $HClO_4$ in the same way as the ammonium halides do. The key step would involve the transfer of a proton from NH_4^+ to ClO_4^- to form neutral molecules of NH_3 and $HClO_4$ which then desorb from the crystal surface. The decompositions of $NH_4H_2PO_4$ to

yield NH_3 and H_3PO_4, $(NH_4)_2SO_4$ to NH_3 and NH_4HSO_4, and NH_4Cl to NH_3 and HCl all suggest that proton holes, i.e: ammonia molecules at normal lattice sites are created after the anions accept the protons.

The electrical conductivity of $NH_4H_2PO_4$ has been attributed to the presence of L defects, i.e. hydrogen vacancies caused by impurities, and NH_3 defects or proton holes, thermally generated in the NH_4^+ sublattice by proton transfer from NH_4^+ to $H_2PO_4^{2-}$.

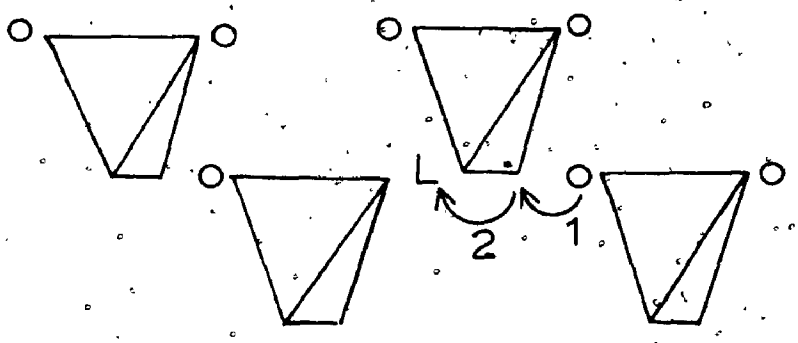

where

 = PO_4^{2-} 1 = interbond jump

O = H 2 = intrabond jump

The motion of L defects in the hydrogen-bonded network of the phosphate lattice involves both interbond and intrabond jumps of a proton; these are collectively regarded as having an activation energy of 0.46 eV. The creation of NH_3 defects requires 0.16 eV but their migration was unfortunately not discussed by Harris and Vella (44). The rotation of the phosphate group is greatly reduced because $NH_4H_2PO_4$ possesses two hydrogen-bond systems, one among the phosphate groups and the

other between the NH_4^+ ions and phosphate ions.

The Herrington-Staveley mechanism (45) for conduction in NH_4Cl consists of three steps: (i) proton transfer from NH_4^+ to Cl^- adjacent to a vacancy; (ii) the jump of either the NH_3 molecule into a cation vacancy or the HCl molecule into an anion vacancy, depending on which type is present; (iii) a reversal of the proton switch to reform NH_4^+ and Cl^-. The final configuration differs from the initial one in that the cation or anion vacancy has moved one lattice site in its own sublattice. The concept of proton holes, generally considered as missing protons in the lattice or in hydrogen bonds, has also been introduced in order to explain the conduction process in ice, in alcohols and in many salts containing no ammonium groups.

The fact that the conductivity of AP is increased by divalent anions and decreased by divalent cations tends to suggest that anion vacancies are the conducting species if we use the conventional model for ionic conductivity of alkali halides. As water vapor, ammonia and HSO_4^- would not introduce any vacancies into AP, their enhancement of conductivity does not support the idea of ionic conduction by anion vacancies. Also, since the ClO_4^- (ionic radius = 2.36 Å) is more bulky than the NH_4^+ (ionic radius = 1.43 Å) and does not undergo free rotation below 513 K, it is inconceivable that ClO_4^- can migrate readily via a vacancy jump mechanism.

In the absence of any impurities, the formation of intrinsic molecular defects NH_3 and $HClO_4$ in AP would be the first

step in the charge transport process,

$$NH_4^+ + ClO_4^- \longrightarrow NH_3 + HClO_4 \qquad (6.1)$$

A proton transfers away from the $HClO_4$ to a neighbouring ClO_4^-, or from a neighbouring NH_4^+ to the NH_3 (proton hole) is then necessary to prevent the reversal of reaction (6.1), if the charge transport process is to proceed any further. The possible fates of the NH_3 and $HClO_4$ formed may be represented by the following equations,

$$NH_3 + NH_4^+ \longrightarrow NH_4^+ + NH_3 \qquad (6.2)$$

$$HClO_4 + ClO_4^- \longrightarrow ClO_4^- + HClO_4 \qquad (6.3)$$

Thus proton transfer could occur within either the NH_4^+ or the ClO_4^- sublattices. Occasionally an inter-lattice jump would happen when NH_3 and $HClO_4$ are in favorable orientations at nearest neighbour sites, resulting in an annihilation of the molecular defects. The proton holes NH_3 migrate in an opposite direction to the proton jumps in the ClO_4^- lattice but the same net effect, i.e. transport of positive charges toward the cathode, is observed. By analogy with electrical conduction in semiconductors, the conductivity of AP can be written as a sum of two terms

$$\sigma = \sigma_{\text{proton hole}} + \sigma_{\text{proton}} \qquad (6.4)$$

An examination of the crystal structure of AP (46) indicates that process (6.2) is an unfavorable one for proton migration. The N-H bond lengths range from 1.028 to 1.058 Å

and the N....N distance between two nearest NH_4^+ is 4.6 Å. Even when the most favorable orientation exists the proton has to traverse the rather long distance of 2.5 Å from one cation to the other. The situation would be somewhat improved if NH_3 molecule can wander closer to the neighbouring NH_4^+. From consideration of ionic radii (1.43 Å for NH_4^+, 2.36 Å for ClO_4^-) and packing structures, this possibility could not be ruled out. However, the NH_3 molecule would have to be oriented properly so that its lone pair electrons could accept a proton from the other NH_4^+. Moreover, a conduction mechanism based solely on process (6.2) can not explain the observed anisotropy in the conductivity of AP.

The next mechanism to be considered would then be process (6.3). For clarity, Fig. 40 shows only the ClO_4^- ions within a unit cell of AP. Each ClO_4^- (X) is surrounded by ten nearest ClO_4^- neighbours, two (A) located at 4.0 Å, two (B) located at 4.7 Å in the mirror plane of X, and six (C) at 5.6 Å. The Cl-O bond lengths are 1.44 ± 0.01 Å and the proton is held electrostatically to the ClO_4^- ion by an O-H bond which is roughly 1.0 Å in length. The proton jump from a $HClO_4$ to its ClO_4^- neighbours at 4.0 and 4.7 Å is more favorable because the proton has to migrate a distance of less than 1 Å when the $HClO_4$ and ClO_4^- are in favorable orientations. Figure 41 shows the projection on the (100) plane of two neighbouring planes of ClO_4^-. The proton jumps in the direction of the b axis from one ClO_4^- to another ClO_4^- situated at 4.0 Å away. Figure 42 shows the projection on

the (010) plane of two neighbouring planes of ClO_4^-. The easiest path for proton migration along the a axis involves the jump from one ClO_4^- to the other ClO_4^- at 4.7 Å. The proton jumps in the direction of the c axis would involve a very long jump between two ClO_4^- at 5.7 Å apart. These structural considerations suggest that a proton transfer mechanism in the anion sub-lattice would lead to a higher conductivity in the (001) plane than along the c axis normal to this plane. Process (6.2) is further supported by Boldyrev's observation (11) that the conductivity of AP was increased by HSO_4^-, a proton-donating impurity.

It should be mentioned that proton transfer in the ClO_4^- sub-lattice comprises several steps. Within a ClO_4^-, a proton can jump from one oxygen to the other with the help of bending & stretching of Cl-O bonds. A proton can also jump from one ClO_4^- to another ClO_4^- when the two ClO_4^- ions are brought into a favorable configuration by a rocking or reorientation motion. While the inter- ClO_4^- jump of a proton is considered to be very easy because of the short jump distance (less than 1 Å), the motion of the ClO_4^- groups may require some energy. The separation of the activation energy for proton migration into the intra- and inter- ClO_4^- parts is obviously impossible on the basis of conductivity theory, and would require detailed calculations not practicable at present.

Equation (6.4) for the conductivity of AP can be rewritten as

$$\sigma = \sigma_h + \sigma_p$$

$$= n_h \mu_h e_h + n_p \mu_p e_p \qquad (6.5)$$

where h = proton hole, μ = mobility,

p = proton, n = conc. of carrier,

and e = charge of carrier.

Based on the previous discussion, the mobility of a proton hole is expected to be smaller than that of a proton, i.e. $\mu_h < \mu_p$. Therefore in pure AP where the concentration of NH_3 and $HClO_4$ are equal, i.e. $n_h = n_p$, the major charge carriers are the protons hopping in the ClO_4^- sub-lattice because of the higher value of $n_p \mu_p e_p$ than $n_h \mu_h e_h$.

Water is known to be an unavoidable contaminant in AP and its effect of the conductivity, if any, would be exhibited in undoped, nominally pure AP. Ammonia and water vapor were found to increase the conductivity of pure AP without altering the activation energy. This statement is at least valid in the high temperature region or when the gases do not completely cover the surface of the AP. The two substances can function as proton acceptors:

$$NH_4^+ + NH_3(a) \longrightarrow NH_3 + NH_4^+(a) \qquad (6.6)$$

$$NH_4^+ + H_2O(a) \longrightarrow NH_3 + H_3^+O(a) \qquad (6.7)$$

where 'a' denotes an adsorbed site. The protonated adsorbed species would then give their protons up to the ClO_4^- ions, as

$$NH_4^+(a) + ClO_4^- \longrightarrow NH_3(a) + HClO_4 \qquad (6.8)$$

$$H_3^+O(a) + ClO_4^- \longrightarrow H_2O(a) + HClO_4 \qquad (6.9)$$

and the migration of protons can proceed as usual i.e. according to eq. (6.3). Thus water and ammonia in fact catalyse the proton transfer in eq. (6.1). Even if the protonated adsorbed species are reluctant to give up their protons, the concentration of proton holes formed in eq. (6.6) or (6.7) is increased and the product of $n_h\mu_h$ is considerably large so that conduction by proton hole can no longer be neglected.

When the coverage of adsorbed NH_3 or H_2O is high the protonated adsorbed species are more likely to transfer their protons to the unprotonated NH_3 or H_2O neighbours than to the ClO_4^-.

$$NH_4^+(a) + NH_3(a) \longrightarrow NH_3(a) + NH_4^+(a) \qquad (6.10)$$

$$H_3^+O(a) + H_2O(a) \longrightarrow H_2O(a) + H_3^+O(a) \qquad (6.11)$$

As the adsorption of NH_3 and H_2O occurs predominantly at the lattice imperfections like dislocations, grain boundaries, the proton transfer along these sub-structures can proceed readily with an extremely low activation energy. From the water vapor and ammonia experiments, the values of 0.05 - 0.30 eV are observed. The theoretical calculation by ab initio methods indicates that the proton jump from NH_4^+ to NH_3 in solution involves an energy barrier of 0.1 eV (47).

For the nominally pure AP in a nitrogen atmosphere, the activation energy of 0.56 eV in the low temperature region would be accounted by processes (6.9), (6.2) and (6.3). A proton transfer from the adsorbed H_3^+O to the ClO_4^- plus the jumps of proton in the ClO_4^- sub-lattice, together with proton hole conduction in the NH_4^+ sub-lattice. When the temperature is increased the formation of molecular defects by direct proton transfer from the NH_4^+ to the ClO_4^- becomes feasible. Instead of acting as a proton acceptor, the water could help stabilize the $HClO_4$ formed through the formation of a hydrate $H_3O^+ClO_4^-$. Similar argument can be drawn to account for the effect of NH_3 on the conductivity of AP. Both H_2O and NH_3 are known to retard the decomposition of AP through their complexing with the $HClO_4$ formed. Therefore the formation of molecular defects in (6.1), together with the migration of proton in (6.3) would correspond to an activation energy of 0.87 eV as observed in the high temperature conductivity of pure AP in N_2, NH_3 and H_2O vapor.

Though the anion vacancies introduced into AP by divalent anions do not migrate, they may play an important role in the conduction process. The absence of a ClO_4^- ion ensures that more room be available to the neighbouring ions, NH_4^+ as well as ClO_4^- or impurity anions. This is extremely important for the anions because they can rock more vigorously than in a perfect lattice. Thus in the vicinity of an anion vacancy the proton transfer from a NH_4^+ to a ClO_4^- is facilitated and

a lowering of activation energy should be observed. The process is represented as

$$NH_4^+ + ClO_4^- + \boxed{-} \longrightarrow NH_3 + HClO_4 + \boxed{-} \quad (6.12)$$

or diagrammatically

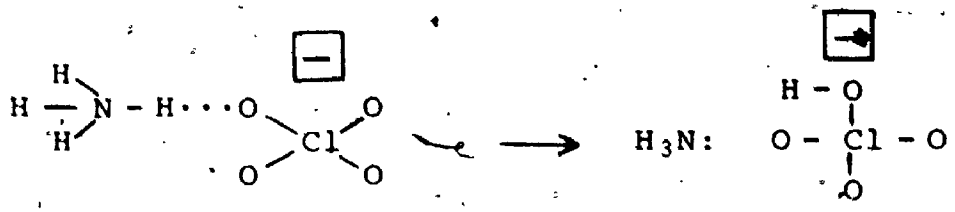

where $\boxed{-}$ denotes an anion vacancy. Similarly the proton can be transferred from a NH_4^+ to an impurity anion. The protonated anion can pass the proton on to other ClO_4^- so that the migration of protons in the ClO_4^- sub-lattice is initiated and proceeds in the usual manner. The proton hole NH_3 left behind has an effective negative charge and with the anion vacancy (an effective positive charge) forms a dipole. Thus the NH_3 is not free to migrate, as in eq. (6.2), and to contribute to conduction. The relaxation of this dipole however could display a transient behavior which will be discussed later. The activation energies of 0.66 and 0.72 eV observed for 0.1% AP:SO_4^{2-} and 0.1% AP:CrO_4^{2-} respectively, are accounted by the formation of protonated anion (ClO_4^- or impurity anion) in eq. (6.12) plus the migration of proton in the ClO_4^- sub-lattice. A slight difference in the environment of the anion vacancy for the two crystals or inherent experimental errors could account for the small difference in the observed activation energies. As 1% AP:CrO_4^{2-} crystals are

heavily doped and may contain precipitates of $(NH_4)_2CrO_4$ or large aggregates of defects, the extra activation energy of 0.85-0.74 = 0.11 eV is likely related to the dissolution of precipitates or aggregates.

The decrease in the conductivity of AP by Pb^{2+} can arise from: (i) Pb^{2+} introduce cation vacancies which destroy anion vacancies due to preservation of the Schottky equilibrium between vacancies of opposite charge. The formation of molecular defects by eq. (6.12) becomes practically non-existent, (ii) cation vacancies have an effective negative charge and may trap some protons and (iii) Pb^{2+} may form amine complexes with proton holes NH_3 and immobilize them. The close resemblance of the conductivity plots for pure AP and AP:Pb^{2+} implies that the same conduction mechanisms operate in both systems. The latter suffers a decrease in conductivity mainly due to reasons (i) and (ii).

Initial conductivity σ_0 occurs on a much smaller time scale than σ_∞. The displacement of charge carriers is relatively short in σ_0 and may involve a few steps only. The decrease of σ_0 to σ_∞ is generally attributed to the presence of traps which capture and immobilize the charge carriers. The same effect would arise if a conducting path is broken. The nature of the traps can not be discussed specifically due to lack of experimental evidence relating to this point. Dislocations and grain boundaries are generally said to break the continuous lattice in the crystals. Point defects are also likely to do so, e.g. an anion vacancy locating in the

path of a proton transfer in the ClO_4^- sub-lattice. Similarly, an impurity which can trap a carrier would reduce the probability of its being transferred toward the electrode. The σ_o curves for pure and anion doped AP have some common features; they are fairly flat at the low temperature and rise gradually when approaching high temperature. For anion doped AP the first sign of an increase in σ_o appears at a much lower temperature than for pure AP. The σ_o curves can be qualitatively decomposed into two parts: (i) the displacement of H along N-H...O bond and (ii) the charge displacement arising from the relaxation of $HClO_4$. The displacement of a proton along the N-H...O bond would require little energy and hence would account for the weak temperature dependence of the σ_o curves. When the temperature is increased the motion of the proton acceptor becomes more vigorous. Its rotation or even rocking would help break the N-H bond and transfer the proton further, giving rise to an increase in σ_o. Although ClO_4^- ions only rotate freely above the transition temperature 513 K, they may rock considerably at lower temperatures. The increase in σ_o for pure AP may be thus related to the increased partial rotation of ClO_4^- ions. The presence of SO_4^{2-} and CrO_4^{2-} in AP increases the concentration of $HClO_4$, the increase in the σ_o becomes detectable at a lower temperature than in pure AP. In AP:Pb^{2+} the concentration of $HClO_4$ is greatly reduced and σ_o hardly shows any increase even at the highest temperature studied.

6-4 Thermal Depolarization Current

NH_4^+ and ClO_4^- are tetrahedrally symmetric and the ions themselves have no dipole moment. Their rotation cannot, therefore, contribute to the transient currents. The thermal depolarization currents of 0.1% AP:SO_4^{2-}, 0.1% AP:CrO_4^{2-} and NH_3- treated AP display two peaks whose positions are only slightly shifted by a large change in the polarization temperature. This implies that the relaxation processes giving rise to the TDC are dipolar in nature. When a low polarization temperature was used, the TDC spectra showed a less complicated structure at their high temperature ends. An examination of these spectra permits one to draw the following conclusions: (i) The high temperature peak appears in the temperature range of 283 - 291 K and the average activation energy is 0.50 ± 0.05 eV. The small differences of ±4 K obtained for the peak position are probably due to some errors in the temperature measurement. (ii) The position of the low temperature peak varies from 232 K for AP:CrO_4^{2-} to 252 K for NH_3-treated AP. The spread is about 20 K and not likely due to the experimental error. The activation energy for AP:SO_4^{2-} and AP:CrO_4^{2-} is about 0.25 ± 0.05 eV and for NH_3-treated AP, 0.35 ± 0.02 eV. Hence it appears that the high temperature peak is due to a common relaxation process operating in all samples, and the difference between the low temperature peaks of NH_3-treated AP and anion-doped AP arise from different relaxation processes.

The conductivity experiments suggest that the molecular

defects NH_3 and $HClO_4$ are responsible for protonic conduction in AP. Both species have a dipole moment and can be aligned by an external electric field. Their reorientation after removal of the field would give to a TDC. The activation energy for the rotation of HSO_4^- in $(NH_4)_2SO_4$ and in $NH_4H_2PO_4$ is about 0.51 ± 0.04 eV as determined from dielectric loss measurements (48). Spin-lattice relaxation measurements on the $H_2PO_4^-$ and $H_2SeO_3^-$ groups in their alkali metal salts indicate that they undergo ultraslow reorientational motions with an activation energy ranging 0.40 to 0.80 eV. In CsH_2PO_4 the activation energy is higher (31). The high temperature peak with E = 0.50 ± 0.05 eV in the TDC spectra therefore most probably corresponds to the relaxation of $HClO_4$. The low temperature peak would then be associated with the relaxation of NH_3 which may have different environments in anion-doped AP and NH_3-treated AP. The values of τ_0 obtained for both peaks in the TDC spectra are unusually large and the calculated time constant at the peak temperature is about 200-300 seconds. It is difficult to imagine an orientational motion of individual dipoles with such long relaxation time in an inorganic material. There are two models that are commonly used to explain the occurence of long dipole relaxation times. The first is the cooperative rotation of several dipoles connected to each other with a certain kind of bonding. The mechanism is known to occur in hydrogen bonded compounds and its operation in an alcohol ROH is illustrated in eq. (6.13)

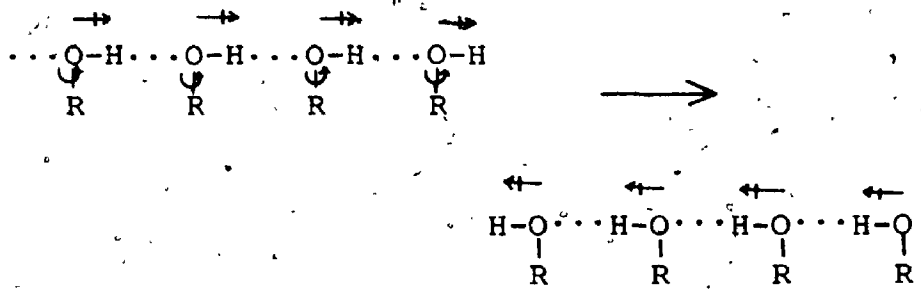

(6.13)

→ dipole moment

↺ rotation of C-O bond

The hydroxyl groups, each constituting a dipole, are hydrogen-bonded to form a giant dipole whose orientation can be reversed by a cooperative rotation of individual hydroxyl groups about the C-O bonds. The second mechanism is known as Maxwell-Wagner polarization. If the hydrogen bonded chains do not pass completely through the material due to the presence of structural disorder, they would appear in the system as conducting filaments surrounded by a non-conducting matrix. This forms a Maxwell-Wagner system which could give rise to a Debye type of dielectric absorption. Sack (49), has used this concept in proposing the 'block' model for the dielectric properties of an ionic crystal containing defects which can move over a certain distance in the crystal before being trapped. If the distance over which the defects can move is reasonably uniform all through the material, a single macroscopic relaxation time will be associated with each type of defect.

In the anion-doped AP crystals, the NH_3 formed in eq. (6.12) has an effective charge of -1 and would associate with the neighbouring anion vacancy to form a dipole. The dipole

can change its direction by proton transfer from one NH_4^+ to the NH_3 as,

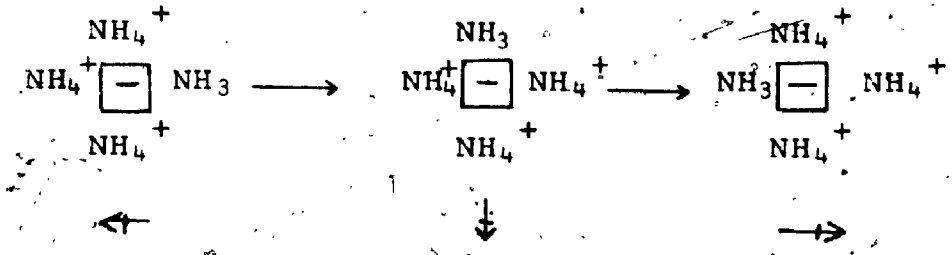

(6.14)

The anion vacancy provides more room for NH_4^+ and NH_3 to approach each other than if the anion site were occupied. The proton transfer between them actually involves a cooperative mechanism in which the lone-pair electrons of NH_3 has to be exactly positioned toward the H of NH_4^+. The migration of NH_3 and NH_4^+, together their attainment of the correct configuration might therefore account for the large τ_0. Thus the low temperature peak of TDC of AP:CrO_4^{2-} and AP:SO_4^{2-} is caused by the same relaxation as shown in eq. (6.14).

When an AP crystal is treated with NH_3, the NH_3 is expected to be adsorbed on the surface and to diffuse internally along favorable paths like dislocations and grain boundaries. The surroundings of such an NH_3 molecule are no longer the same as depicted in eq. (6.14) for AP doped with anions and hence a different relaxation may arise. Due to the structural complexity of large defects, it is difficult to discuss the relaxation process in detail.

Similarly the proton transfer from one ClO_4^- to the other is also cooperative type of process in which correct orientation of participating anions is critical. The large τ_0 for the

relaxation process is partly caused by the reluctance of ClO_4^- to rotate which obviously would reduce the chance of achieving a correct orientation.

The low temperature peak observed in AP:Pb^{2+} can be attributed to the relaxation of NH_3 around Pb^{2+} which would give rise to TDC but does not contribute to σ_∞. The position of high temperature is shifted by a change in the polarization temperature, indicating that a non-polar process is involved. Unfortunately, this type of process in TDC is poorly understood for any ionic crystals so far investigated.

The presence of large aggregates of defects or precipitates of $(NH_4)_2CrO_4$ in 1% AP:CrO_4^{2-} results in complicated TDC. Variations of peak positions, intensities and parameters with the length of annealing time were observed but the available data are not sufficient to permit a conclusive discussion.

6-5 D.C. Polarization Current

Most previous studies have been made on the alkali halides which are known to display several kinds of polarization effects. The underlying causes are not simple; for instance, some effects seem to predominate over others in different temperature regions. In the low temperature region from 200 K to room temperature, polarization currents in alkali halides have been interpreted in terms of the relaxation of divalent impurity-vacancy complexes (20). From room temperature up to about 620 K, the polarization seems to be closely connected with the presence of line defects and large

clusters of defects (22,35). Above this temperature the polarization displays the characteristics of space-charge polarization due to blocking electrode effects (21). For other materials in which these different effects may not be well separated the study of d.c. polarization currents would not be an easy task.

The dissimilarity between AP and the alkali halides has been emphasized previously and greater complexities are expected for the polarization behavior of AP. The results of the d.c. polarization currents also look more complicated than that of the steady state conductivity and thermal depolarization experiments. The following model does nevertheless appear to fit qualitatively the main body of the experimental data: the polarization currents are attributed to the trapping of charge carriers at some special sites and σ_∞ is ascribed to the net flow of free carriers through the sample. The increase in the polarization currents after thermal treatment can be associated with an increase in the number of trapping sites, while the increase in σ_∞ can arise from the generation of free carriers due to the dissolution of impurities, the dissociation of complexes, or thermal decomposition.

The thermal depolarization experiments have indicated that polarization at a high temperature would introduce some complicated features in the TDC which do not belong to a dipolar relaxation. The d.c. polarization currents were measured at a much higher temperature than the TDC and hence may contain some of these effects.

The observed anisotropy in the polarization currents is likely caused by the distribution of trapping sites. Investigations of dislocations in AP (50,51) have revealed that the arrangement of dislocation systems is anisotropic leading to preferential alignment of etch pits and decomposition nuclei in the [010] direction on the (001) plane. Without further experimentation, however, it is difficult to work out the details of the distribution of traps according to the arrangement of dislocations.

The polarization current observed for pure AP when ⊥(001) showed little temperature dependence. It seems to arise, therefore, from a situation in which the traps are completely filled. While the concentration of carriers increases with the temperature, the trap being already saturated at a low temperature would not capture more carriers to cause an increase in the polarization current. If this is true the values of and E obtained from Fig. 32 cannot be interpreted literally. The activation energies obtained for AP:$SO_4^{=}$ and AP:$CrO_4^{=}$ range from 0.56 to 0.66 eV are slightly higher than that for the relaxation of protonated anions, indicating that this relaxation process plays an important part in the d.c. polarization effect.

For the case (210), an interesting observation was noted. Based on the values of and E for the TDC peaks, their corresponding were calculated at several temperatures in the temperature region where the polarization currents were measured. For each of AP:$SO_4^{=}$ and AP:$CrO_4^{=}$ the of

the two relaxation processes are fairly close. It would thus be impossible to resolve two relaxation processes from the $I_p(t)$ curves and the $\log\tau^{-1}$ vs. T^{-1} plot thus corresponds to that of a single relaxation process.

The comparison of relaxation times from d.c. polarization and from extrapolation of TDC measurements are shown in Fig. 43. This indicates that the dipolar relaxation processes observed for TDC are the dominant processes occurring during d.c. polarization.

Pure AP, AP:ClO_4^- and AP:SO_4^{--} all show an activation energy of 0.36 to 0.45 eV but the time constant of pure AP is about a factor of ten larger than that for the other two. The shorter τ of the AP doped with anions may also mean the density of traps is higher and the relaxation mechanism takes fewer steps to reach equilibrium.

6-6 Conclusion

Complete understanding of electrical conduction processes in AP is handicapped by its complicated structure and chemical properties. Instead of restricting the investigation to conductivity measurements only, more experimental techniques should be employed. For the first time, thermal depolarization and d.c. polarization of AP have been studied in conjunction with d.c. conductivity in this work, all of which have revealed the anisotropic nature of AP. The investigations on thermal depolarization and d.c. conductivity, being far more fruitful than on d.c. polarization, support proton transfer

mechanisms in AP. Anion vacancies, though immobile, influence the formation of charge carriers as well as their later migration. A preliminary model of carriers being trapped at large defects has been tentatively proposed for d.c. polarization. It only provides a qualitative picture but appears to be a logical step toward the understanding of this phenomenon. As mechanical deformation would produce dislocations in crystals, future work on the d.c. polarization shall take this into consideration. The concentration of charge carriers is not discussed due to lack of knowledge on the mobility of protons in AP. An estimate of the proton mobility could be obtained from experiments on the diffusion of tritium in AP. Conductivity measurements on deuterated AP should help to confirm proton transfer.

TABLE 1

Conductivity of AP pellets in NH_3

(as ratios to values in N_2).

Atmosphere	σ at 370 K	σ at 410 K
N_2	1	1
50 torr NH_3	5.01	1.66
100 torr NH_3	14.5	2.45
200 torr NH_3	23.5	4.16
400 torr NH_3	66.1	7.08

TABLE 2

TDC of 0.1% AP:SO_4^{2-}

Spectrum No.	1	2	3
T_p/K	300	240	240
P_{m_1}/C	0.145×10^{-8}	0.497×10^{-9}	0.180×10^{-9}
τ_{m_1}/s	0.308×10^{-8}	0.366×10^{-7}	0.300×10^{-8}
E_{T_1}/eV	0.60	0.54	0.65
T_{m_1}/K	283	283	285
P_{m_2}/C	0.995×10^{-9}	0.650×10^{-9}	---
τ_{m_2}/s	0.224×10^{-3}	0.134×10^{-9}	---
E_{T_2}/eV	0.29	0.26	---
T_{m_2}/K	241	241	---

Symbols defined in eq. (1.10). Subscripts 1 and 2 refer to high- and low-temperature peaks, respectively.

TABLE 3

TDC of 0.1% AP:CrO_4^{2-}

Spectrum No.	1	2	3
T_p/K	300	220	200
P_{o1}/C	0.108×10^{-7}	0.547×10^{-9}	0.118×10^{-9}
t_{o1}/s	0.572×10^{-7}	0.534×10^{-5}	0.131×10^{-5}
E_{r1}/eV	0.56	0.45	0.47
T_{m1}/K	294	295	288
P_{o2}/C	0.624×10^{-9}	0.111×10^{-9}	$.709\times10^{-10}$
t_{o2}/s	0.321×10^{-3}	0.545×10^{-2}	0.107×10^{-2}
E_{r2}/eV	0.28	0.22	0.25
T_{m2}/K	238	237	233

Symbols: see Table 2.

TABLE 4

TDC of 1% AP:$CrO_4^{=}$, T_p = 21.5 K

Spectrum No.	1	2	3
	Annealed at 346 K + 12 hrs	Annealed at 373 K + 5 hrs	Annealed at 373 K + 16 hrs
P_{o1}/C	---	0.233×10^{-9}	0.181×10^{-9}
τ_{o1}/s	---	0.282×10^{-6}	0.789×10^{-6}
E_{r_1}/eV	0.24	0.51	0.51
T_{m_1}/K	300	292	302
P_{o2}/C	---	0.619×10^{-10}	0.493×10^{-10}
τ_{o2}/s		0.531×10^{-3}	0.523×10^{-4}
E_{r2}/eV	0.24	0.26	-0.33
T_{m2}/K	235	232	252

Symbols: see Table 2.

TABLE 5

TDC of NH_3-treated AP

T_p/K	300	260
P_{o1}/C	0.798×10^{-10}	0.535×10^{-10}
τ_{o1}/s	0.292×10^{-6}	0.254×10^{-6}
E_{r1}/eV	0.50	0.50
T_{m1}/K	286	283
P_{o2}/C	0.291×10^{-10}	0.236×10^{-10}
τ_{o2}/s	0.158×10^{-4}	0.244×10^{-4}
E_{r2}/eV	0.36	0.35
T_{m2}/K	254	252

Symbols: see Table 2.

FIG. 1 POINT DEFECTS IN IONIC SOLIDS

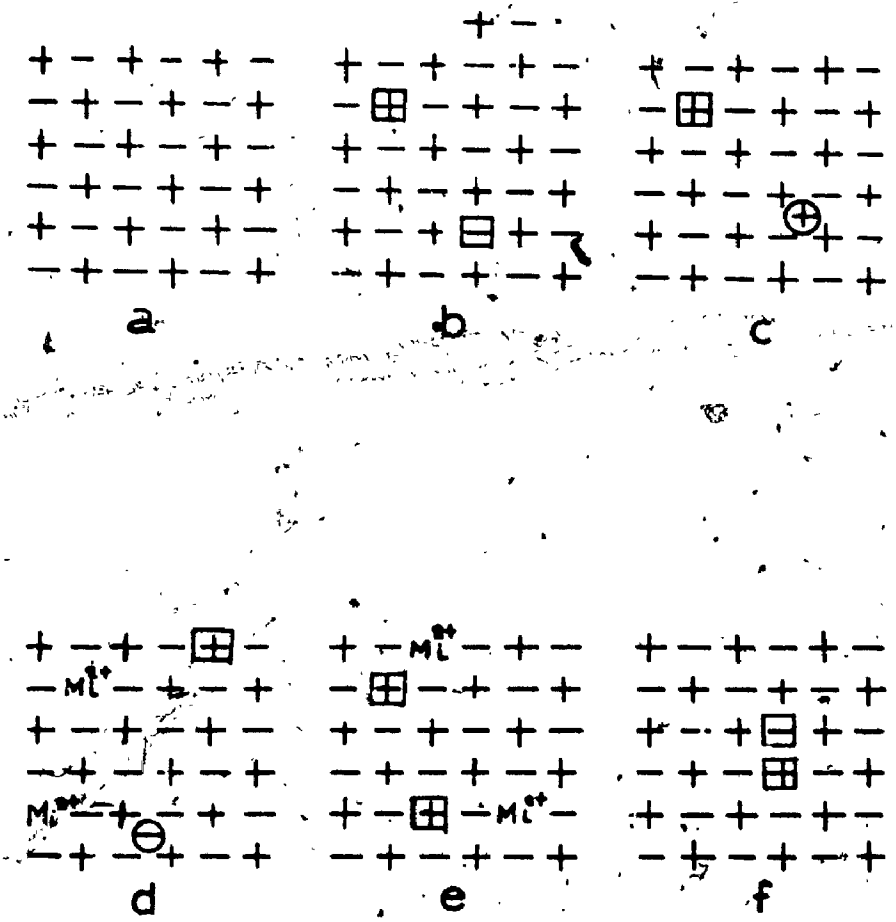

FIG. 2 TIME SCHEMATIC OF TDC EXPT.

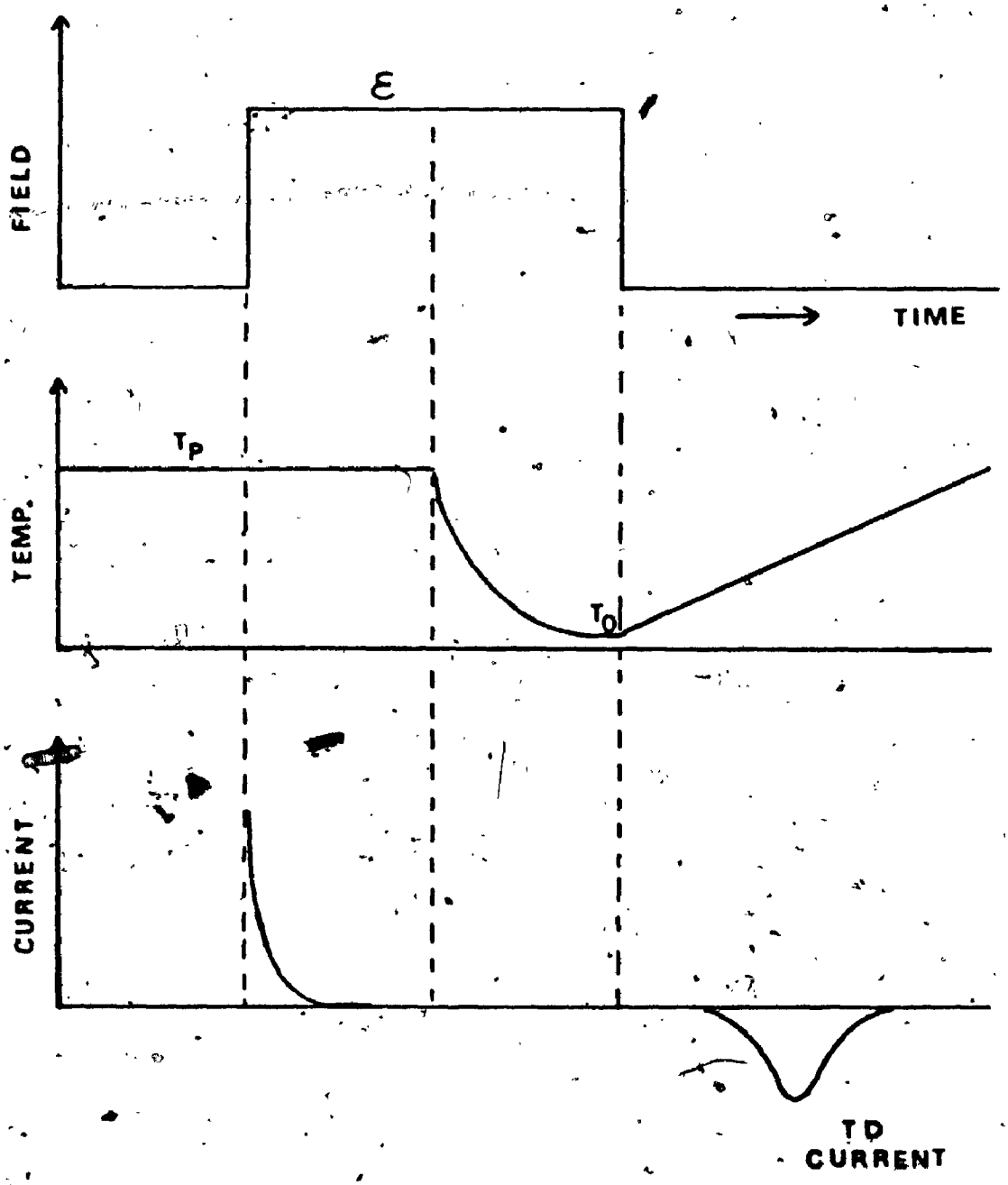

FIG. 3

CRYSTAL GROWTH TANK

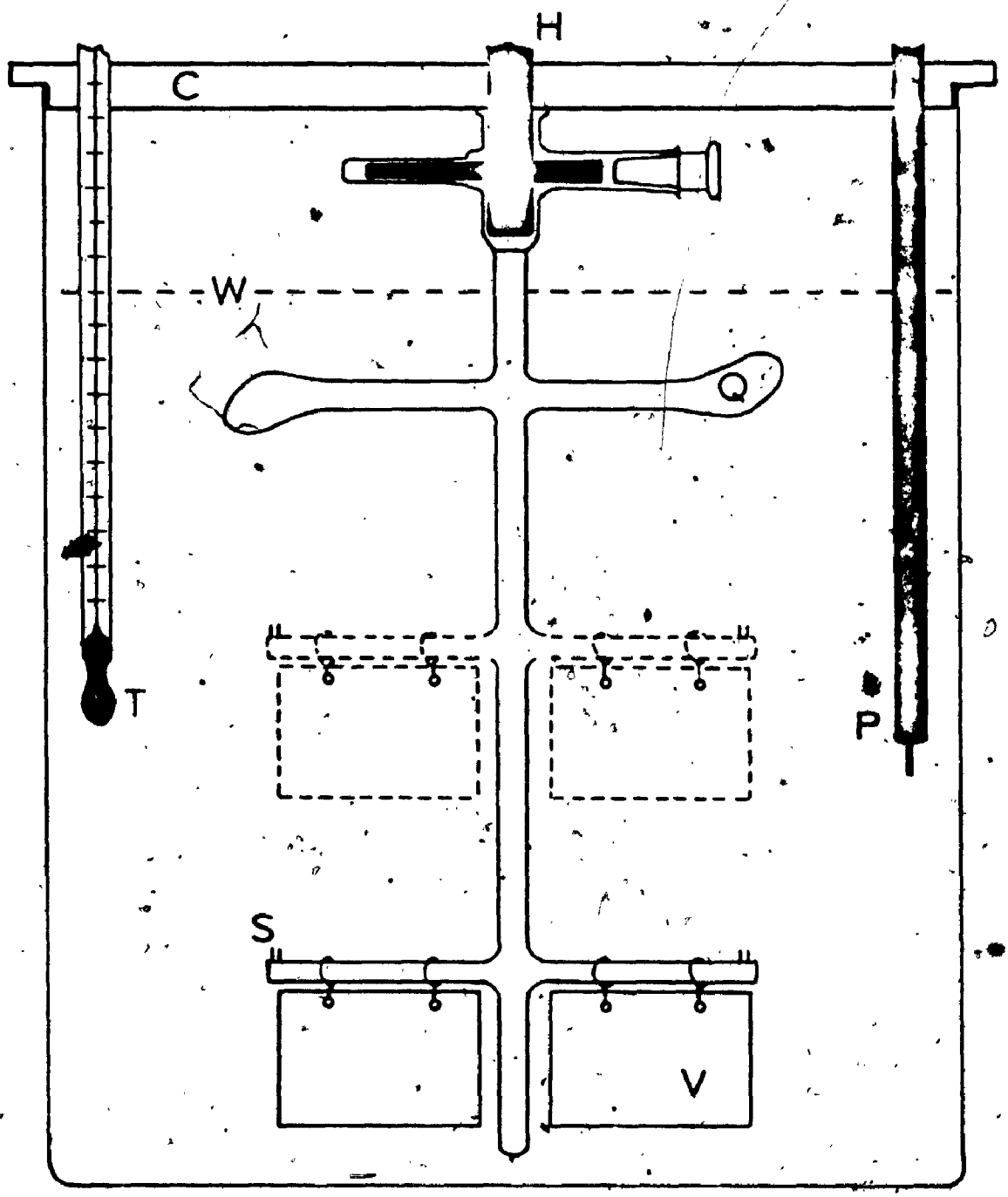

LEGEND FOR FIG. 3

T	Thermometer
P	Probe of temperature control
V	Thin glass plate
C	Plexiglass lid
Q	Stirring propeller
H	Rotating shaft
W	Solution level
S	Socket

FIG. 4 ROTATING UNIT

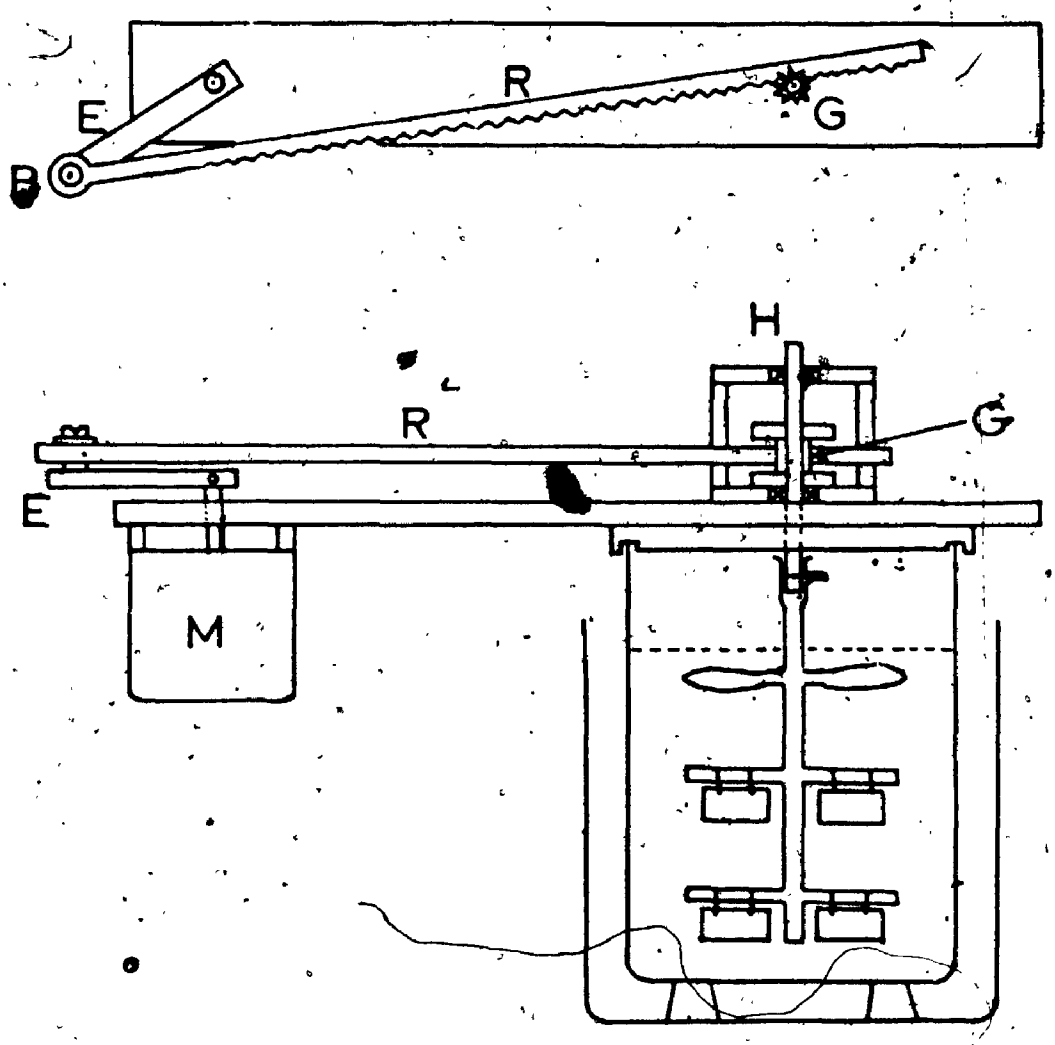

G Pinion

R Rack

M Motor

H Rotating shaft

B Bearing

E Eccentric arm

FIG. 5

CONDUCTIVITY CELL

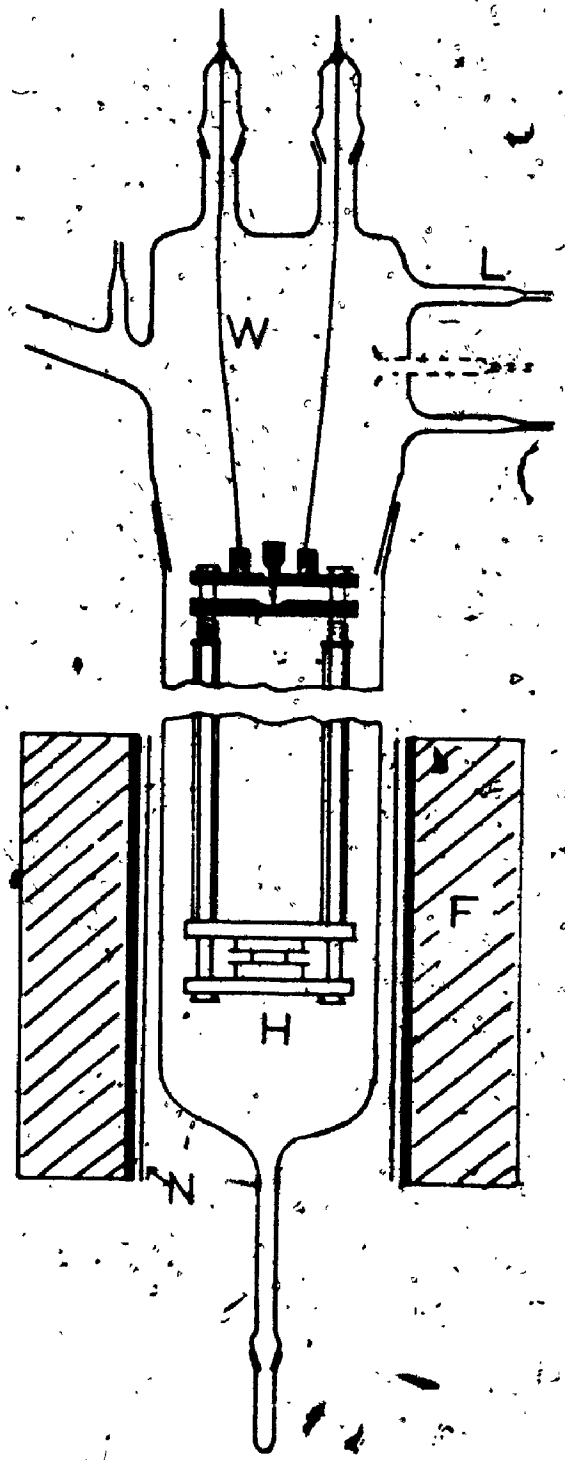

W Tungsten wire

L Sleeve

F Furnace

N Nickel sheet

H Sample holder

FIG. 6 SAMPLE HOLDER FOR CONDUCTIVITY CELL

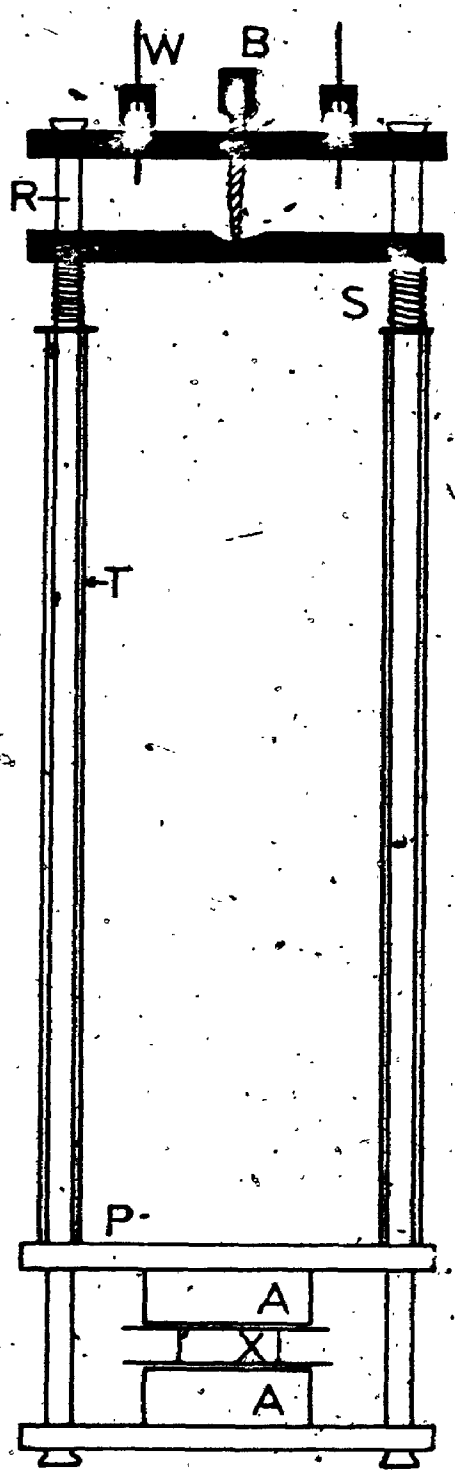

A Alumina disc

X Sample

P Quartz plate

S Spring

T Quartz tube

R Quartz rod

B Screw

W Tungsten wire

FIG. 7 VACUUM LINE FOR CONDUCTIVITY CELL

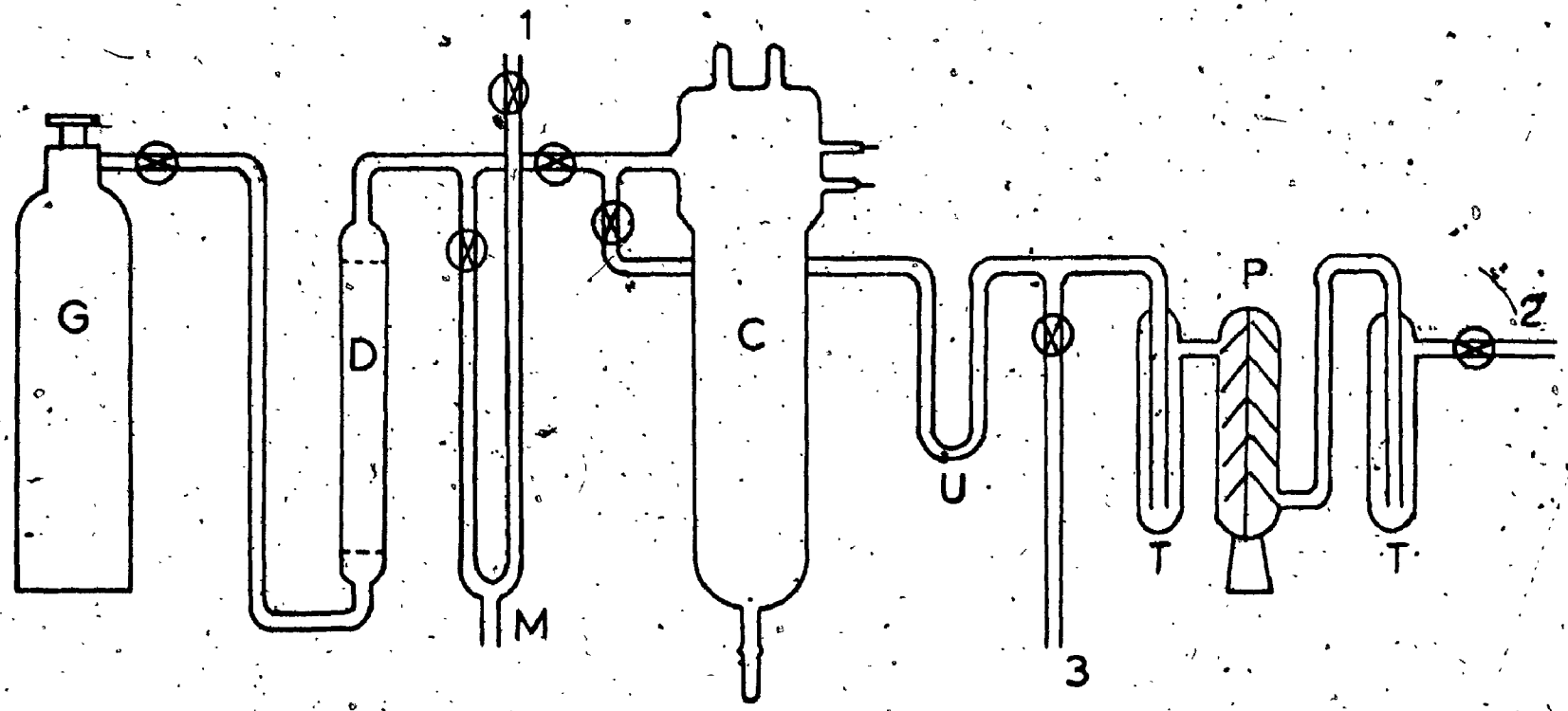

LEGEND FOR FIG. 7

G	Gas cylinder
D	P_2O_5 drying column
M	Manometer
C	Conductivity cell
U,T	Traps
P	Mercury diffusion pump
1,2	To rotary pump
3	To McLeod gauge

FIG. 8 THERMAL DEPOLARIZATION APPARATUS

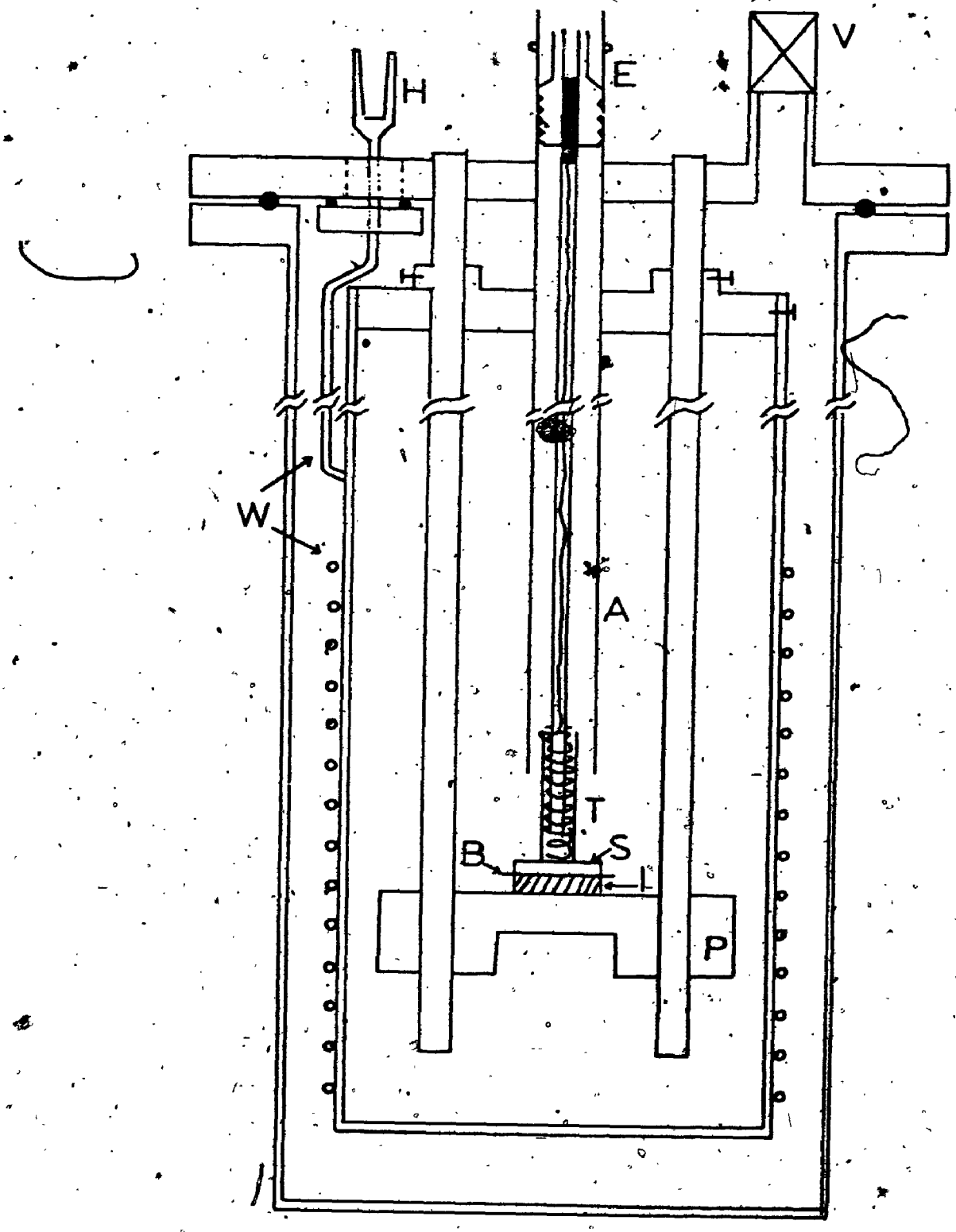

LEGEND FOR FIG. 8

W	Thermocoax wire
S	Sample
B	Pt electrode
I	Sapphire insulator
V	Veeco valve
A	Steel shield
T	Upper electrode
H	Terminal of Thermocoax wire
E	BNC teflon connectors
P	Platform

FIG. 9 TOP OF THERMAL DEPOLARIZATION APPARATUS

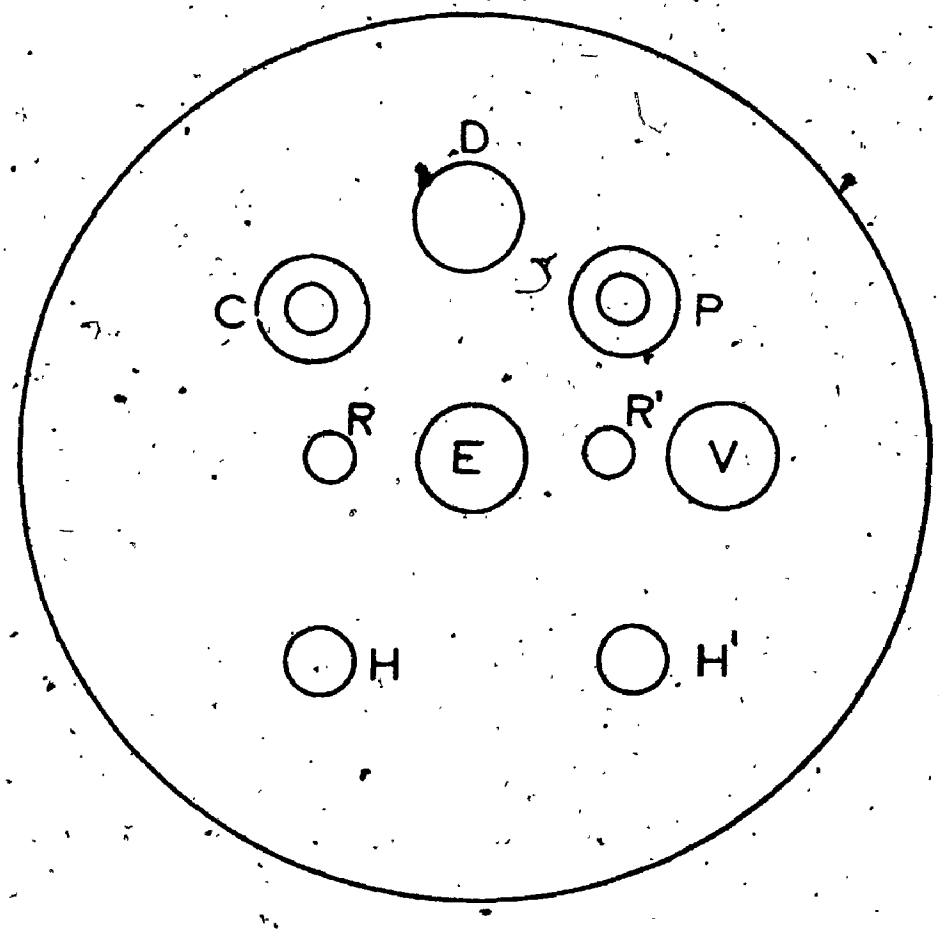

V Veeco

C, P Cajon ultra-torr adapters

H, H' Terminals of Thermocoax wire

E, D BNC teflon connectors

R, R' Supporting rods

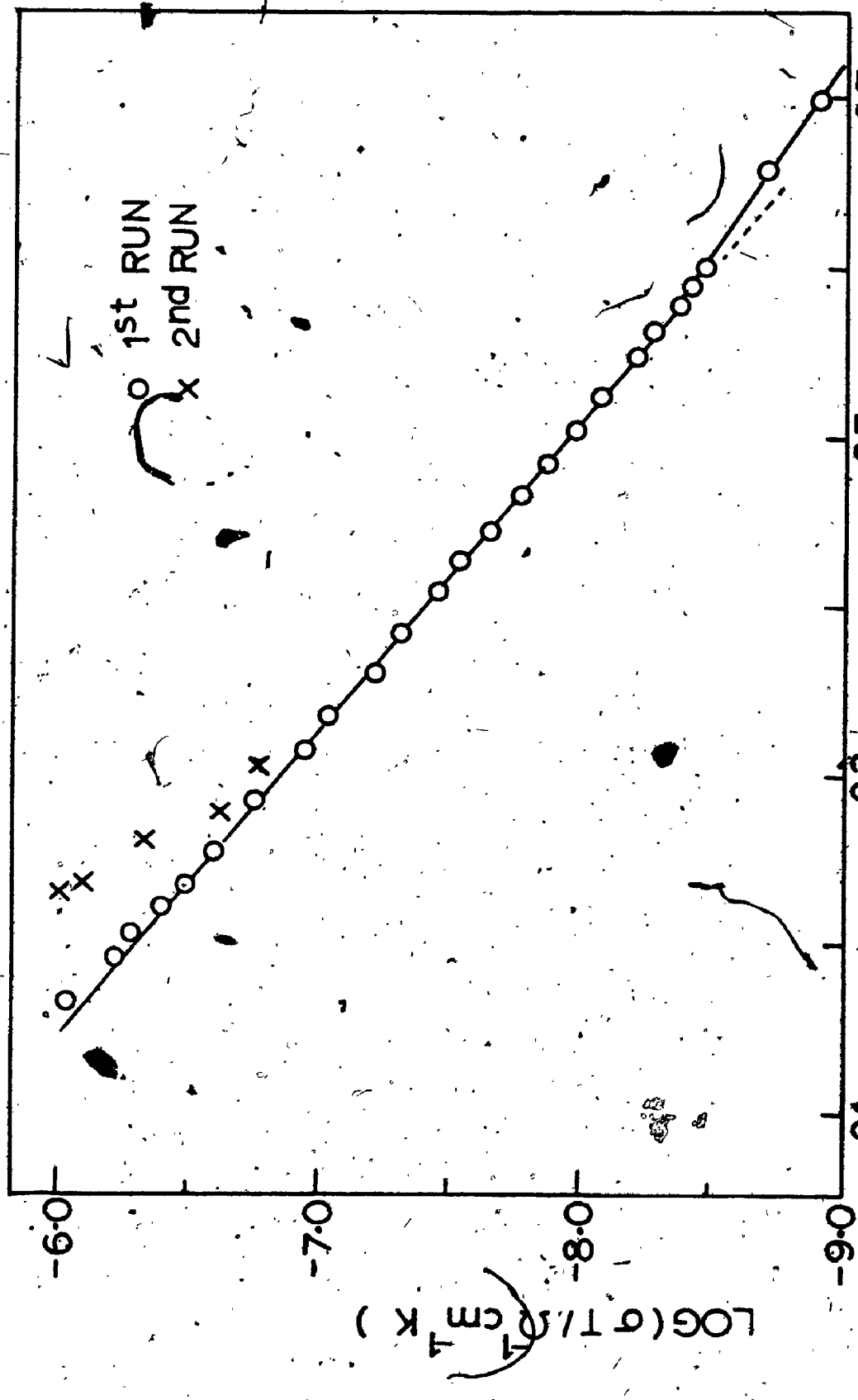

FIG. 10 CONDUCTIVITY OF AP PELLET

FIG. 11 CONDUCTIVITY OF AP PELLET IN NH_3

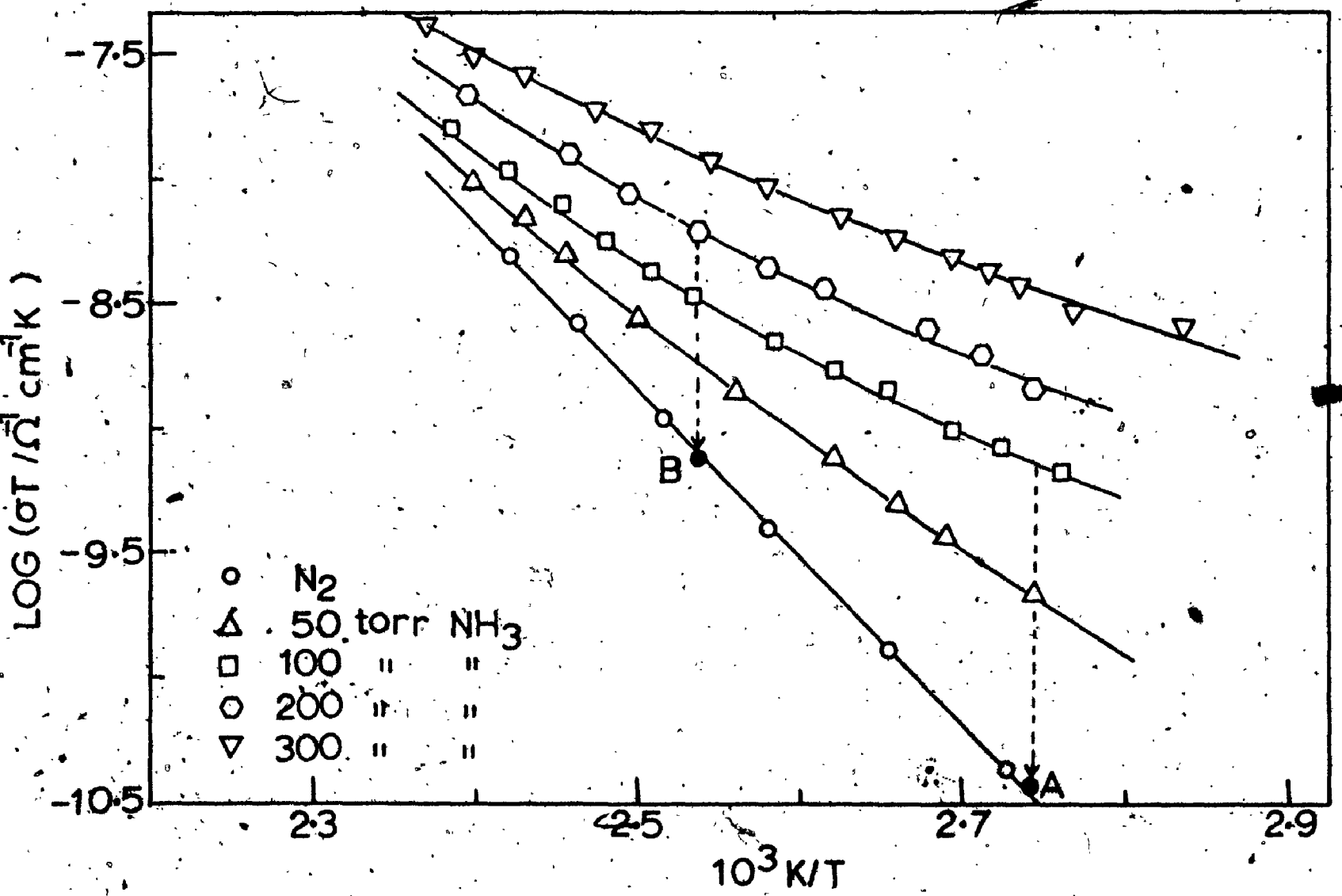

FIG. 12 CONDUCTIVITIY OF PURE AP CRYSTAL

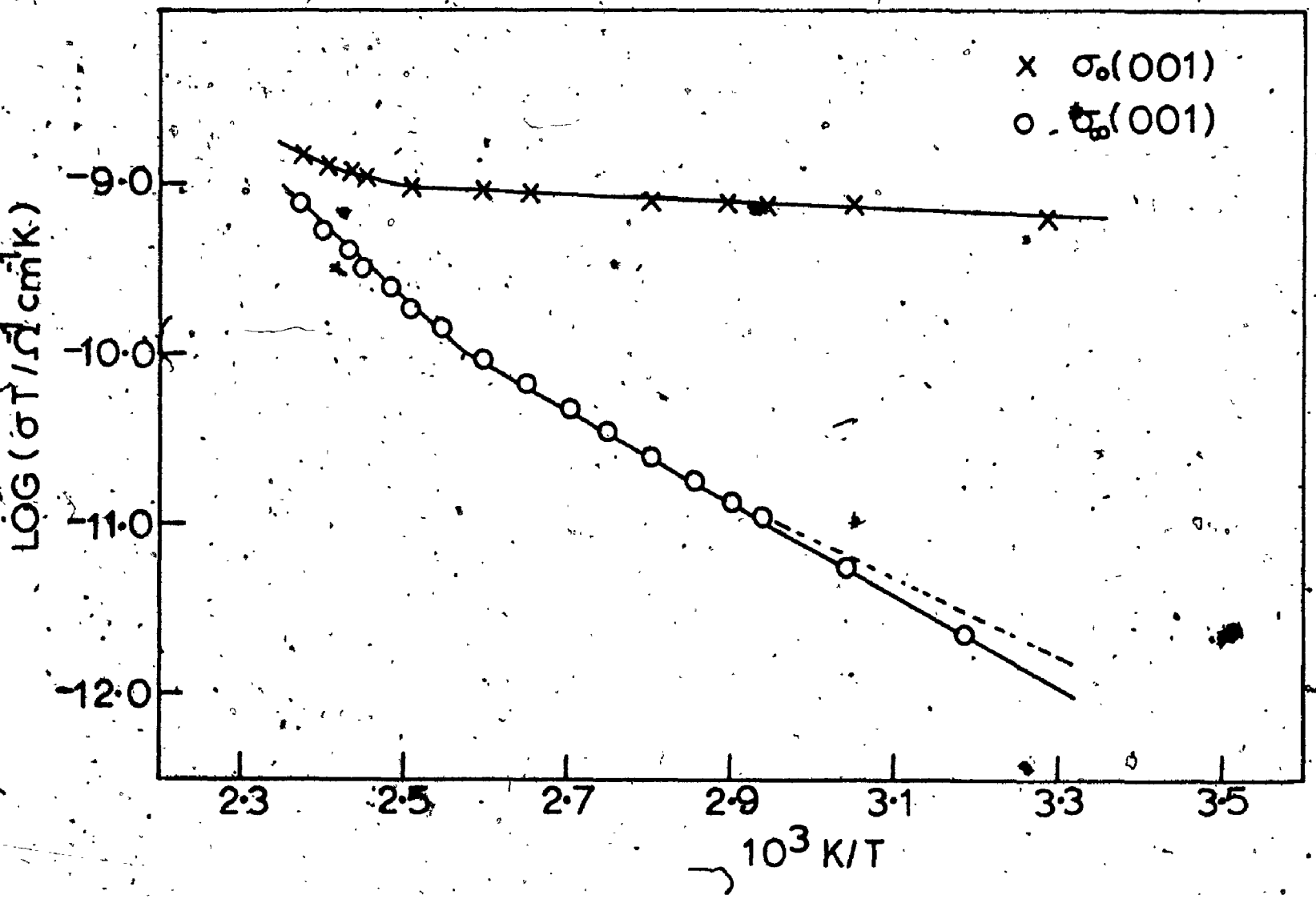

FIG.13 CONDUCTIVITY OF AP CRYSTAL IN H_2O VAPOR

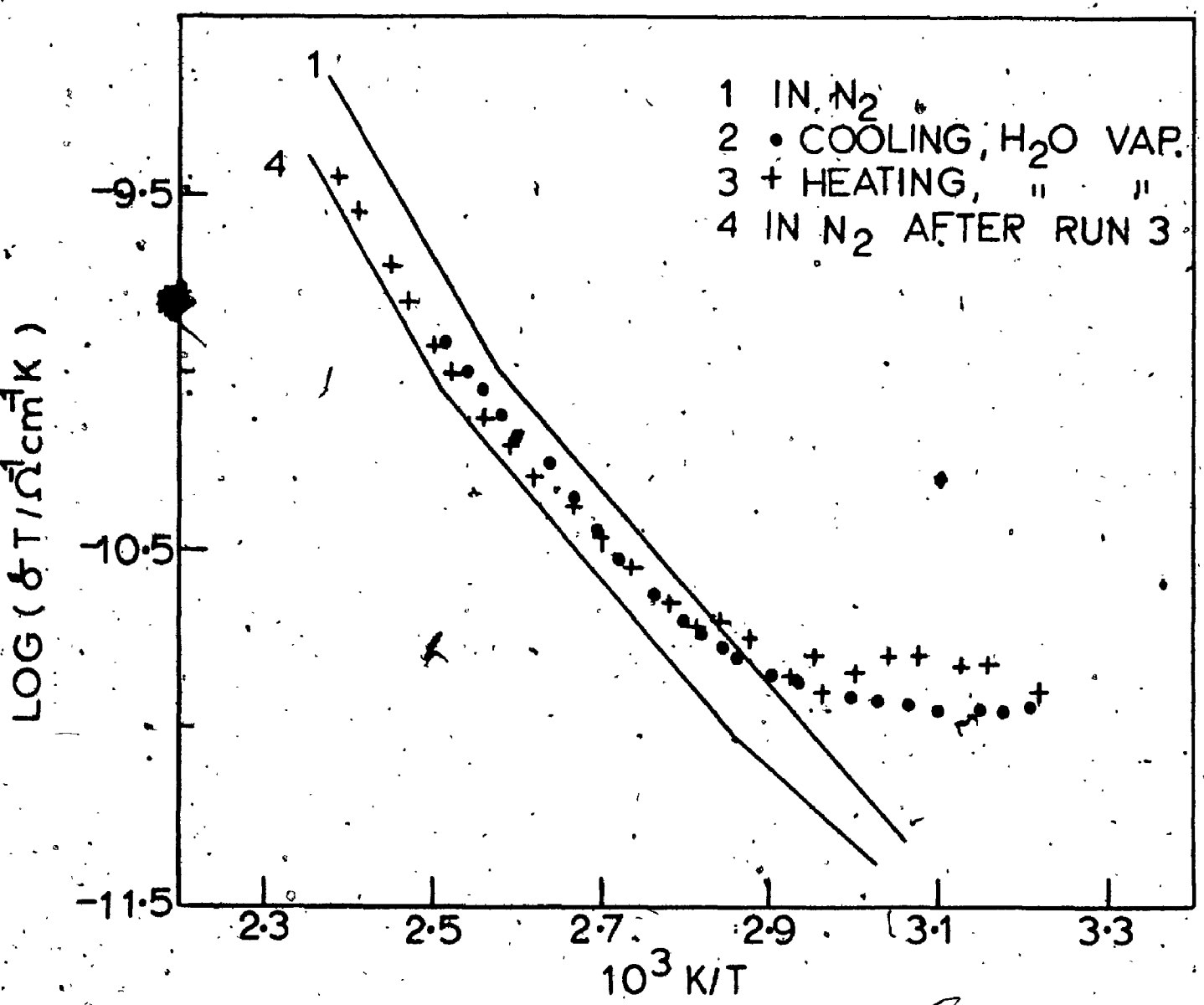

FIG.14 CONDUCTIVITY OF AP CRYSTAL IN NH_3

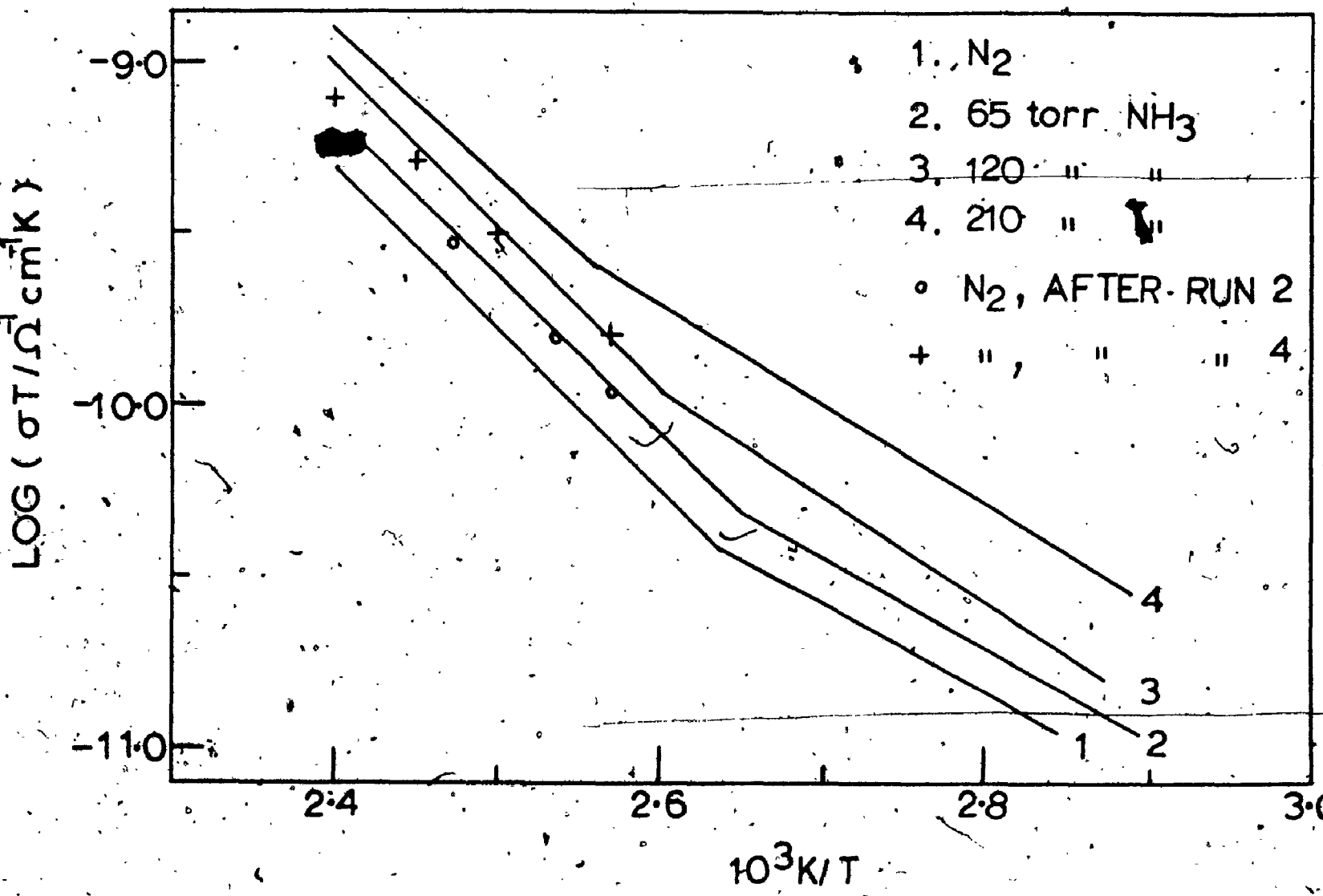

FIG.15 - CONDUCTIVITY OF AP CRYSTAL IN NH_3

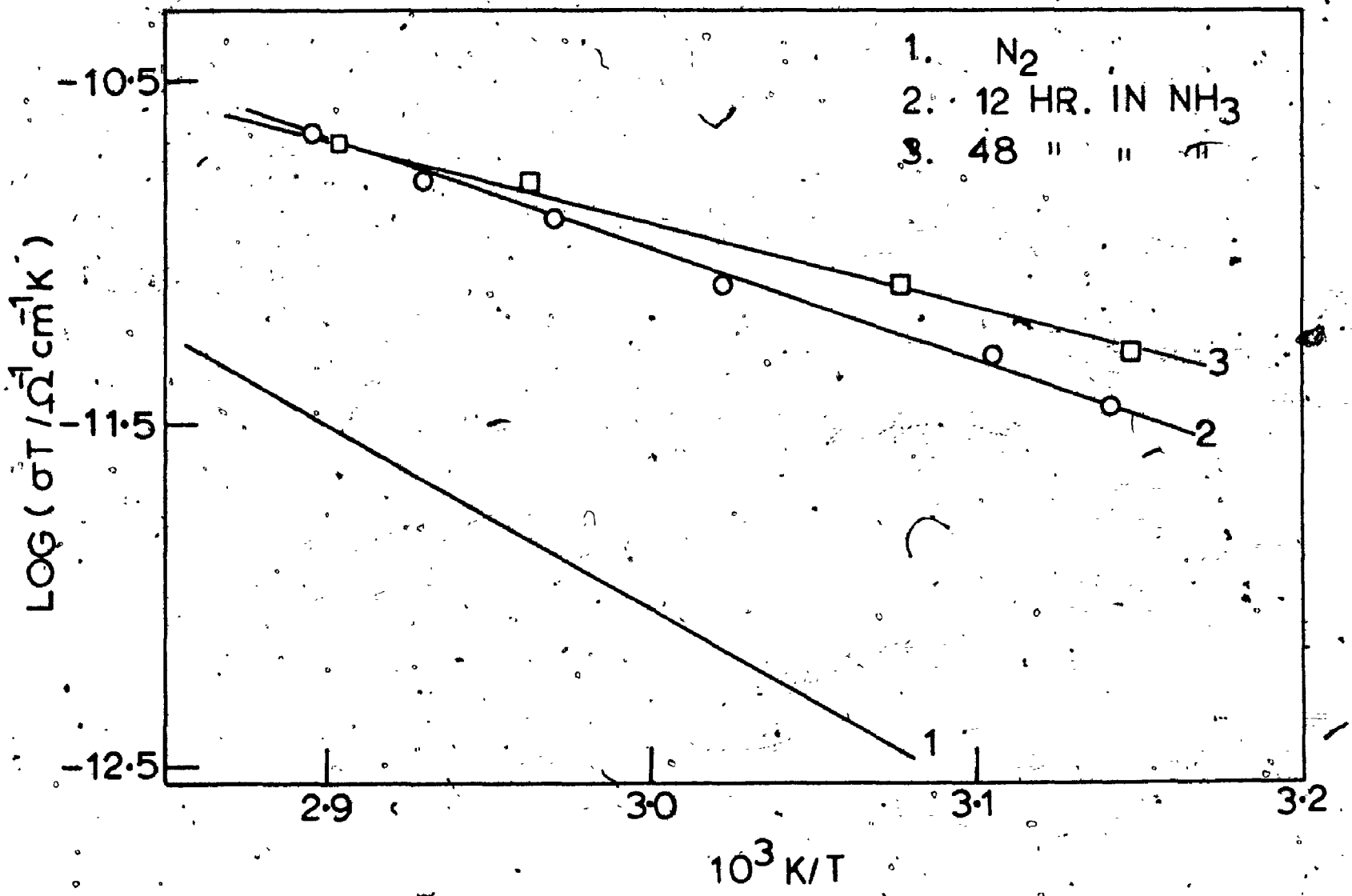

FIG.16 CONDUCTIVITY OF 1% AP : Ba^{2+}

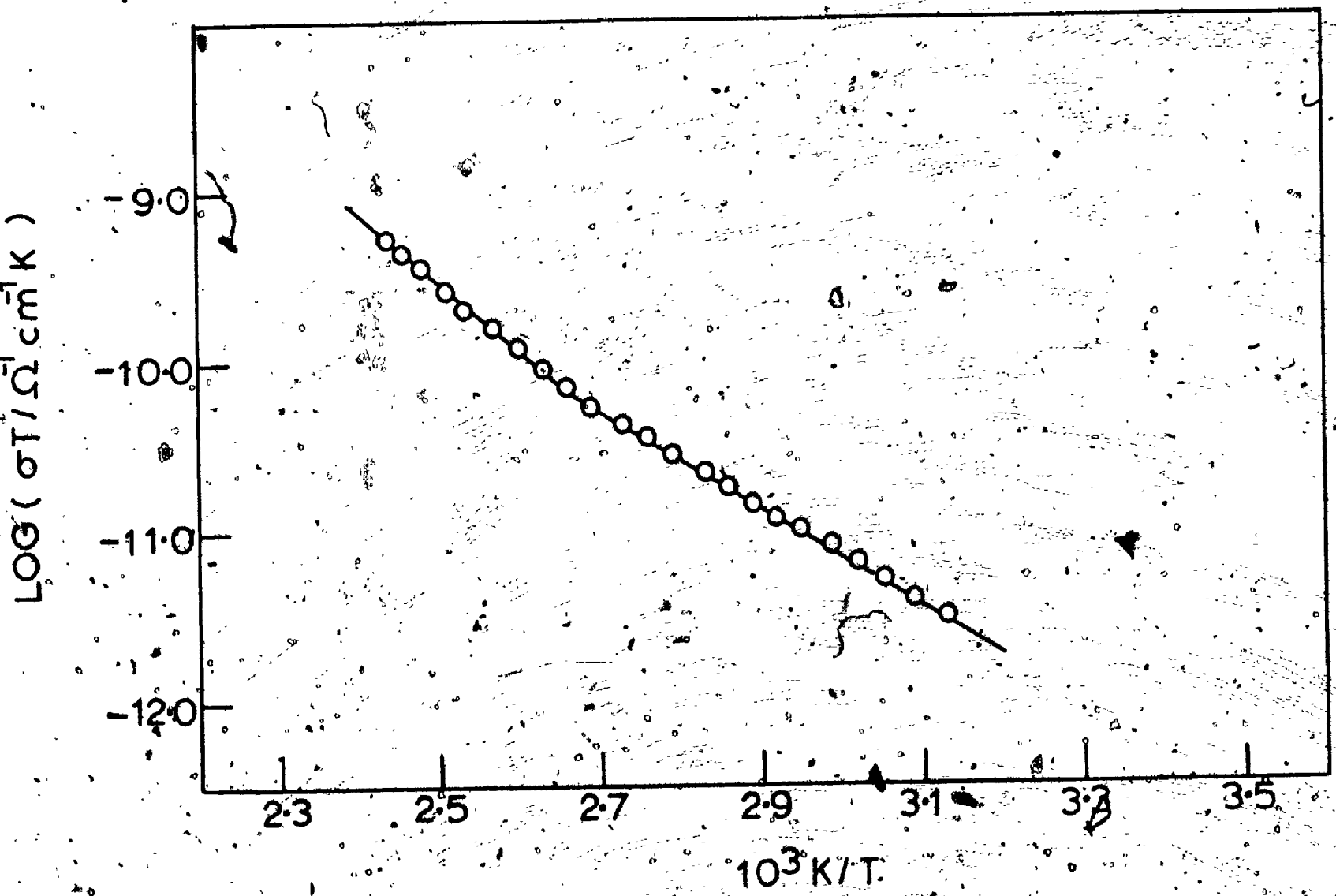

FIG 17 CONDUCTIVITY OF 5% AP: Pb^{2+}

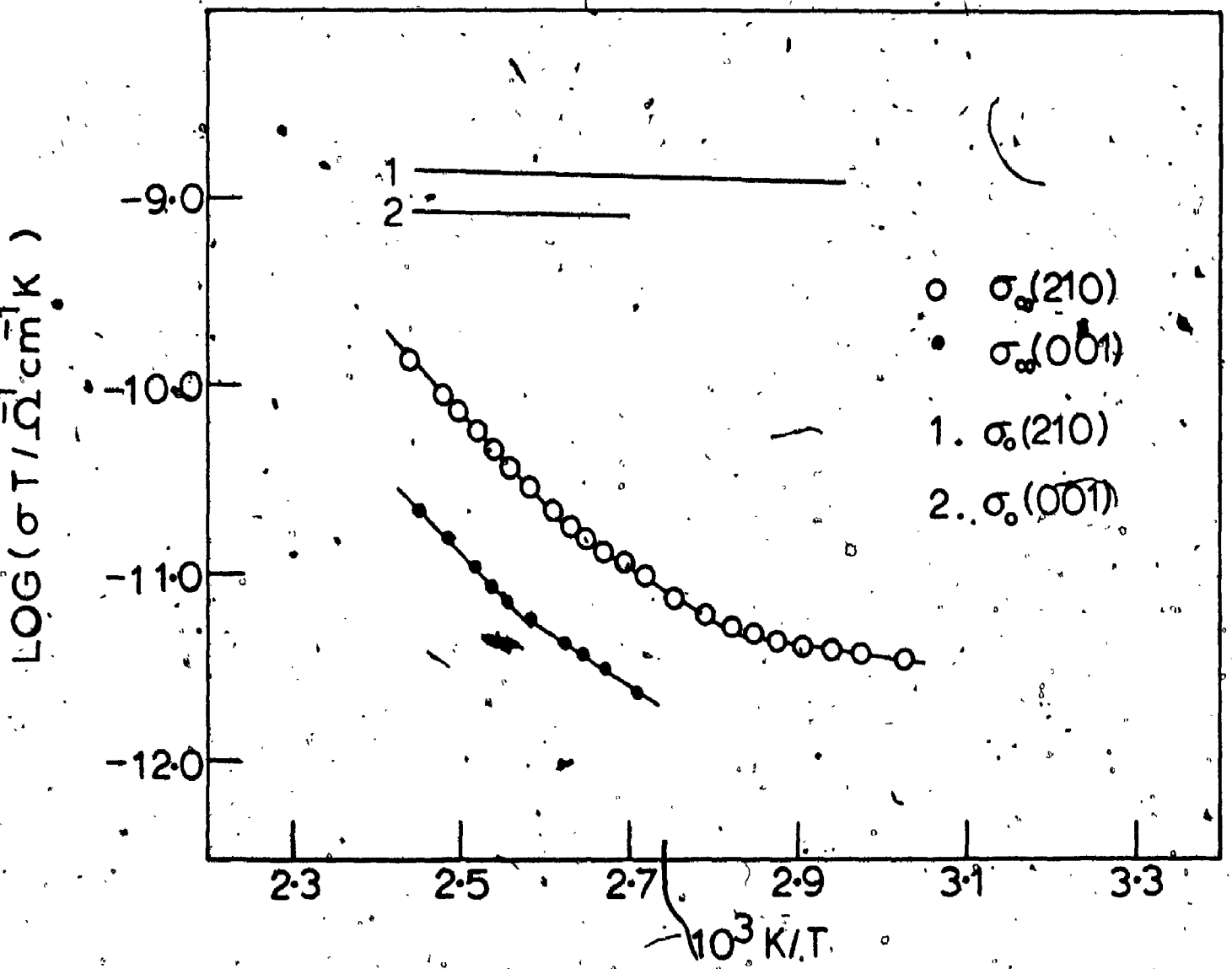

FIG.18 CONDUCTIVITY OF 0·1% AP:SO_4^{2-}

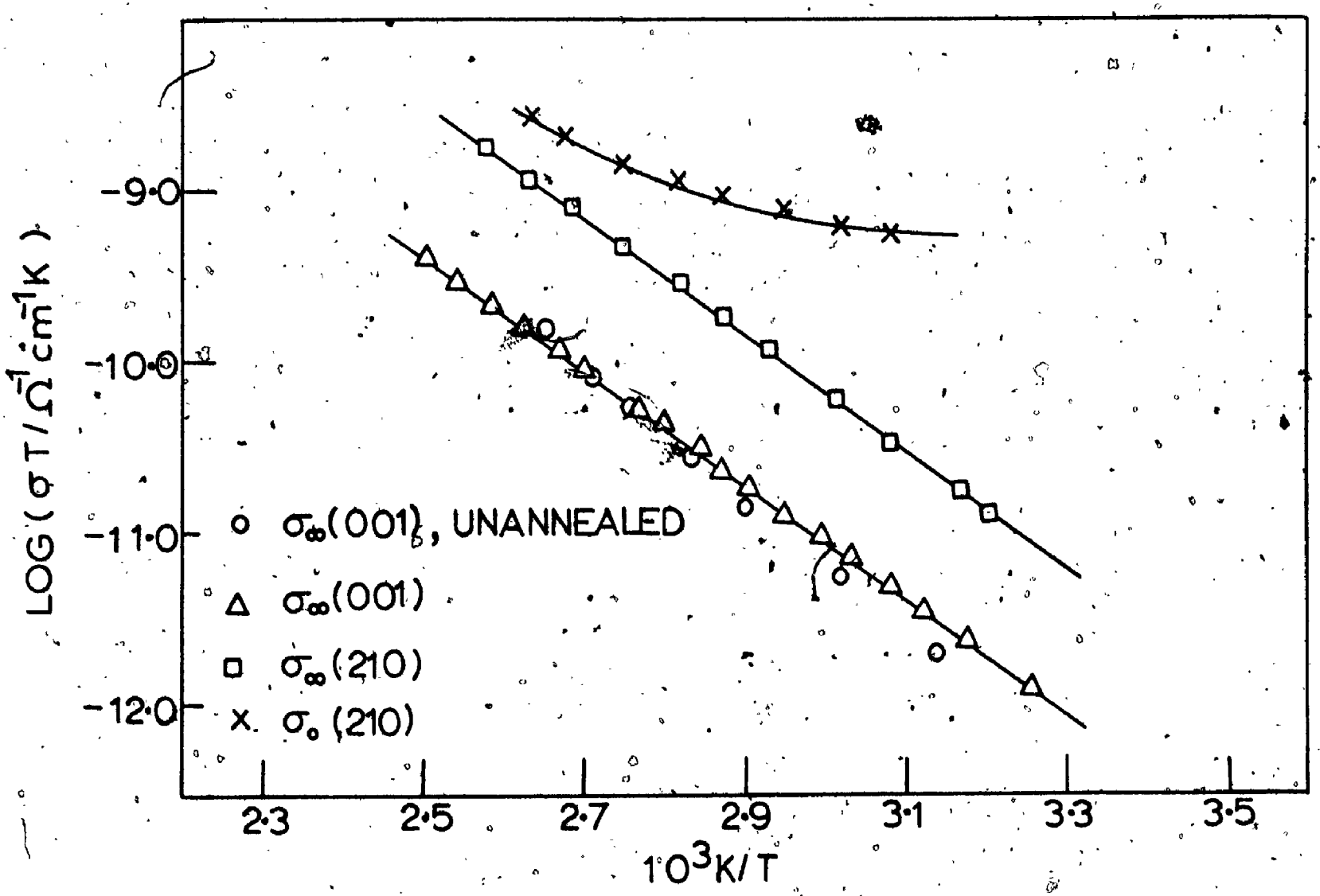

FIG. 19 CONDUCTIVITY OF 0·1% AP:CrO_4^{2-}

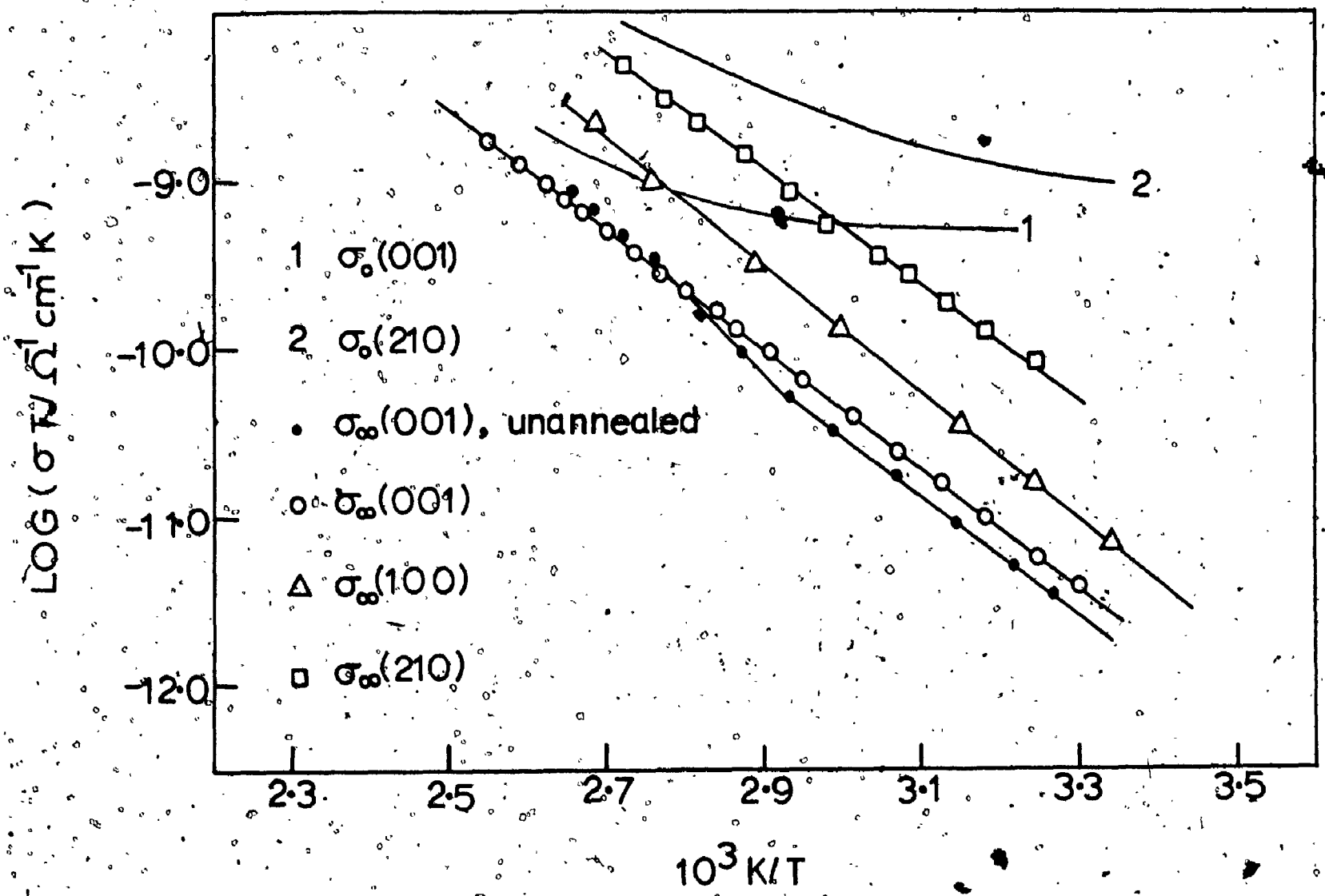

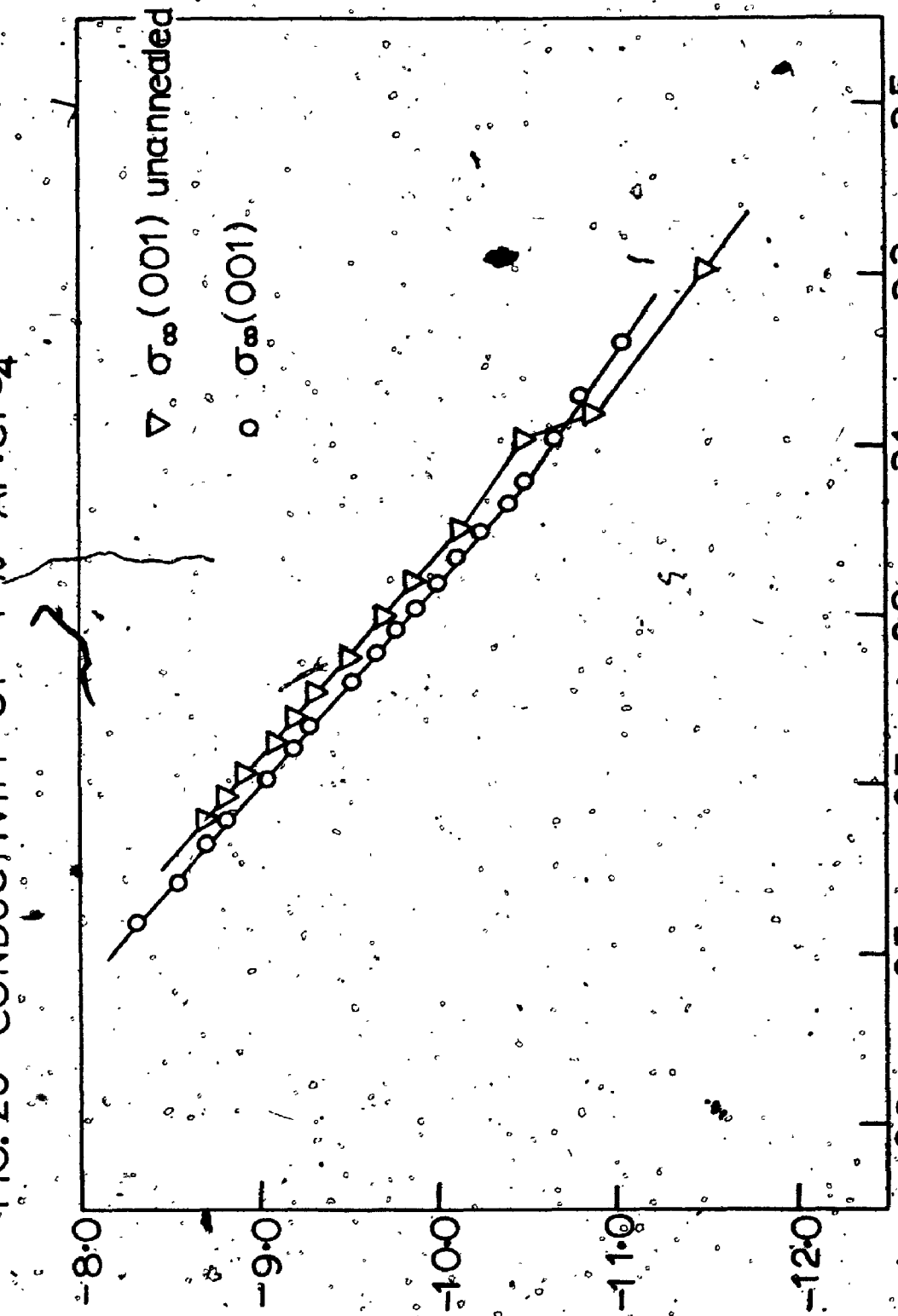

FIG. 20 CONDUCTIVITY OF 1% AP:CrO_4^{2-}

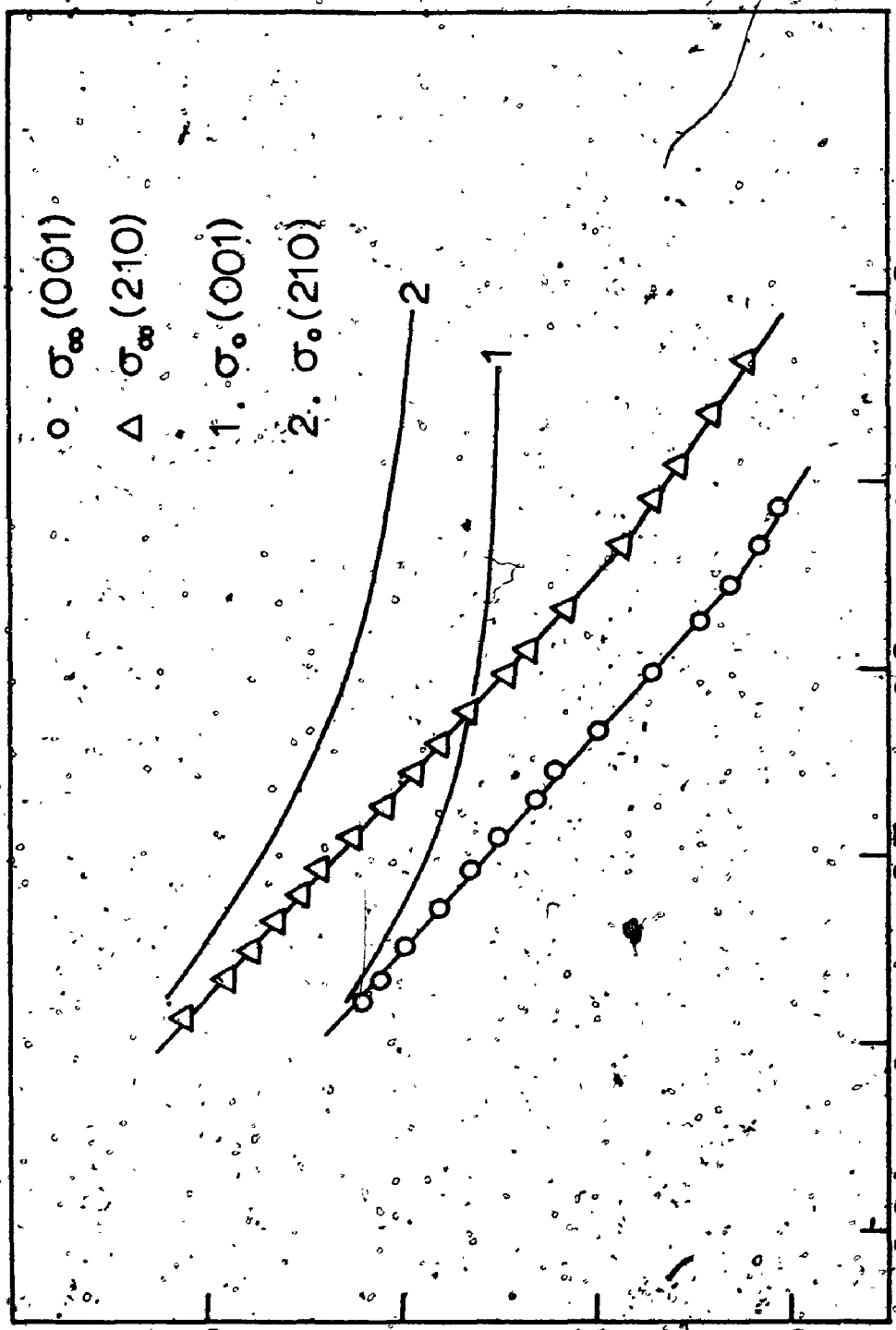

FIG. 21 CONDUCTIVITY OF 1% AP:CrO_4^{2-}

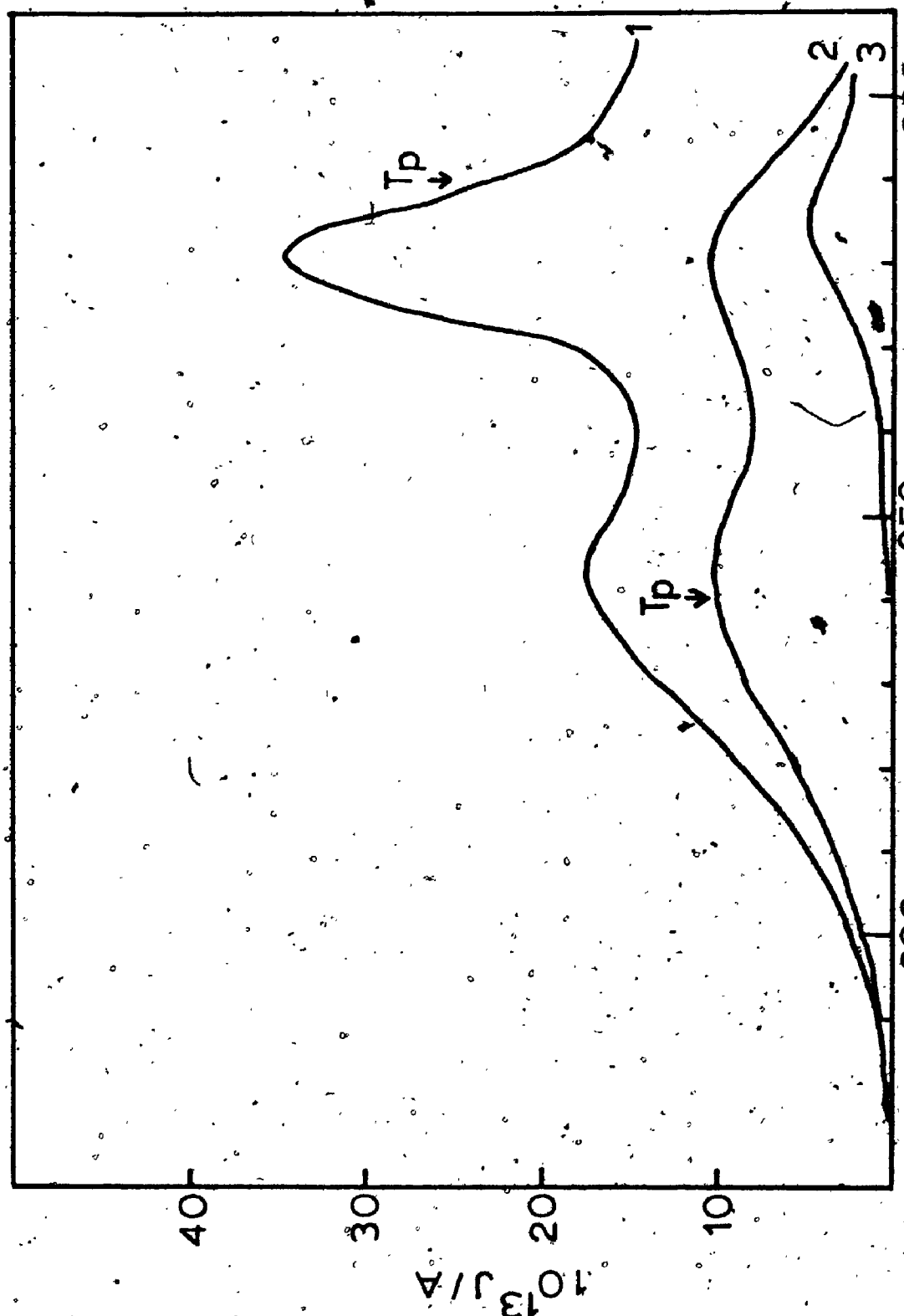

FIG. 22 TDC OF 0.1 % AP: SO_4^{2-}

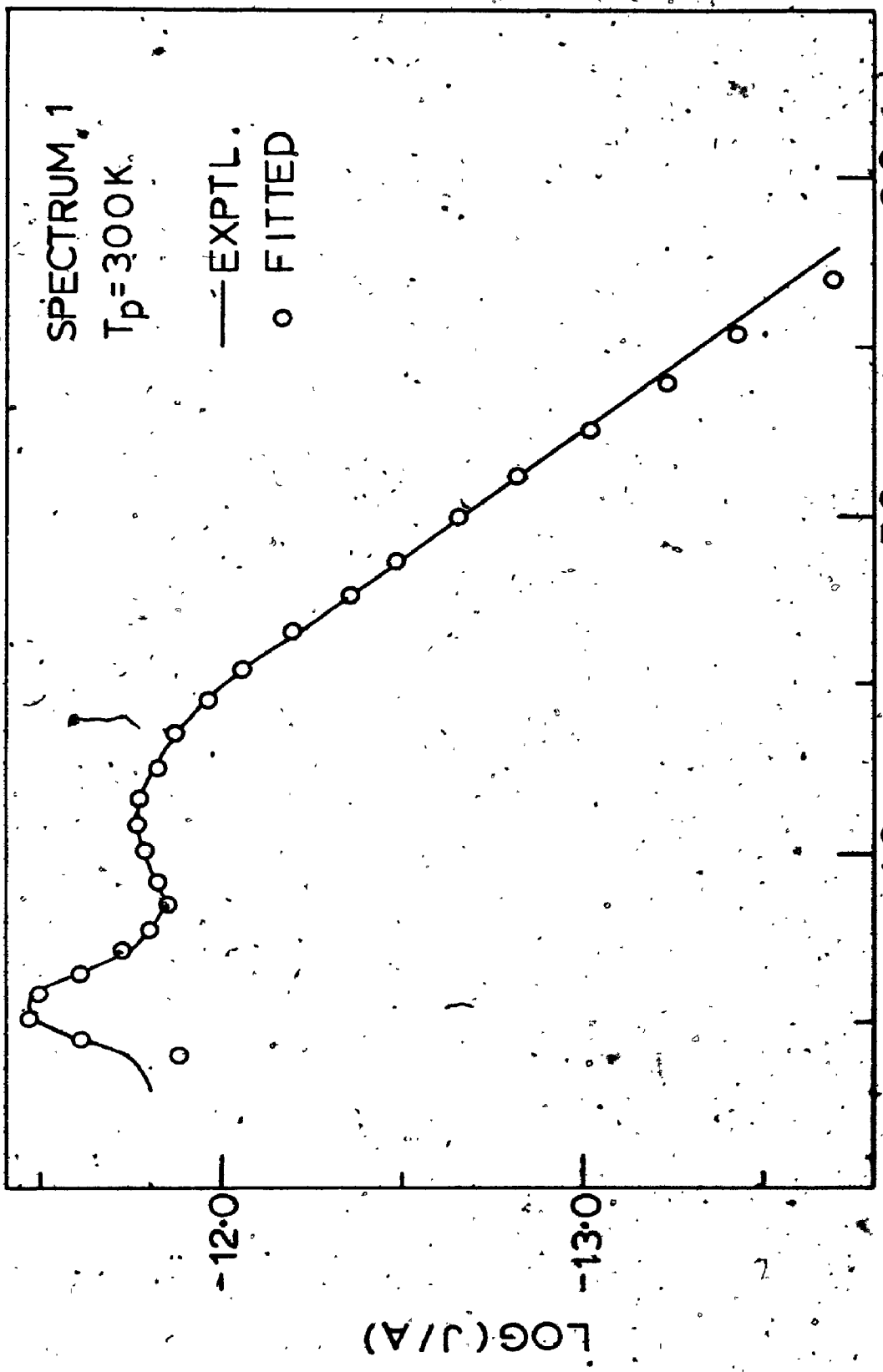

FIG. 23 TDC OF 0.1% AP:SO_4^{2-}

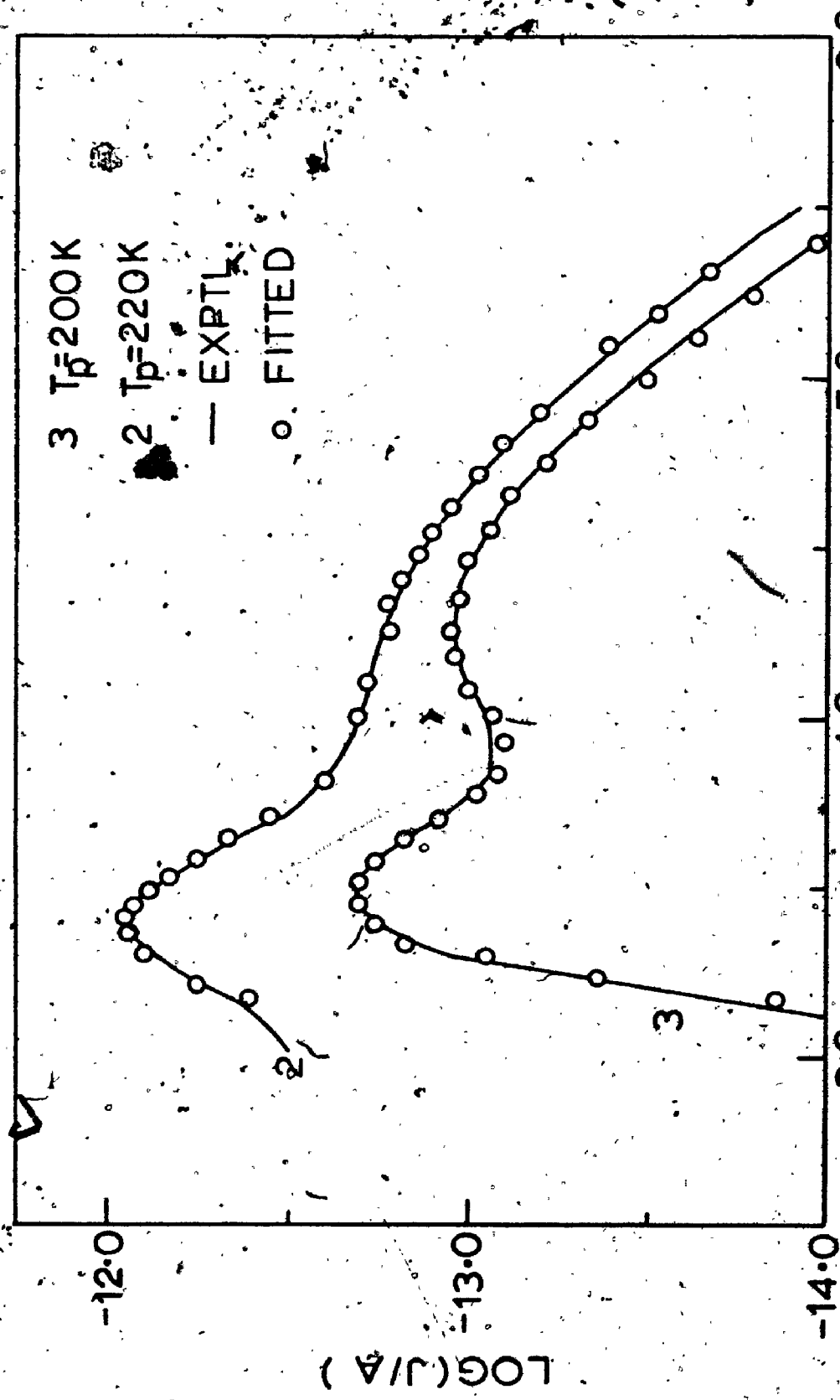

FIG. 24 TDC OF 0·1% AP:CrO_4^{2-}

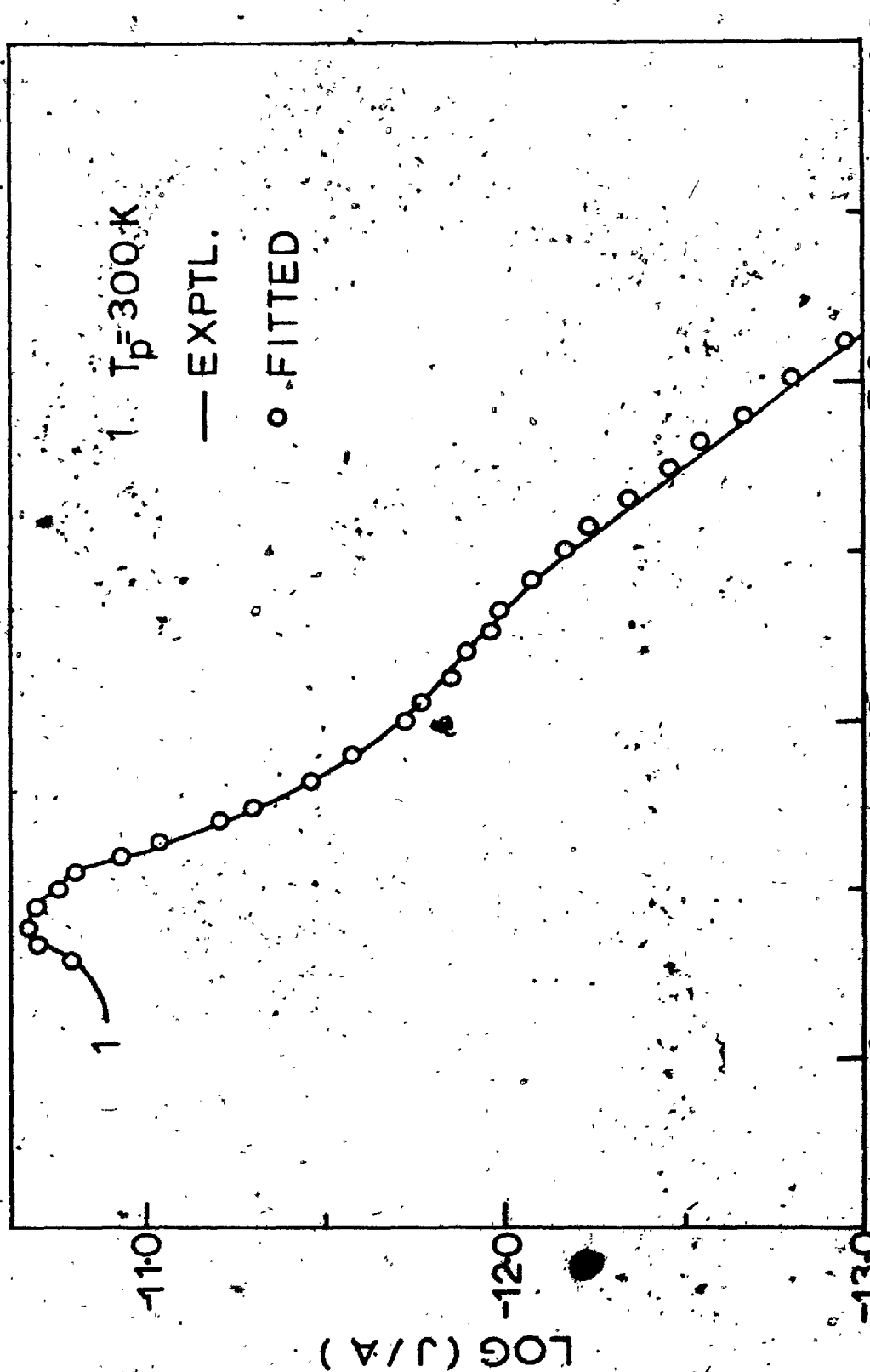

FIG. 25 TDC OF 0·1% AP:CrO_4^{2-}

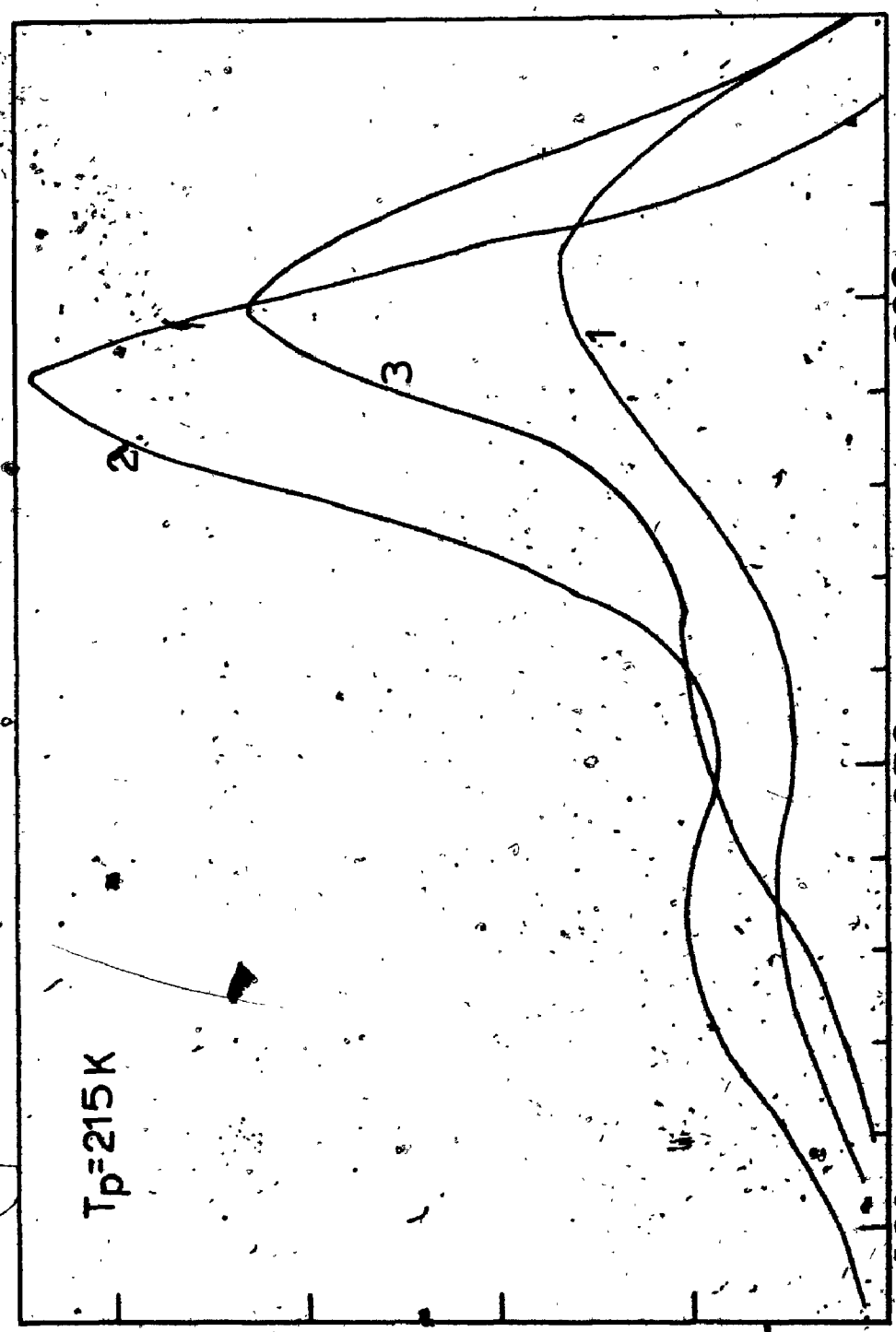

FIG. 26 TDC OF 1% AP:CrO_4^{2-}

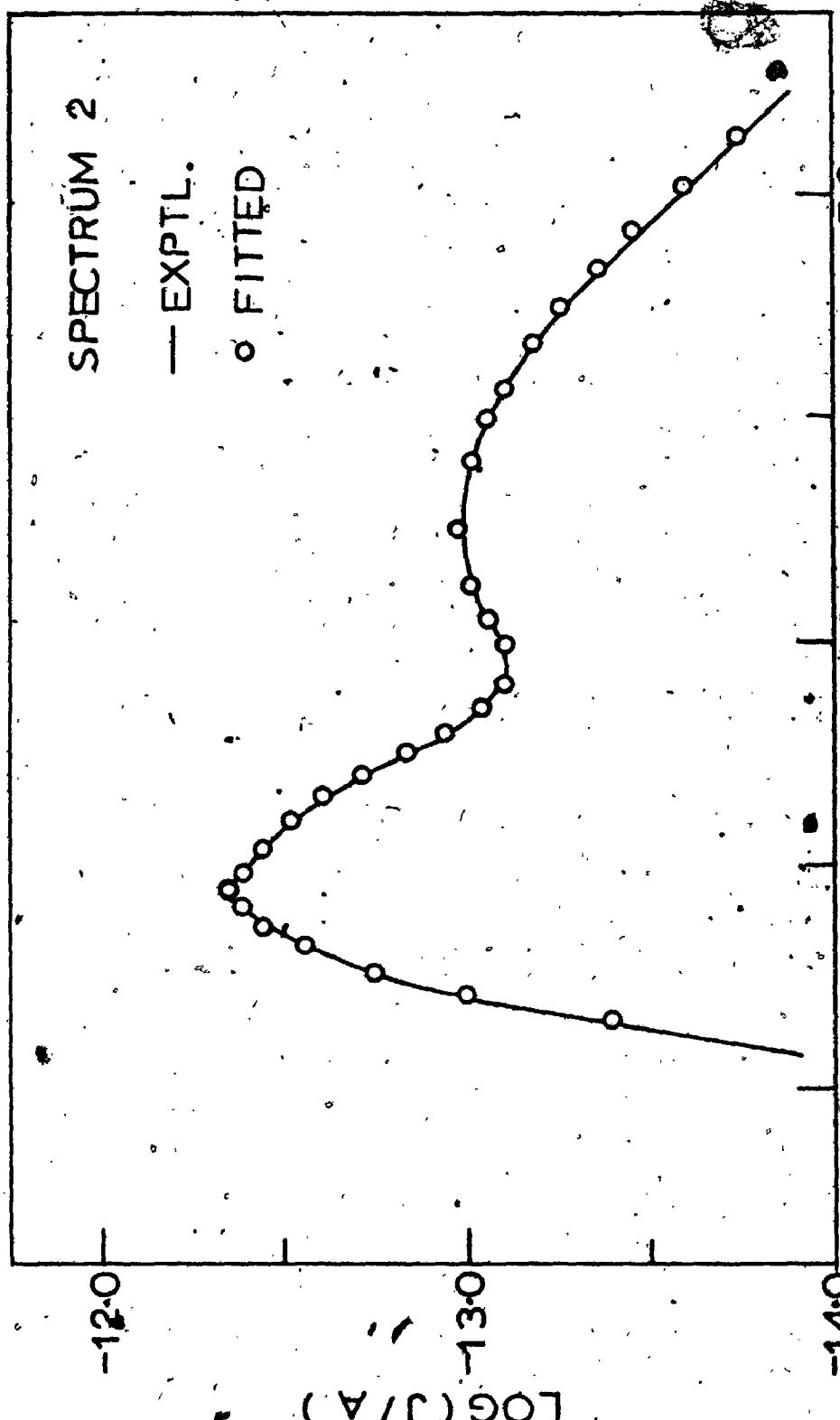

FIG. 27 TDC OF 1% $^tAP:CrO_4^{2-}$

FIG. 28 TDC OF 1% AP:CrO_4^{2-}

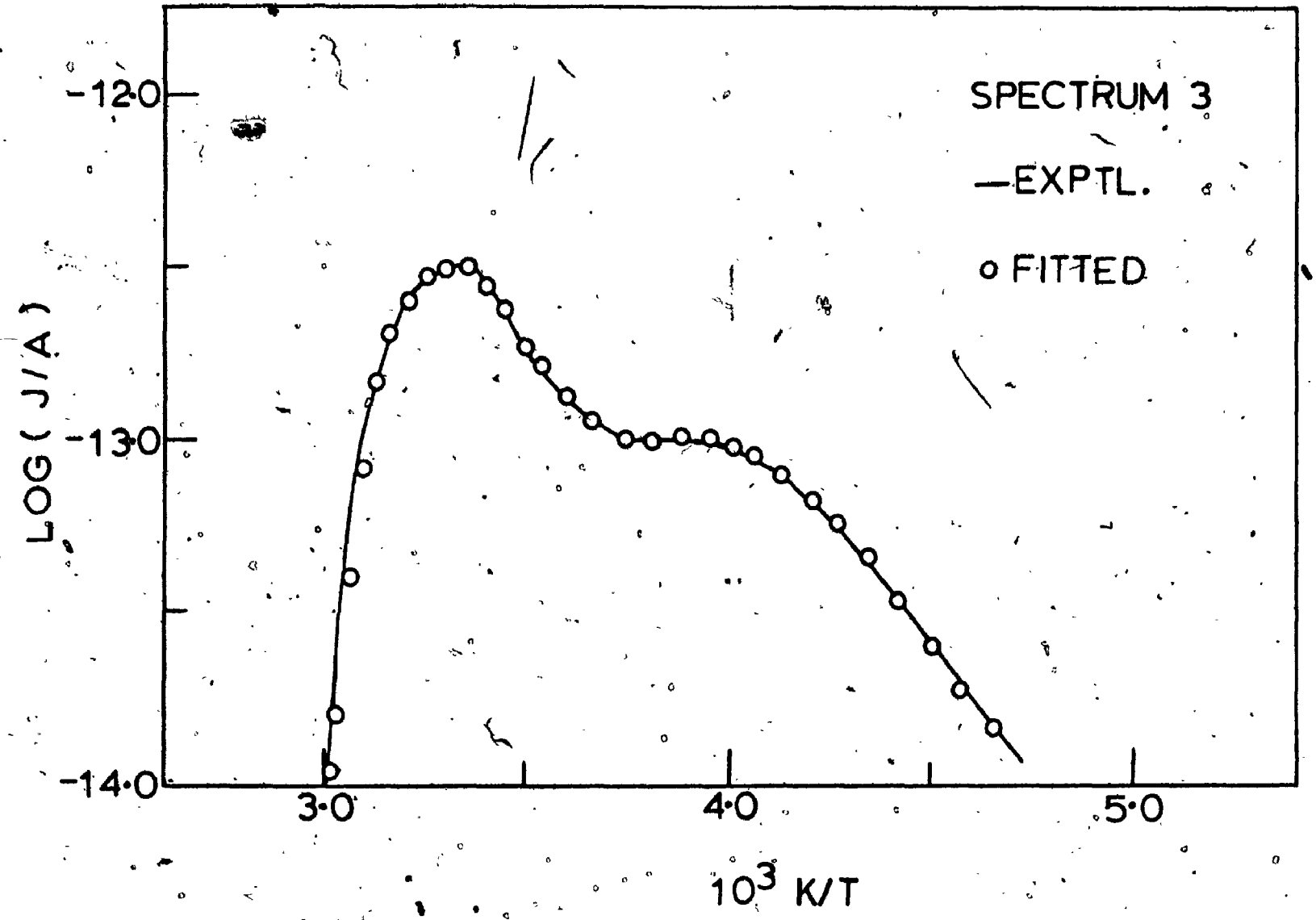

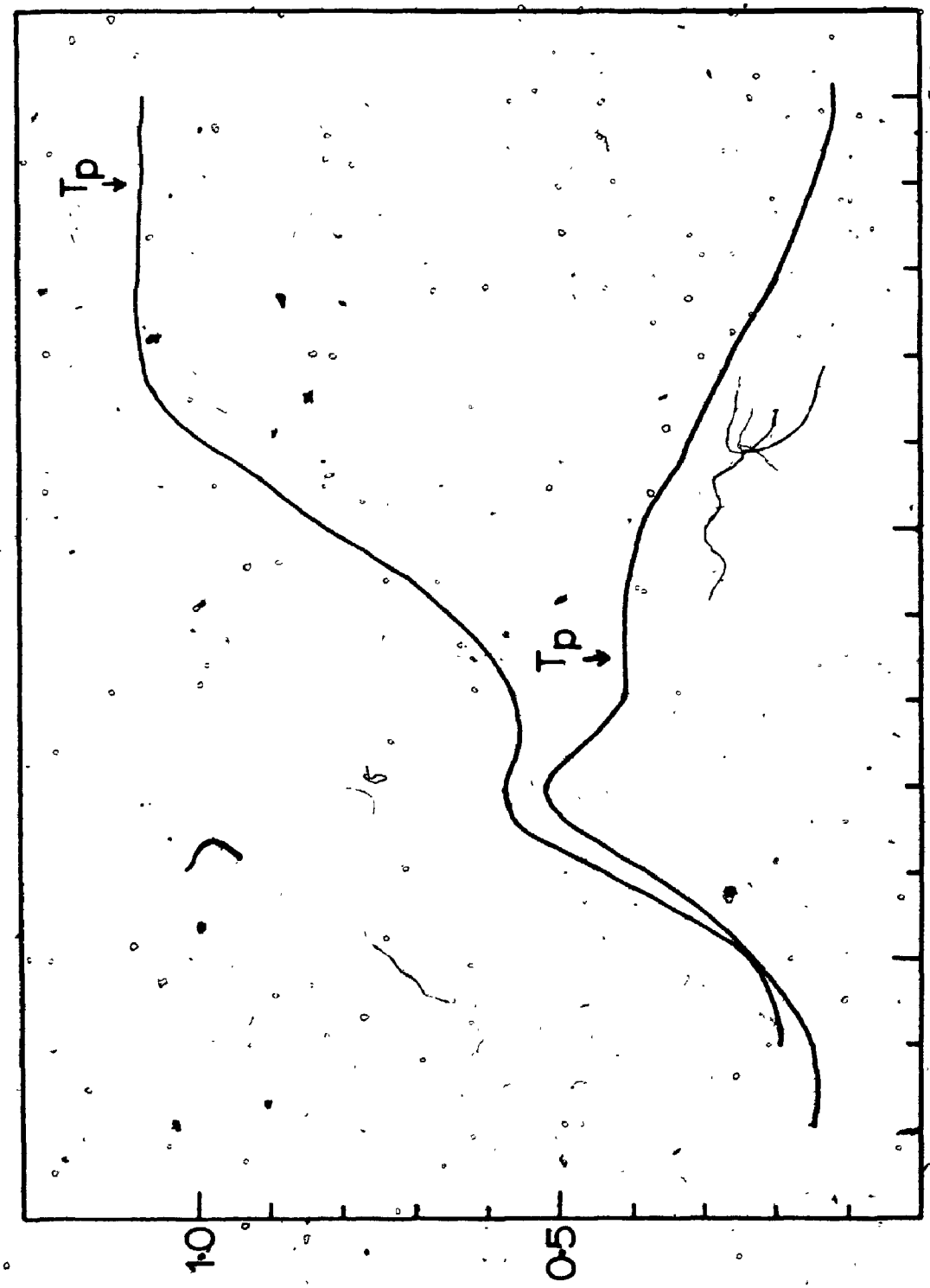

FIG. 29 TDC OF 5% AP: Pb^{2+}

FIG. 30 TDC OF NH_3-TREATED AP

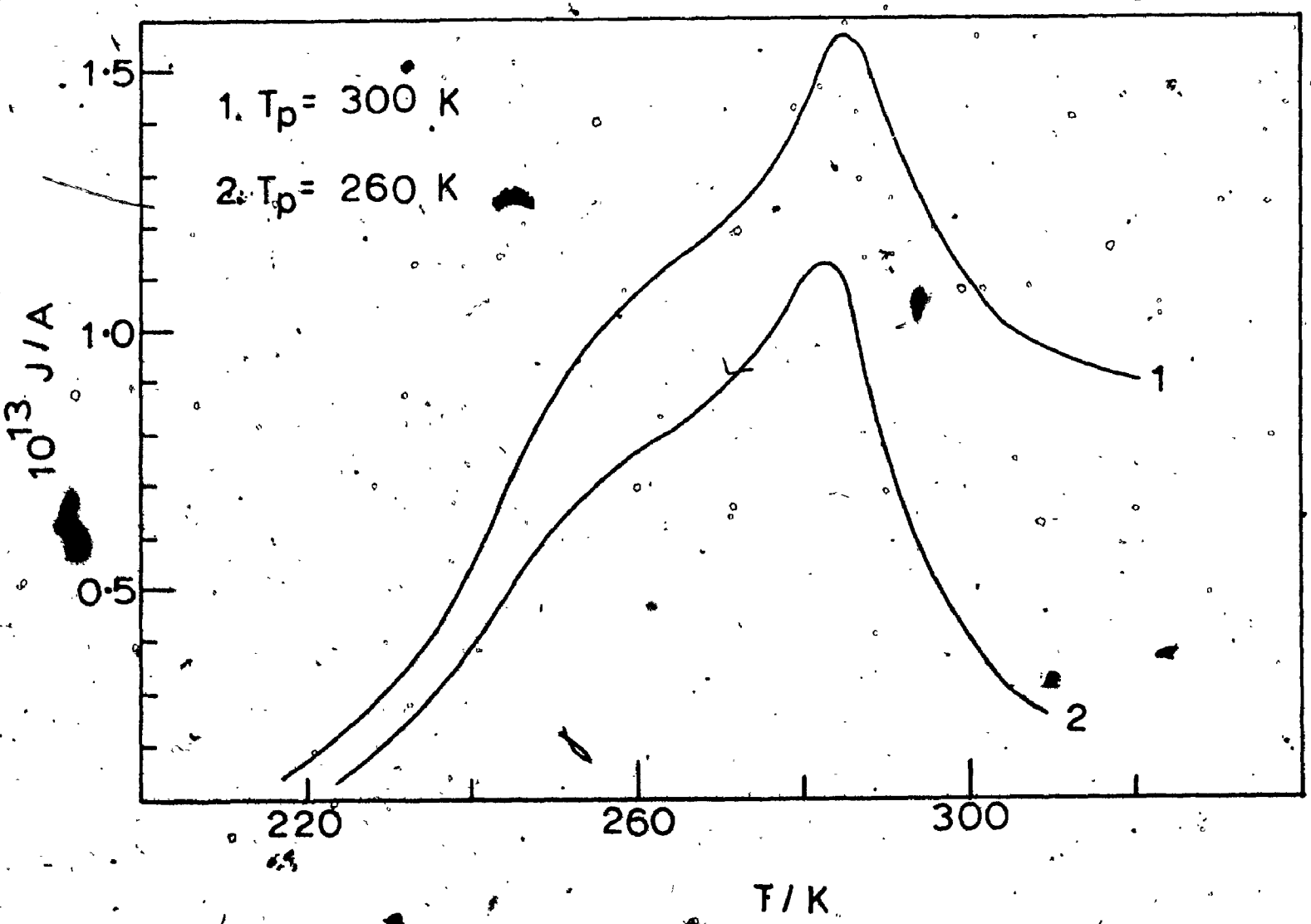

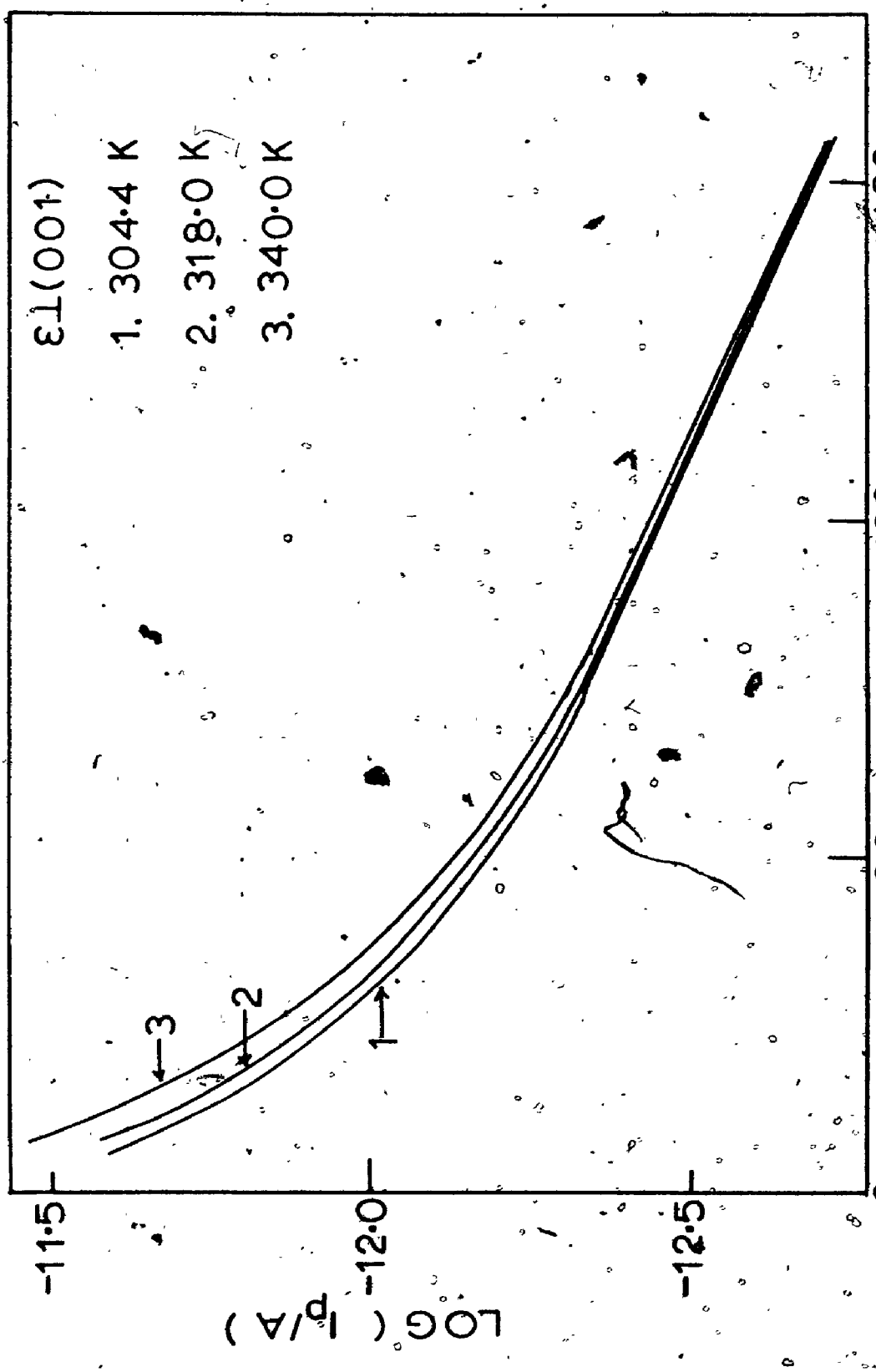

FIG. 31 POLARIZATION CURRENTS IN PURE AP

FIG. 32 LOG(τ^{-1}) VS. T^{-1} FOR PURE AP, ε_4(001)

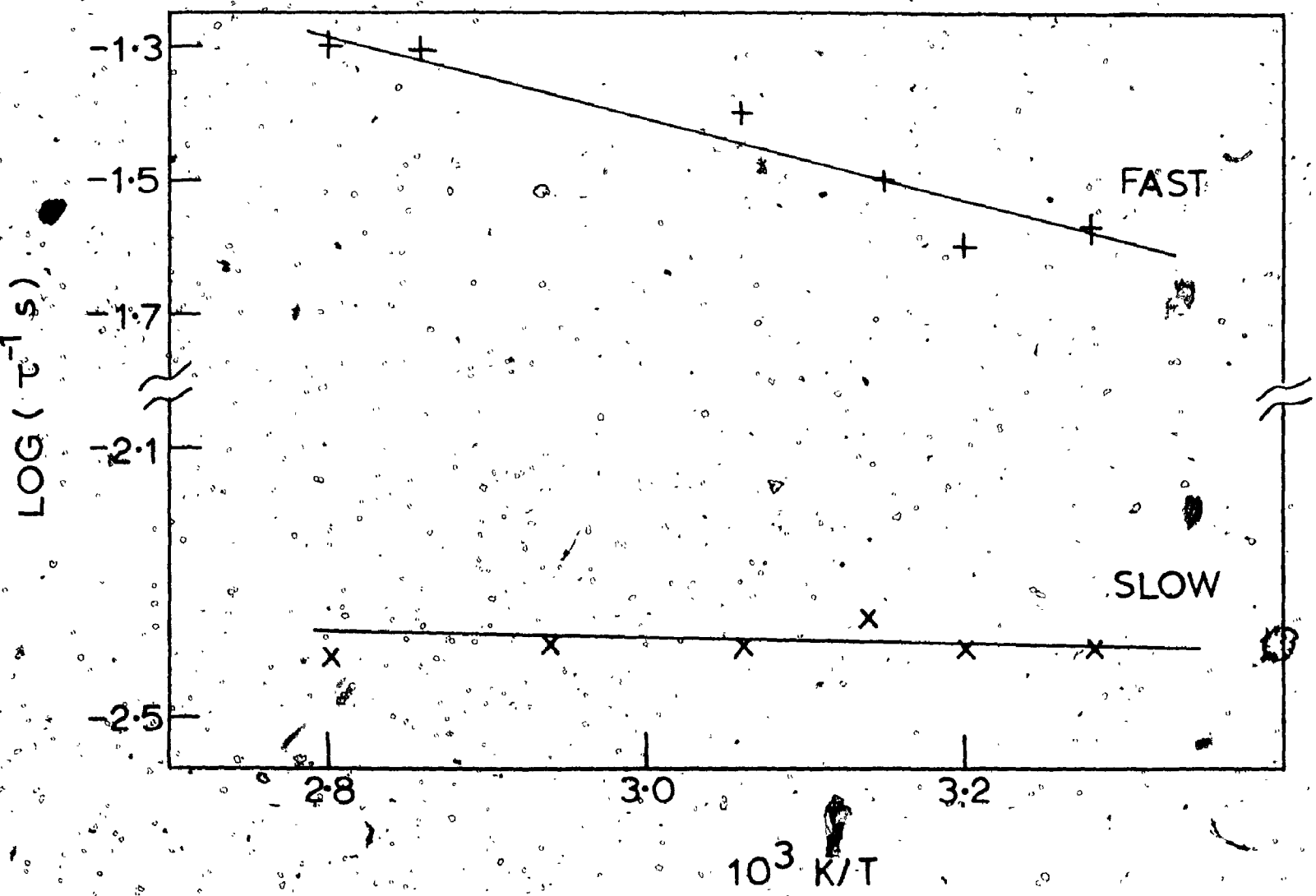

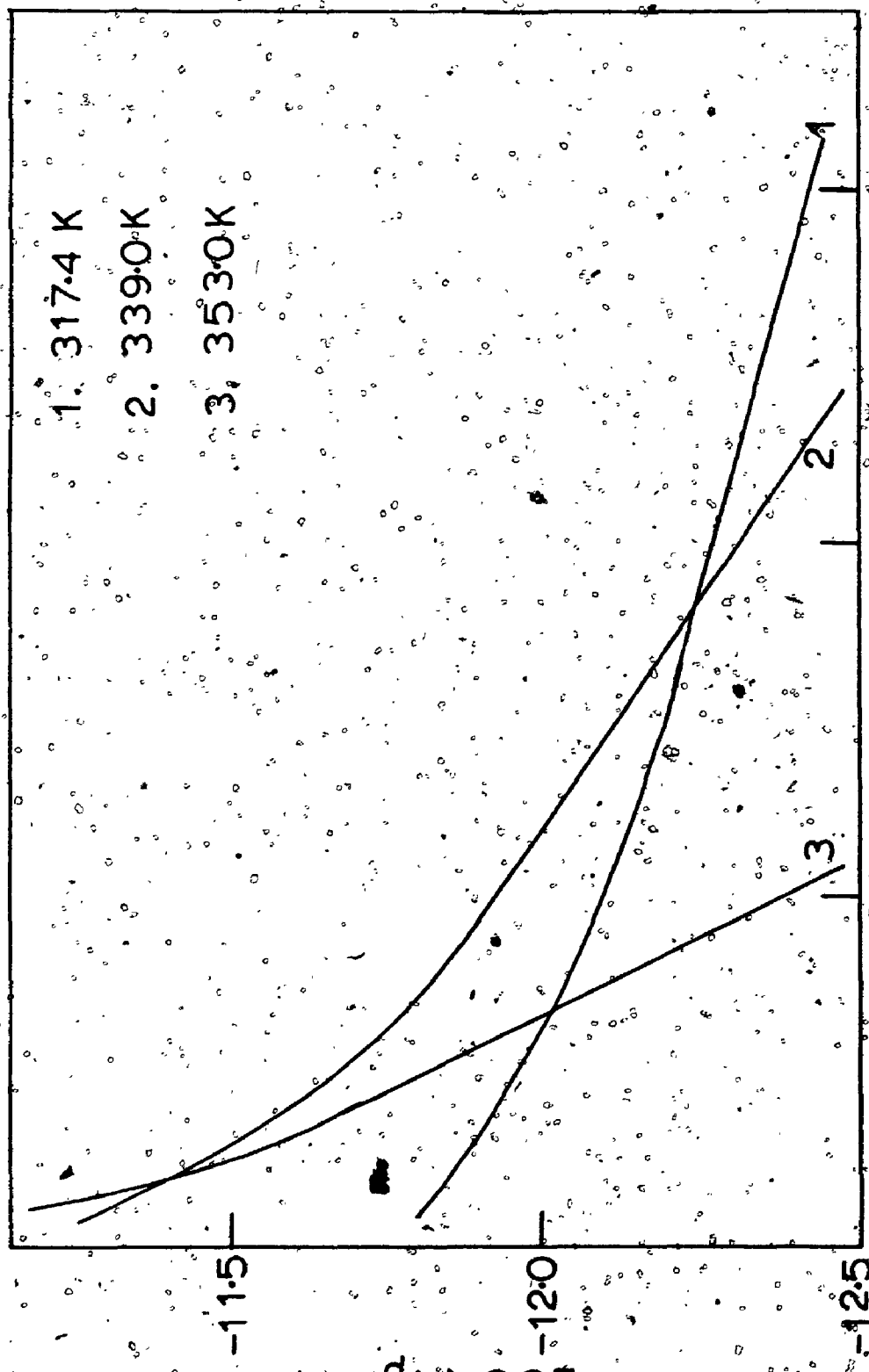

FIG. 33. POLARIZATION CURRENTS IN 0·1%. AP: SO_4^{2-}, Cu(001)

FIG. 34 POLARIZATION CURRENTS IN 0·1 % AP:CrO_4^{2-}, $\varepsilon_\perp$(001)

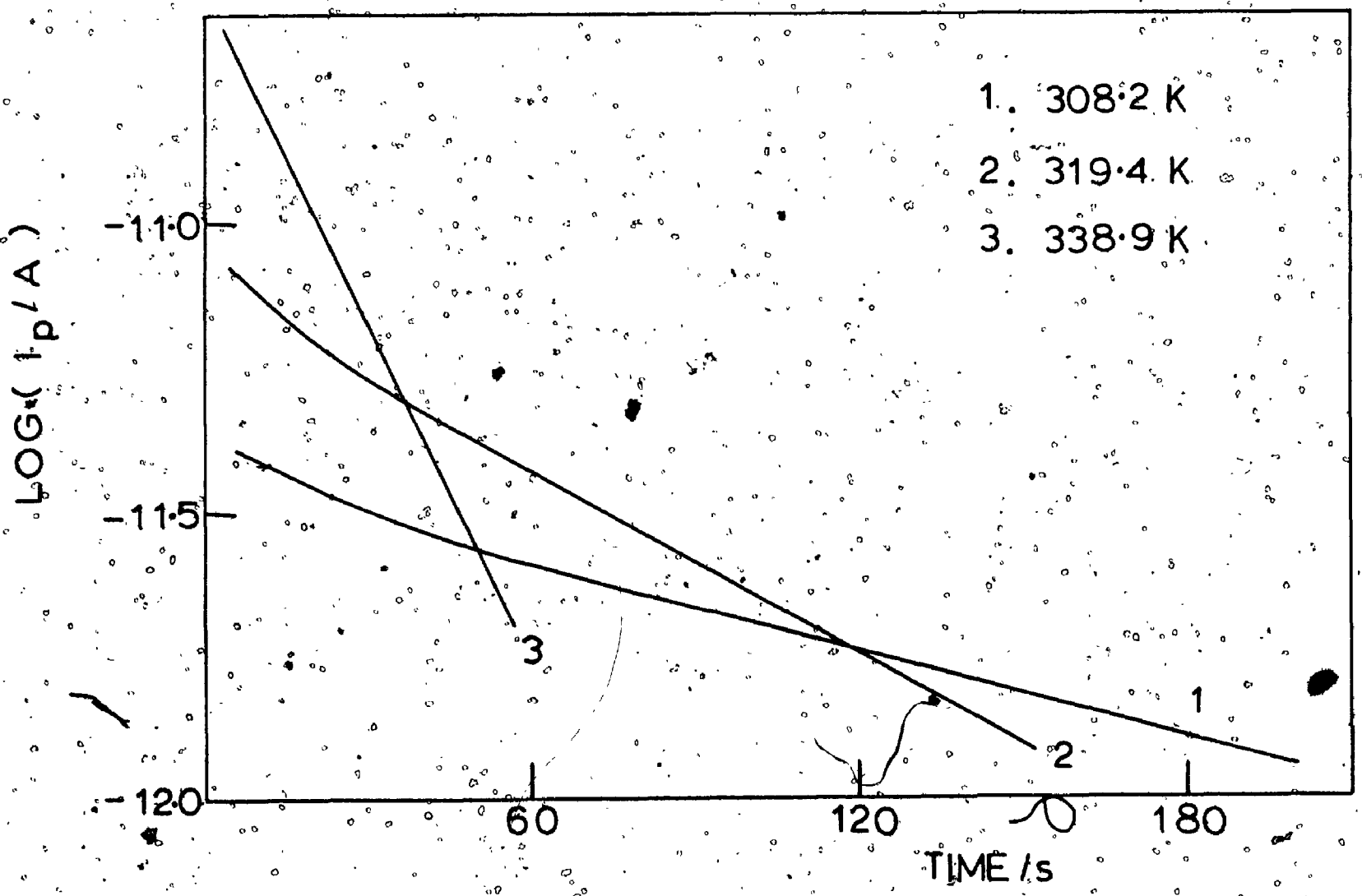

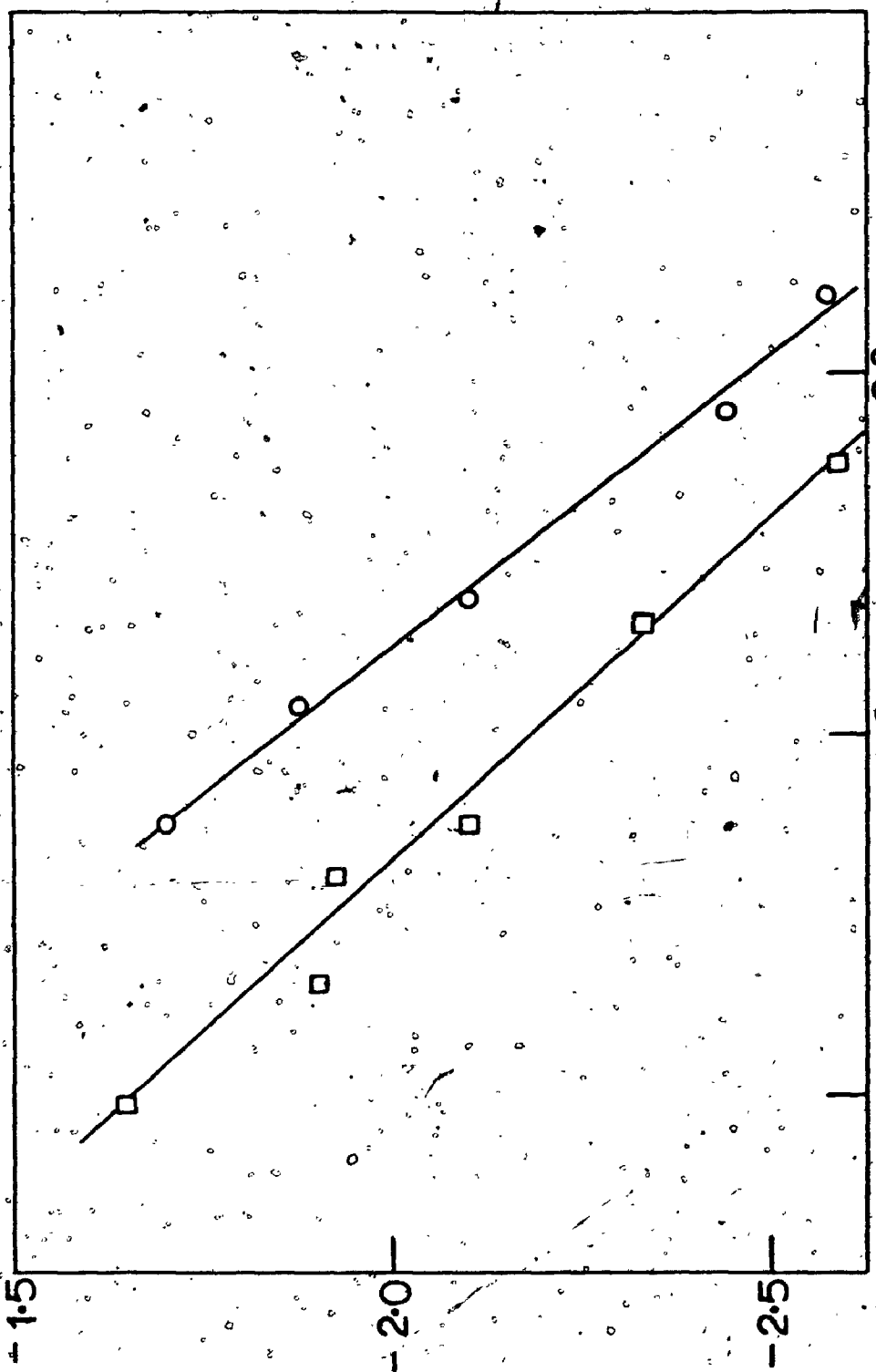

FIG. 35 LOG (τ^{-1}) VS. T^{-1} FOR 0·1% AP:SO_4^{2-} & 0·1% AP:CrO_4^{2-} , $\varepsilon\perp$(001)

FIG. 36 POLARIZATION CURRENTS IN PURE AP, $\varepsilon_{\perp}(210)$

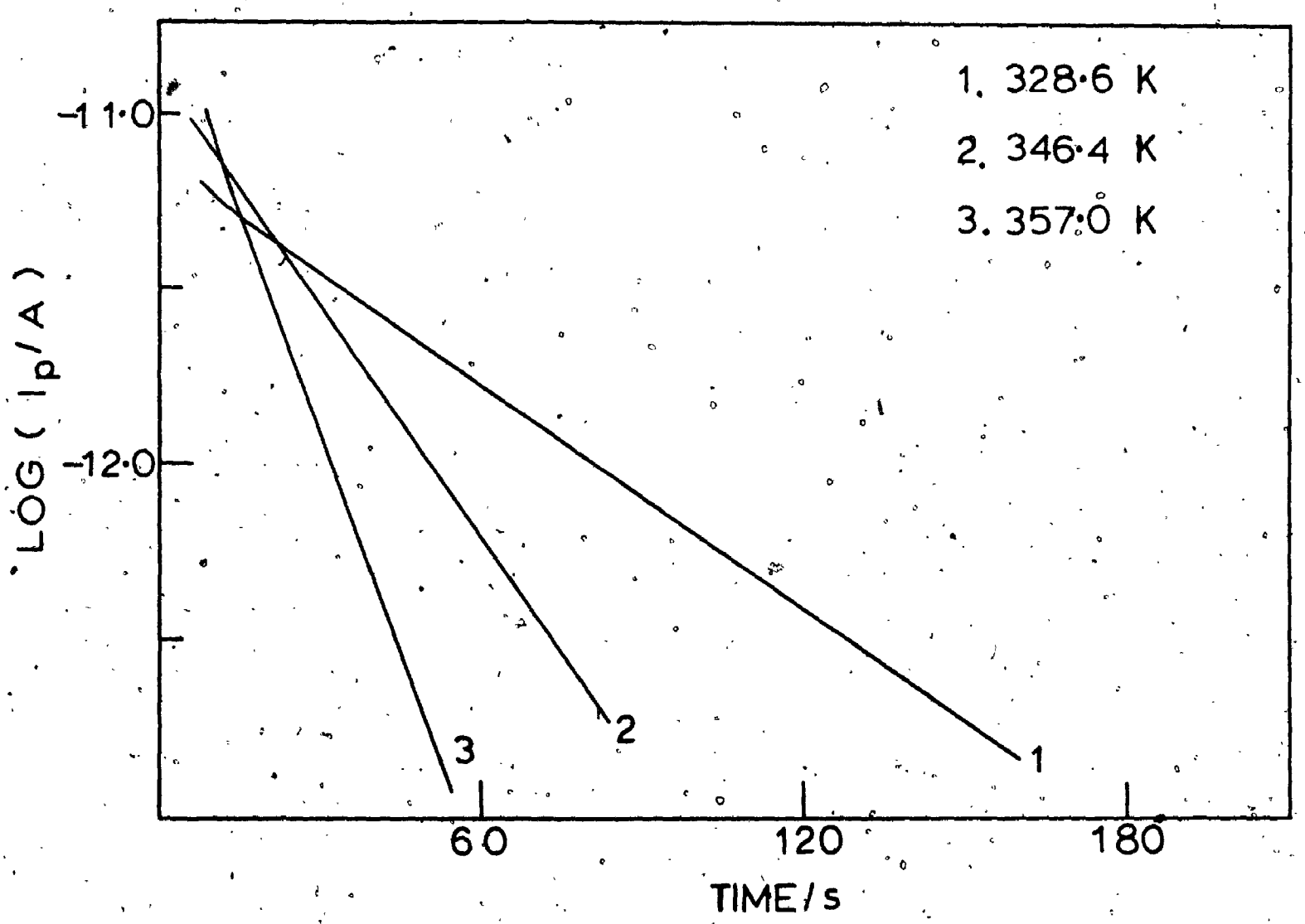

FIG. 37 POLARIZATION CURRENTS IN 0·1 % AP:CrO_4^{2-}, E⊥(210)

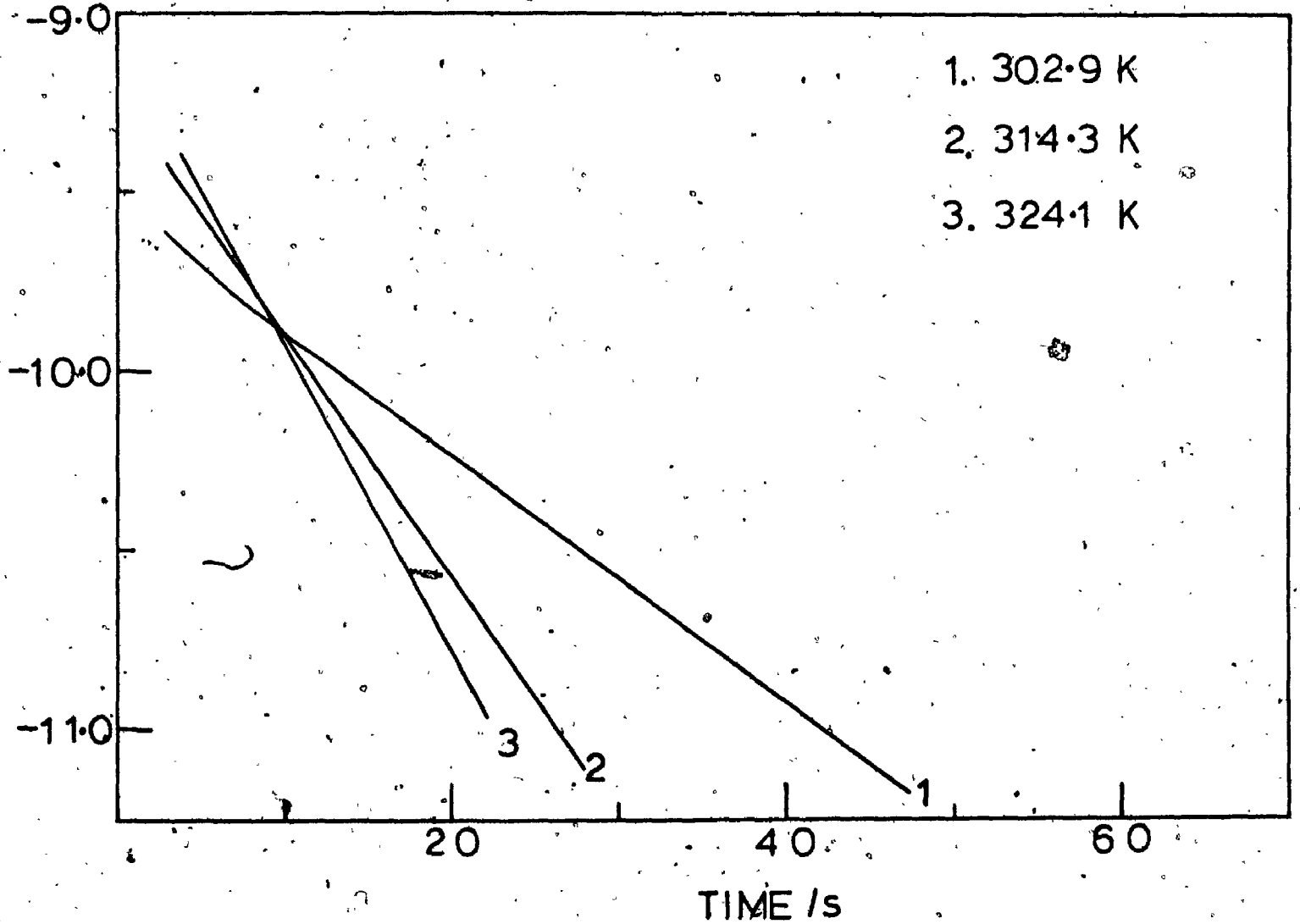

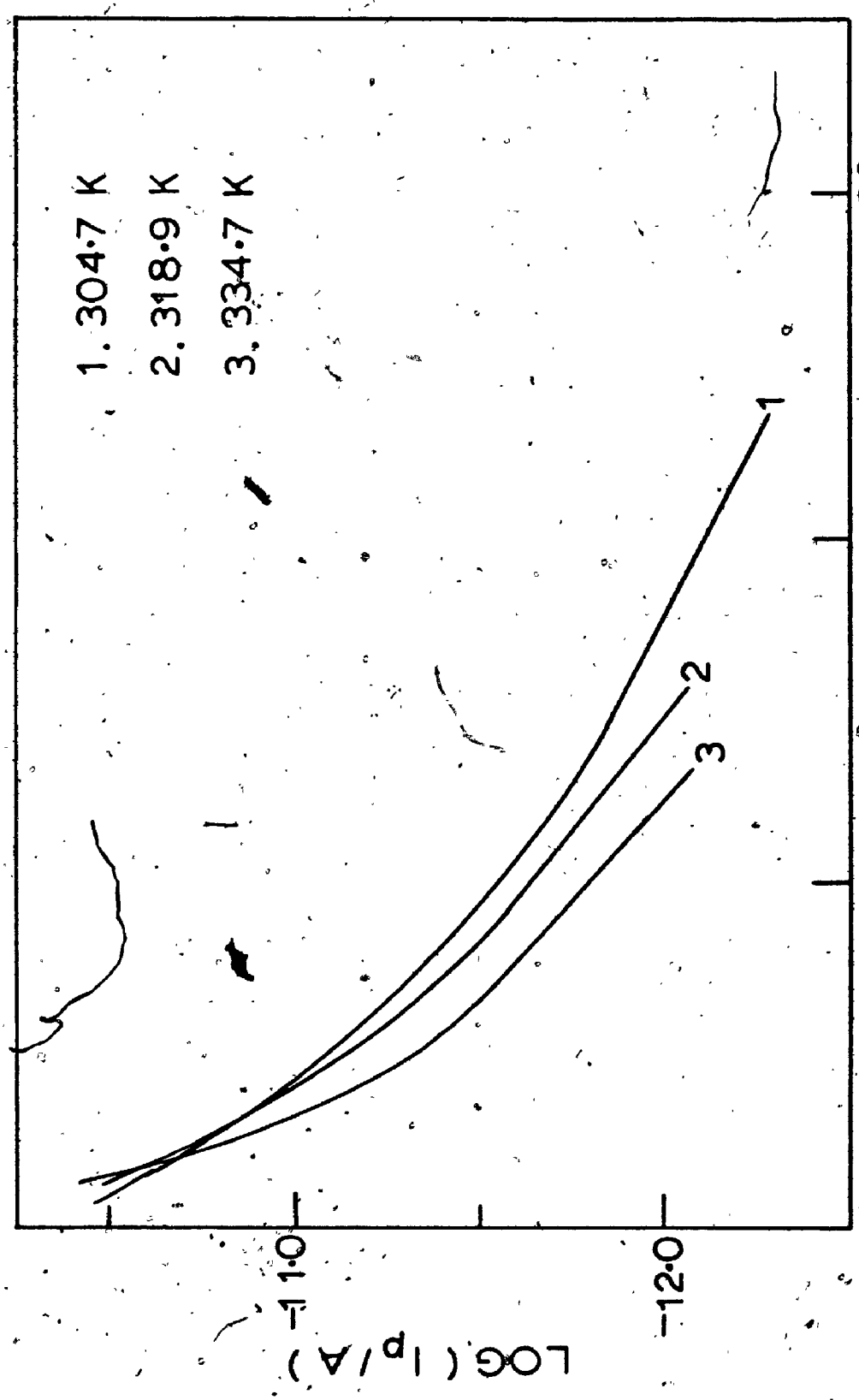

FIG. 3.8 POLARIZATION CURRENTS IN 0·1%, ÀP: SO_4^{2-}, Eɪ(210)

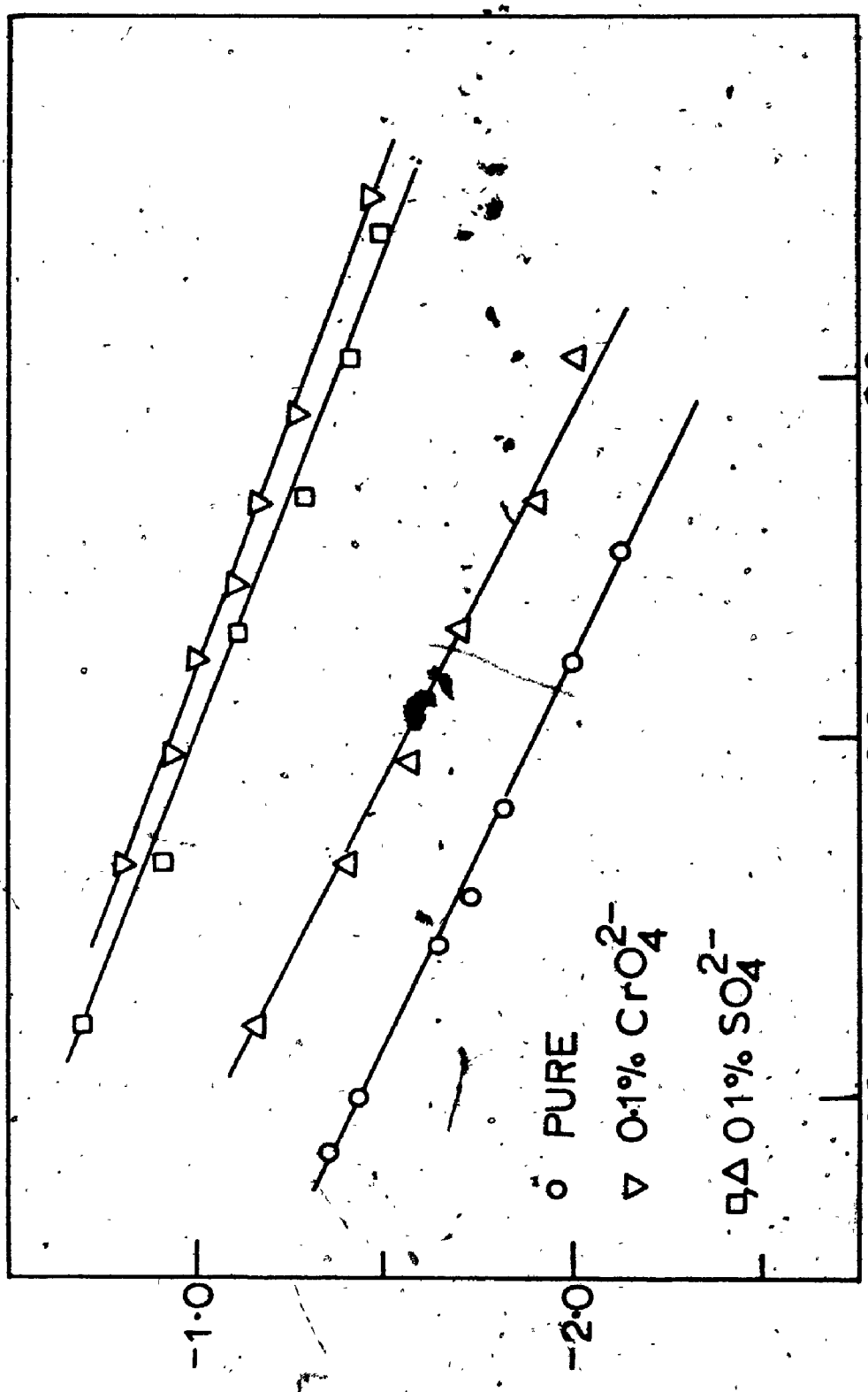

FIG. 39 LOG (τ^{-1}) VS. T^{-1}, $\varepsilon_\perp$('210)

FIG.40 THREE PLANES OF ClO_4^- IN A UNIT CELL OF AP

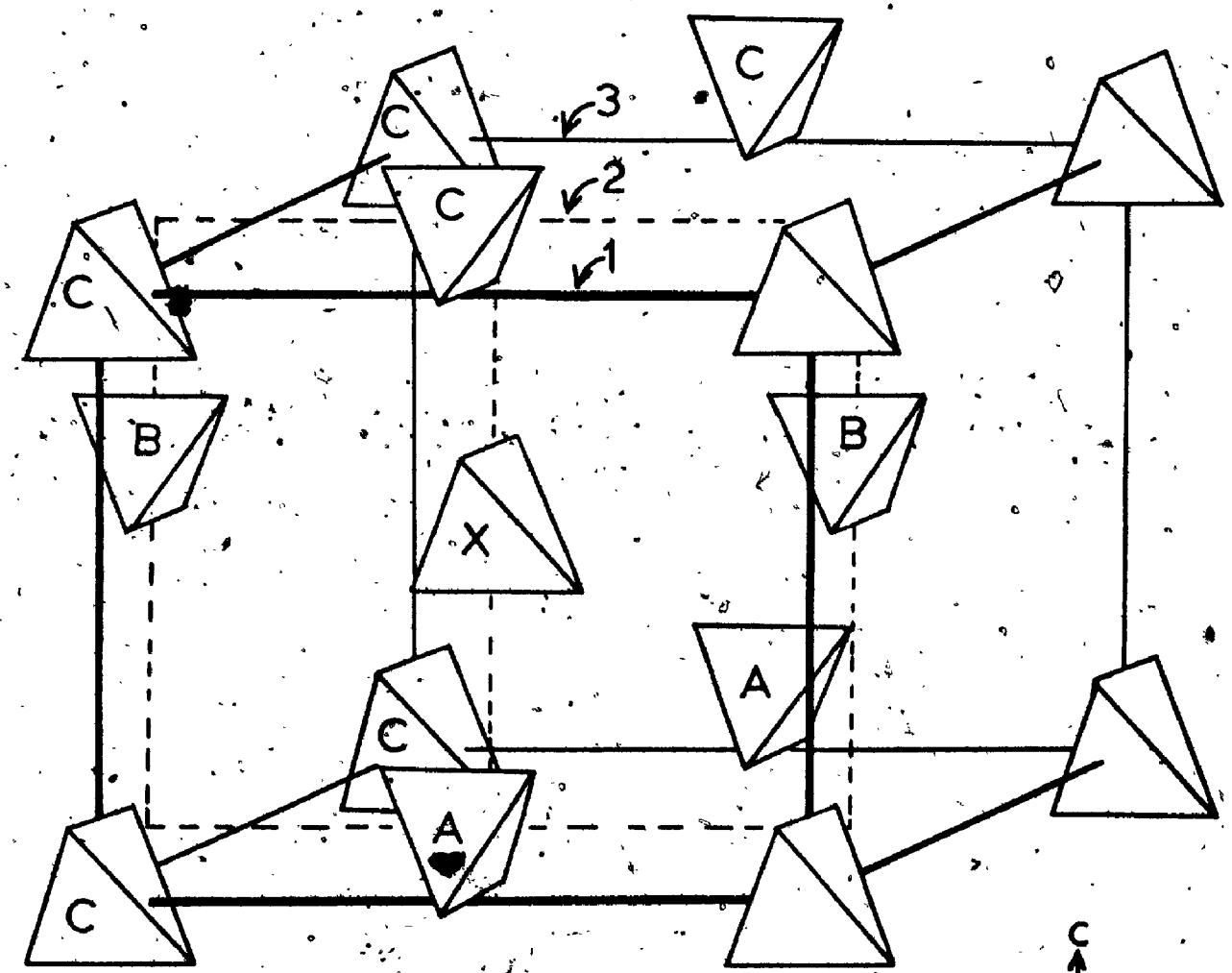

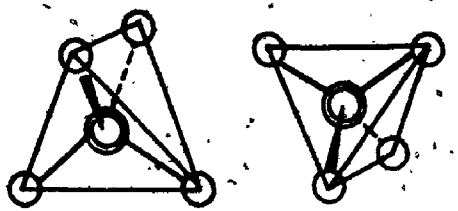

O = OXYGEN

O = CHLORINE

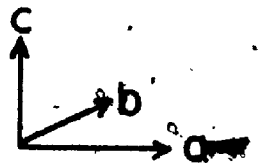

FIG. 41

PROJECTION ON THE (100) PLANE OF TWO NEIGHBOURING PLANES OF ClO_4^-

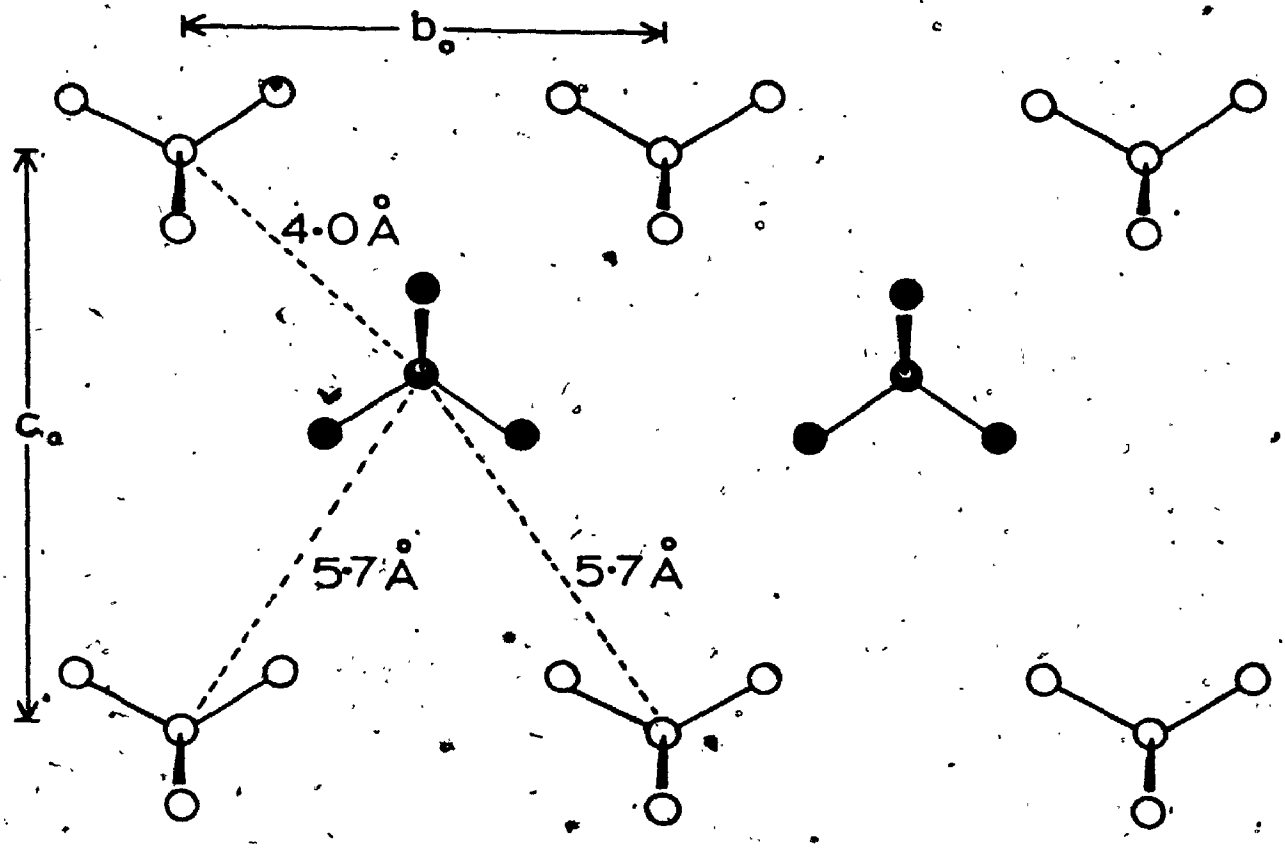

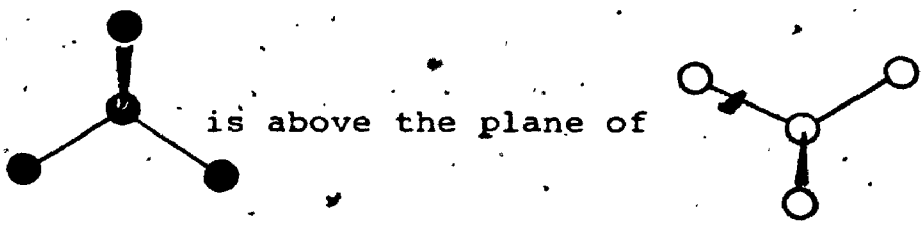

FIG. 42 PROJECTION ON THE (010) PLANE OF TWO NEIGHBOURING PLANES OF ClO_4^-

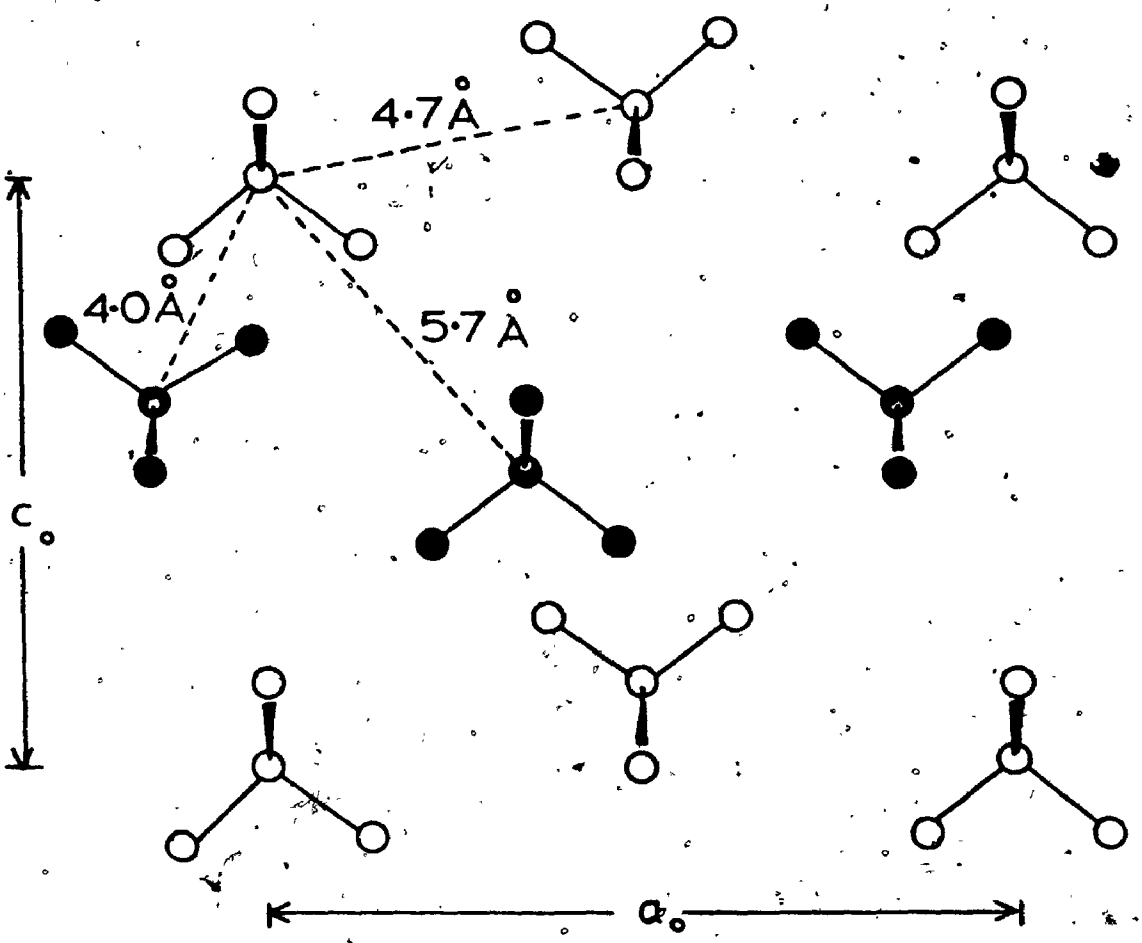

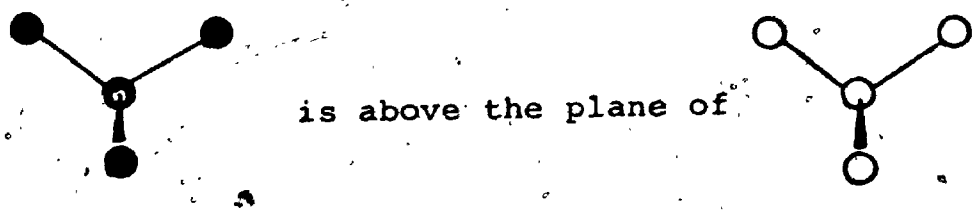

is above the plane of

FIG. 43 COMPARISON OF VALUES OF τ OBTAINED FROM FROM D.C. ROLARIZATION AND TDC

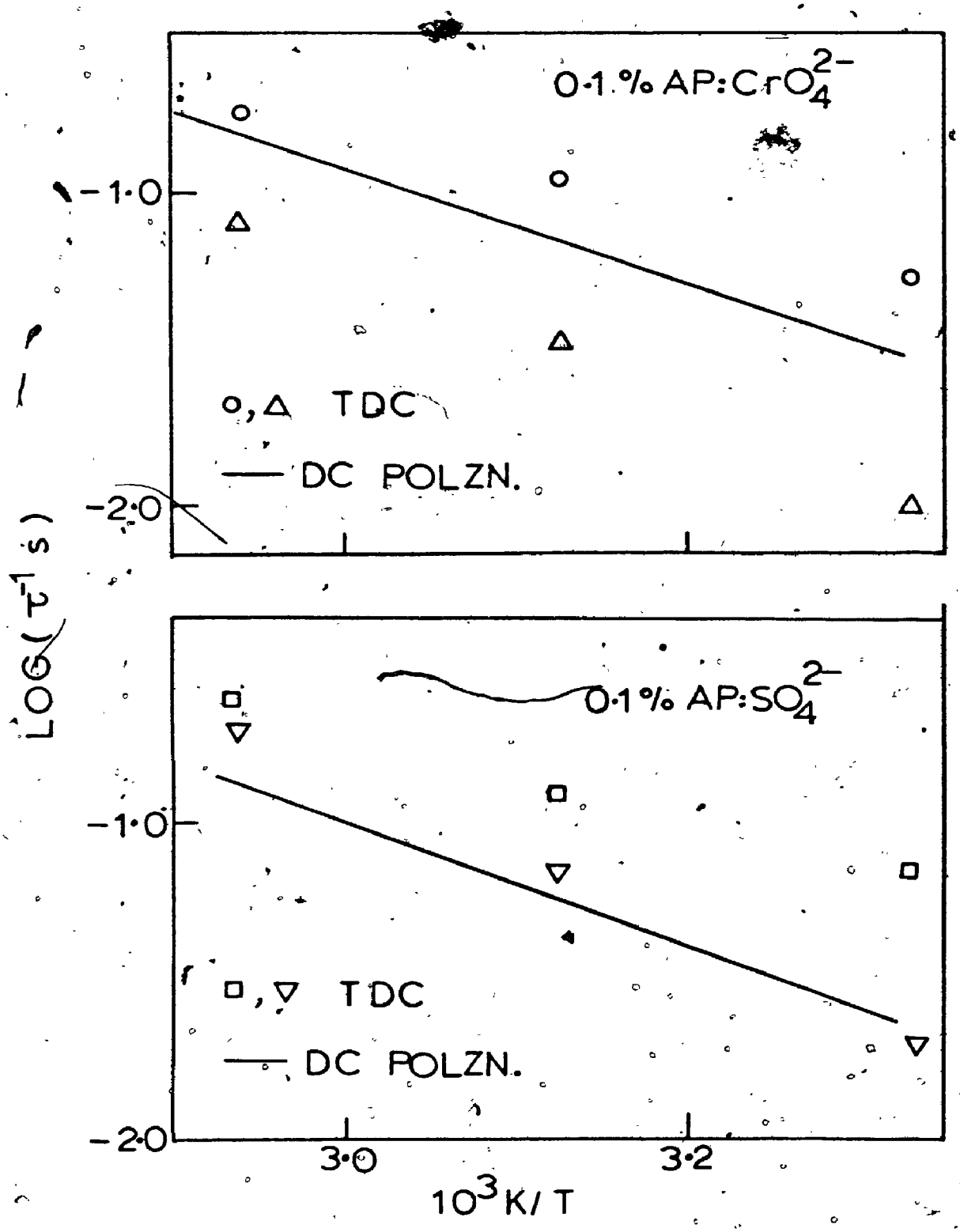

REFERENCES

1. P.W.M. Jacobs and H.M. Whitehead, Chem. Rev. 69, 551 (1969).

2. A.G. Keenan and Robert F. Siegmund, Quant. Rev. Chem. Soc. 23, 430 (1969).

3. P. Zirkind and E.S. Freeman, Nature 199, 1280 (1963).

4. H. Wise, J. Phys. Chem. 71, 2843 (1967).

5. J.N. Maycock and V.R. Pai Verneker, Proc. Roy. Soc. (Lond.) A 307, 303 (1968).

6. J.N. Maycock, V.R. Pai Verneker and C.S. Gorzynski, Solid State Comm. 5, 227 (1967).

7. P.W.M. Jacobs and Wee Lam Ng, J. Phys. Chem. Solids, 33, 2031 (1972).

8. P.W.M. Jacobs, Francis E. Lovatt and Wee Lam Ng, Can. J. Chem. 50, 3154 (1972).

9. G.P. Owen, J.M. Thomas and J.O. Williams, J.C.S. Dalton 808, (1972).

10. G.P. Owen, J.M. Thomas and J.O. Williams, J.C.S. Faraday Trans. 1, 68, 2356 (1972).

11. E.F. Khairetdinov and V.V. Boldyrev, J. Solid State Chem. 11, 67 (1974).

12. A.G. Keenan and M.G. Ohanian, J. Solid State Chem. 16, 151 (1976).

13. M. Goldstein and A.G. Keenan, J. Solid State Chem. 7, 286 (1973).

14. A.B. Lidiard, in "Handbuch der Physik", ed. S. Flugge, Springer-Verlag, Berlin, 1957, vol. 20, p. 246.

15. J. Corish and P.W.M. Jacobs, in "Surface and Defects Properties of Solids" (Specialist Periodical Reports), ed. M.W. Roberts and J.M. Thomas, The Chemical Society, London, 1973, vol. 2, p. 160.

16. L.W. Barr and A.B. Lidiard, in "Physical Chemistry - An Advanced Treatise," ed. H. Erying, D. Henderson and W. Jost. Academic Press, New York, 1970, vol.X, p. 151.

17. P. Süptitz and J. Teltow, Phys. Stat. Sol. 23, 9 (1967).

18. J.M. Thomas and J.O. Williams, Progr. Solid-State Chem. 6, 119 (1971).

19. R.E. Howard and A.B. Lidiard, Rep. Progr. Phys. 27, 161 (1964).

20. R.W. Drefus, Phys. Rev. 121, 1675 (1961).

21. A.R. Allnatt, P.W.M. Jacobs, and J.N. Maycock, J. Chem. Phys. 43, 2526 (1965).

22. K.C. Kao, W. Whitham, and J.H. Calderwood, J. Phys. Chem. Solids, 31, 1019 (1970).

23. C. Bucci, R. Fieschi, and G. Guidi, Phys. Rev. 148, 816 (1966).

24. B.J. Klein, Jr., Ph.D. Thesis, University of North Carolina, Chapel Hill, 1970.

25. M.M. Perlman and S. Unger, J. Appl. Phys. 45, 2389 (1974).

26. D.W. Marquardt, "Least-squares Estimation of Non-linear Parameters", Share Distribution No. 3094, E.I. Du Pont de Nemours and Co., Inc. Wilmington, Delaware, 1966.

27. R. Capelletti and E. Okuno, "Electrets, Charge Storage and Transport in Dielectrics", Ed. M.M. Perlman, The Electrochemical Soc. 1973, p. 13.

28. C. Bucci and S.C. Riva, J. Phys. Chem. Solids 26, 363 (1965).

29. A. Kessler, Solid State Comm. 12, 697 (1973).

30. A. von Hippel, J. Chem. Phys. 54, 145 (1971).

31. R. Blinc and J. Pirs, J. Chem. Phys. 54, 1535 (1971).

32. M. O'Keefe and C.T. Perrino, J. Phys. Chem. Solids, 28, 211 & 1086 (1967).

33. B.V. Hammon and R.J. Meakins, Austrl. J. Sci. Res. A. 5. 671 (1952).

34. A. Kawada, A.R. McGhie, and M.M. Labes, J. Chem. Phys. 52, 3121 (1970).

35. P.H. Sutter and A.S. Nowick, J. appl. Phys. 34, 734 (1963).

36. M.A. Maidique, A. von Hippel and W.B. Westphal, J. Chem. Phys. 54, 150 (1971).

37. S.V. Moore, G.R. Owen, J.M. Thomas and J.O. Williams, J. Chem. Soc. Dalton, 1029 (1974).

38. Wee Lam Ng, Ph.D. Thesis, University of Western Ontario, London, Canada, 1971.

39. J. Bruinik, J. Appl. Electrochem. 2, 239 (1972).

40. L. Glasser, Chem. Rev. 75, 21 (1975).

41. V.V. Boldyrev and E.F. Khairetdinov, J. Inorg. Nucl. Chem. 31, 3332 (1969).

42. S.P. Tang and J.B. Fenn, J. Phys. Chem. 77, 940 (1973).

43. R.T.V. Kung and R. Roberts, J. Phys. Chem. 78, 1433 (1974).

44. L.B. Harris and G.J. Vella, J. Chem. Phys. 58, 4550 (1973).

45. T.M. Herrington and L.A. Staveley, J. Phys. Chem. Solids, 25, 921 (1964).

46. C.S. Choi, H.J. Prask and E. Prince, J. Chem. Phys. 61, 3523 (1974).

47 J.J. Delpuech, G. Serratrice, A. Strich, and A. Veillard, J. Chem. Soc. Comm. 817, (1972).

48. E.F. Khairetdinov, A.I. Burshtein, and V.V. Boldyrev, Sov. Phys. Solid State, 15, 2018 (1974).

49. R.A. Sack, Austrl. J. Sci. Res. (A), 5, 135 (1952).

50. P.J. Herley, P.W.M. Jacobs, and P.W. Levy, Proc. Roy. Soc. Lond. (A), 318, 197 (1970).

51. A.V. Raevskii, G.B. Manelis, V.V. Boldyrev, and L.A. Votinova, Dokl. Akad. Nauk SSSR, 160, 1136 (1960).